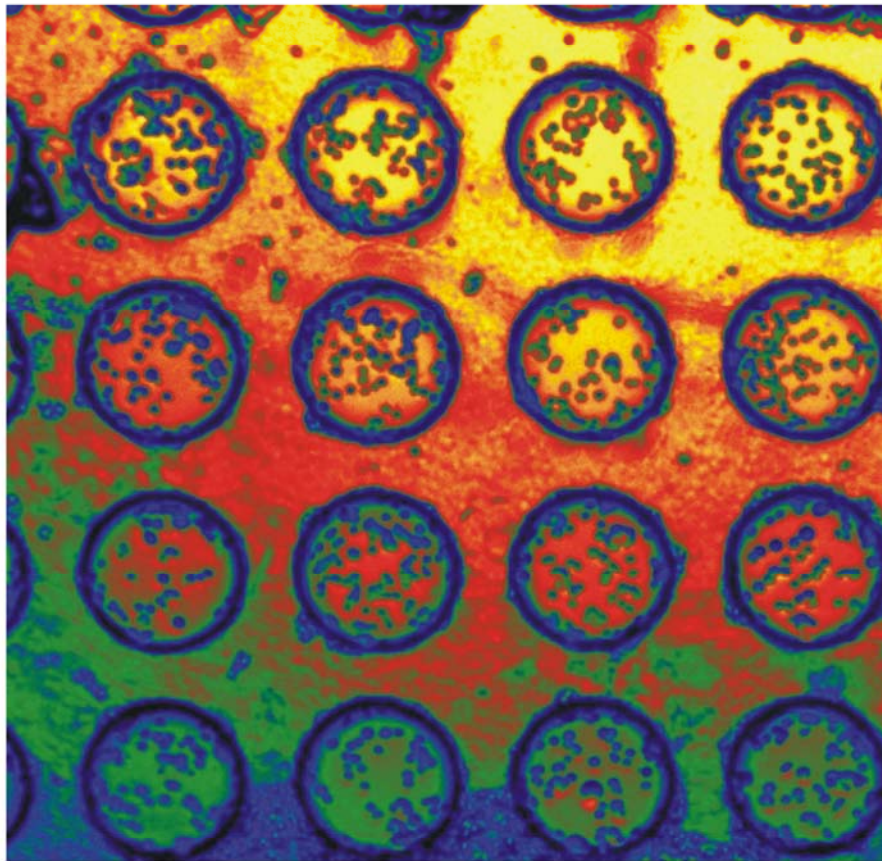


Microfluidic Imaging: Pixelation and Pre-concentration for Biological and Chemical Sample Analyses



 Institute for
Analytical Sciences

 technische universität
dortmund

Kaoru Tachikawa

Microfluidic Imaging: Pixelation and Pre-concentration for Biological and Chemical Sample Analyses

Zur Erlangung des akademischen Grades eines
Dr. rer. nat.

der Fakultät Bio- und Chemieingenieurwesen BCI
der Technischen Universität Dortmund
vorgelegte Dissertation

vorgelegt von
M.Sci. Kaoru Tachikawa

aus
Kanagawa, Japan

bearbeitet am
ISAS - Institute for Analytical Sciences

Tag der mündlichen Prüfung: 29.04.2008
1. Gutachter: Prof. Dr. A. Manz
2. Gutachter: Prof. Dr. A. Schmid

Dortmund 2008

Abstract

The novel concept “microfluidic imaging” that spatially resolves the composition of complex biological and chemical samples by pixelation within a microfluidic platform was explored. The approach integrates two different microfluidic techniques: sample pre-concentration and droplet-based pressure driven flow system.

An electrokinetic pre-concentration method for amino acid enrichment was explored. This technique can be integrated to manipulate pixelated sample that have low-abundant analytes in very small volumes. Agarose gel excelled in fixing various samples on the surface and in the parallel uptake and pixelation step.

The presented device was designed and fabricated to image samples by discretising targeted areas into droplets suspended in a two-phase microflow. These droplets are transferred from parallel to serial mode for data readout similar to a CCD camera, thus referred as “microfluidic imaging”. Three major process steps conducted within the device were parallel sample pixelation and uptake, transfer from parallel to serial mode into a microchannel for individual analysis and image generation. This microfluidic pixelation method is capable of obtaining non-averaged data from heterogeneous specimen, with reduced arduous preparation steps while retaining the spatial information.

The ability to convert the compartmentalised information from a parallel to serial manner is an advantage this device has allowing to approach closer to automation and to implement preparation, separation and detection steps. In this respect, this method has clear superiority over currently available tedious techniques for capturing of cells from tissue, such as laser microdissection or capillary capture methods. With further pixel size reductions, controlled encapsulation of single cells in single droplets comparable in size to the cell diameter is accomplishable. This way the application of the concept in high throughput screening, clinical diagnosis, single cell bioreactors, and the investigation of stem cell differentiation can be appreciated, emphasising the importance of cellular heterogeneity within a population at single cell level.

Zusammenfassung

Das neuartige Konzept des “Microfluidic Imaging” wurde untersucht, welches die Zusammensetzung biologischer und chemischer Proben durch Pixelierung innerhalb einer mikrofluidischen Plattform räumlich auflöst. Der Ansatz vereint zwei mikrofluidische Prinzipien, die Aufkonzentration von Analyten und ein auf Tropfen basiertes, druckbetriebenes Fließsystem.

Dabei wurde eine Konzentrationsmethode für die Anreicherung von Aminosäuren untersucht. Diese Technik kann eine pixelierte Probe mit niedrig konzentrierten Analyten selbst in kleinen Volumina bearbeiten. Als Oberfläche zeichnete sich dabei Agarose-Gel sowohl durch ausgezeichnete Fixierung von verschiedensten Proben als auch durch die parallele Aufnahme aus.

Der präsentierte Chip wurde so konzipiert und hergestellt, dass er Proben in diskrete Flächen einteilen und als suspendierte Tropfen in ein zweiphasiges Mikroflusssystem aufnehmen kann. Diese Tropfen werden zur Datenausgabe vom parallelen in den seriellen Modus übertragen, ähnlich wie bei einer CCD-Kamera, und somit als “Microfluidic Imaging” bezeichnet. In der Apparatur müssen drei Schritte vollzogen werden: Die Probepixelierung und -aufnahme, die Umwandlung von parallelem zu seriellem Betrieb im Mikrokanal, um die individuelle Analyse sicherzustellen, und die Generierung des ursprünglichen Bildes. Diese mikrofluidische Pixelierungsmethode ist fähig nicht gemittelte Daten aus heterogenen Proben zu erzielen, ohne mühsame Vorbereitungsschritte und bei gleichzeitiger Erhaltung der räumlichen Information.

Die Fähigkeit Information von paralleler in serielle Weise umzuwandeln ist ein Vorteil dieses Chips, welcher die Grundlage für die vollständige Automatisierung und Implementierung von Probenvorbereitung, Trennung und Detektion darstellt. Die Methode ist somit klar besser als Techniken zur Zellisolation aus Geweben, wie Lasermikrodissektion oder kapillare Isolationssysteme, und mit einer weiteren Reduzierung der Pixelgröße wird die Isolation von einzelnen Zellen in Tröpfchen mit ähnlichem Durchmesser wie dem der Zellen, möglich. So kann dieses Konzept künftig für “High Throughput Screening”, klinische Diagnosen, Einzelzellreaktoren und zur Untersuchung von Stammzellendifferenzierung genutzt werden, und unterstreicht die Wichtigkeit der zellulären Heterogenität innerhalb einer Population.

Declaration

The work in this thesis is based on research carried out at the ISAS - Institute for Analytical Sciences, Dortmund, Germany. No part of this thesis has been submitted elsewhere for any other degree or qualification and it is all my own work, unless referenced to the contrary in the text.

Dortmund, 8th February 2008

Copyright © February 2008 by Kaoru Tachikawa.

“The copyright of this thesis rests with the author. No quotations from it should be published without the author’s prior written consent and information derived from it should be acknowledged”.

To my parents and my brothers

Acknowledgment

“LIVE LIFE TO ITS FULLEST”

As I left my home country, Japan, at the age of twelve, little did I know how my life voyage would unfold itself... at twenty-four years-old, I moved to a country whereby I opened up, yet again, a completely new chapter in my life.

This has been three fantastic and satisfying years at ISAS, Dortmund. Having moved to a new city, where I spoke no language of, it was difficult for me to adjust at the beginning. I believe it was, after all, my self-strength and -belief that got me through the tough times, by making the most of what I had in given circumstances. But undoubtedly, to have reached where I am now, I certainly CANNOT forget to pay my gratitude to the many people, from whom I constantly received the warm support and assistance, along this wonderful journey so far. Now, I finally have the opportunity to express my true appreciation to all of them...

My greatest gratitude goes to my supervisor, **Andreas Manz** for giving me the life time opportunity to work at ISAS. I am honoured to have been supervised by the world top-class scientist and the real McCoy of the μ TAS field. For endless inspiring ideas that bubbles out his magical hat and the encouraging comments he gave at those downfall moments, it made me feel like I had the most exciting project in the world. The way he motivated his students and gave freedom to nurture your own mind are his ability I look up to and would like to adopt for myself. I truly respect him in every way.

I would like to pay my special thanks to **Petra Dittrich** for the constant motivation, realistic guide and support she gave me throughout the time of my PhD, and for the supervision and the correction of my work. **Joachim Franzke** for his scientific advice, thoughtful discussions and creating wonderful and fun atmosphere in the group. Also **Dirk Janasek** (a.k.a. “DJ”), who was always helpful for when I needed “that” answer.

Two of my encouraging PhD mates, Helke and Claus - they started almost at the same time and “lived” together in the office the entire time. Thank you for putting up with me throughout the last three years. I won’t forget the tough and the fun times we’ve been through! I hope to look back on this day to bring smile on my face. I am sure the office would miss us...

Helmut for the joy he gave me in and outside of ISAS from discussing physics problems to ballroom dancing; Sabine, Ying, Carmen, Kathrine, Lindsey and Melissa for the girly chats; Hendrik, Marco, Sven, Ingo and Jean-Phillip for the boy energies; Peter, Micheal, Uli, Johnny and Sebastian for fruitful discussions; Ken-ichi for bringing back the taste of Japan in my life; all the members of miniaturisation group at ISAS, all of my friends from BCI at the University of Dortmund and all the people who have left but have touched my world - they played a major role in my development during this period, both on a scientific and a personal level. I thank them for creating an inspiring working environment and wonderful social life.

I am so grateful for Daniel for making the time for proof-reading my thesis, filling me in with biology knowledge and making me laugh despite the miserable day I might have had. It was he, who always directed me into the right path when I was losing my focus and provided me the shoulder to cry on. I thank you for everything and for being there for me!

My most sincere appreciation goes to the Tachikawa family members - my father Toshiko, my mother Yoshiko and my brothers Hidemi and Takane, who live thousands of miles away. Whether we were together or apart, they always supported me for the last 27 years. It was their encouragement and belief that allowed me to reach this point in my life. I thank you forever, truly from the bottom of my heart.

...I thank you all.

Dortmund, Feb. 2008

Kaoru Tachikawa

Contents

Chapter One — Introduction	1
1.1 Miniaturisation and Microfluidics	1
1.2 Research Goals	2
1.3 Thesis Outline	6
Chapter Two — Micro Total Analysis Systems (μTAS) Concept	7
2.1 Overview	7
2.2 Motivation for Miniaturisation	7
2.3 μ TAS: Latest Advancements and Trends	10
2.4 Summary	15
Chapter Three — Fabrication of Microfluidic Chips	17
3.1 Producing Microstructured channels	17
3.1.1 Choice of Materials	17
3.1.2 Mask Design	19
3.1.3 Lithography Techniques	19
3.2 Glass/Glass Chip Fabrication	21
3.2.1 Exposure using Direct Write Laser (DWL)	21
3.2.2 Design Etching using Hydrofluoric Acid (HF)	23
3.2.3 Preparative Steps before Bonding	23
3.2.4 Bonding	24
3.3 PDMS/Glass Chip Fabrication	26
3.3.1 Formation and Casting of PDMS	26
3.3.2 Plasma Bonding	28
3.4 PMMA Chip Fabrication	29
3.5 Summary	30

Chapter Four — Pixelation of Planar Biological and Chemical Samples	31
4.1 Droplet Based Microfluidic Platforms	33
4.1.1 Experimental Outline	37
4.1.2 General Experimental Setup	37
4.2 Pixelating and Capturing Samples	41
4.2.1 Pixelation from the Hard Surface	41
4.2.2 Pixelation from the Soft Surface	45
4.3 Total Fluidic Approach	48
4.3.1 Chip Design	48
4.3.2 Three PMMA Layer Chip	49
4.3.3 PDMS-PMMA-PDMS Chip	51
4.4 Micropillar Manifolds Approach	54
4.4.1 Experimental	54
4.4.2 Results and Discussion	54
4.5 Sample Pixelation, Injection, Transport and Stability	56
4.5.1 Experimental	57
4.5.2 Sample Pixelation	60
4.5.3 Segmented Flow System	61
4.6 Testing the Chip Application	68
4.6.1 Aqueous Dye Manipulation	69
4.6.2 Yeast Cell Manipulation	69
4.7 Summary	71
Chapter Five — Towards Electrophoretic Focussing of Amino Acids	73
5.1 Existing Pre-concentration Techniques	74
5.2 Mathematics for Electrophoretic Sample Stacking	77
5.2.1 Electrophoresis and Mobility	77
5.2.2 Electroosmotic flow (EOF)	78
5.2.3 Electrophoretic focussing	79
5.2.4 Field-amplified sample stacking (FASS)	80
5.3 Theory of the Gel-Buffer Interface Pre-concentration Method	81

5.3.1	Effect of the electric field amplification	82
5.3.2	Effect of the counteraction of the bulk flow at the interface	84
5.3.3	Effect of the electric field gradient	87
5.4	Experiments, Results and Discussions	88
5.4.1	Conservation of Mass	90
5.4.2	pH Change in Microchannel	91
5.4.3	Summary	96
Chapter Six — Summary and Suggestions for Future Research		99
6.1	Summary of Achievements	99
6.2	Suggestions for Future Research	100
Appendix A — Additional Information on Pixelation Study		105
A.1	Sample Pre-Treatment	105
A.2	Chip Design	105
Appendix B — Adaptation of the Pre-concentration Method		110
B.1	Chip Design with the Circular Electrode	110
B.2	Experimental	112
B.3	Results	115
Appendix C — Publications		119
Appendix D — Table of Abbreviations		120
Bibliography		121

List of Figures

1.1	Organ printing and commercially available microfluidic chips	2
1.2	Flow chart of the research outline	4
2.1	Examples of μ TAS systems	14
3.1	Photolithography mask fabrication procedure	20
3.2	Glass-glass chip fabrication procedure	22
3.3	Schematic illustration of under-etching	24
3.4	Temperature gradient for the bonding programme	25
3.5	PDMS/Glass fabrication procedure	27
3.6	Reaction mechanism for PDMS formation	28
3.7	The setup for the O ₂ plasma cleaner	29
4.1	Schematic drawing of a CCD device	32
4.2	A conceptual flow diagram for microfluidic imaging	34
4.3	Droplet formation in microchannels	35
4.4	Examples of droplet work	36
4.5	The chemical structure of erythrosine B	39
4.6	Comparison of a hole plate against PMMA stamp	42
4.7	Pixelation from the hard surface	43
4.8	Application of pressure on a the soft surface	44
4.9	Pixelation from the soft surface	46
4.10	SW 480 cell pixelation from the alginate surface	47
4.11	The chip design for the total fluidic approach	48
4.12	Three PMMA layer chip: design and assembly	49
4.13	Alignment and the leakage test on the three PMMA layer chip	50
4.14	PDMS-PMMA-PDMS chip composition and alignment	51
4.15	Sample injection using PDMS-PMMA-PDMS chip	53

4.16	The micropillar manifolds approach and the injected samples	55
4.17	Device design and realisation of microfluidic imaging	58
4.18	Efficiency of sample uptake with PMMA perforations	61
4.19	Retention of the droplet inter-spacing	63
4.20	Droplet size distribution	64
4.21	Contact angle setup and measurement on PMMA surface	65
4.22	Variance of water droplet contact angle over time and its average	67
4.23	Contact angle of droplet in microchannel	68
4.24	Measurement of the fluorescence intensity	70
5.1	A photo of the setup from the original work	74
5.2	Published work on pre-concentration	76
5.3	Schematic representation of the EOF	79
5.4	Schematic of an equilibrium gradient	80
5.5	Schematic of FASS	81
5.6	Side view of the microfluidic chip layout	83
5.7	Counteraction of the bulk flow	85
5.8	Structural formula of fluorescamine labelled amino acids	87
5.9	Side view of the two- and three-electrodes microfluidic chip layout	89
5.10	The effect of EOF at the gel-buffer interface	91
5.11	Pre-concentration of bromophenolblue with varying potential	92
5.12	Time against current graph and sequential agarose gel images	93
5.13	Sample migration and stacking of bromophenolblue with varying potential	94
5.14	Ohm's law plot	95
5.15	TRIS-borate ion formation	96
6.1	Sample pre-treatment layer	101
6.2	Two designs for the total fluidic approach	103
A.1	Sample pre-treatment layer	106
A.2	Serpentine channel design on PMMA	107
A.3	Perforations layer made of PMMA	108

A.4	PMMA agarose gel holder	109
B.1	Schematic representation of the electric field	111
B.2	Reaction mechanisms for fluorescamine	113
B.3	Experiments with two electrodes microfluidic chip	114
B.4	Circuit diagram for microfluidic environment	116

List of Tables

2.1	Scaling law of parameters	9
3.1	Material choice for chip fabrication	18
3.2	Etching solutions	23
3.3	Solvents used for glass/glass bonding	24
3.4	Temperature gradient for the bonding programme	25
4.1	Comparison of sample pixelation surfaces	60
4.2	Comparison of aqueous-in-oil and -gas systems	72
5.1	Existing on-line preconcentration techniques	76
5.2	Electrophoretic mobility of amino acids	87

Introduction

1.1 Miniaturisation and Microfluidics

Miniaturisation is an active process to minimise many hands-on equipments including mechanical, optical parts and electronic devices. The trend to understand the processes at molecular and atomic level can be traced back to ancient times both as an abstract science and a physical practice and the use of early microscopes. To the present day, it is the success in miniaturisation that assisted maturation of the current sciences of nanotechnology in molecular biology to electronics. Familiar examples in the day-to-day life are electronic based equipments such as TV plasma screens and digital cameras. Tending toward ever-smaller scale, the number of pixels were increased. A higher resolution to compose clearer and more accurate images with enhanced quality are the ultimate goal of these devices for the end-user satisfaction.

Often associated with miniaturisation is microfluidics that deals with the behaviour, precise control, transport and manipulation of fluids that are geometrically constrained to a small, typically micro-scale volume. Common fluids utilised in microfluidic systems are various buffers and suspension of blood samples, protein and cell. Especially with the rapid advancement in cell biology and pharmaceutical drug discovery, it has found unique applications in molecular and enzymatic analysis (*e.g.*, glucose and lactate assays) [1], protein [2–4] and DNA analysis (*e.g.*, polymerase chain reaction (PCR) and high-throughput sequencing). A commercially available everyday example of microfluidic system is the ink-jet technology, which the effort was first made in the early 1950's [5]. With dynamic evolution of microfluidics, this technology has even been adapted to medicine and biomedical engineering applications, such as drug screening, genomics, biosensors [6–8] and 3D organ printing¹ [9, 10], as the tiny droplet generated are reproducible in size and deposited with $>100 \mu\text{m}$ positional accuracy (Figure 1.1).

¹referred as to tissue engineering that place various cell types into a soft scaffold fabricated by a computer-aided design template

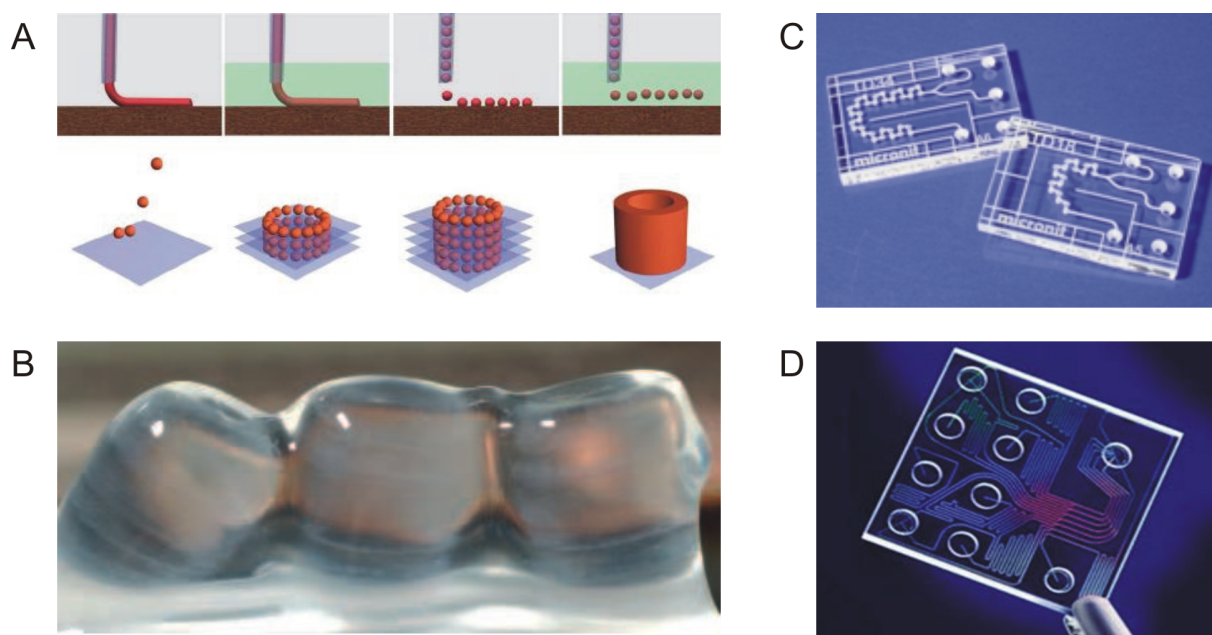


Figure 1.1: Schematic depicting organ printing procedure (A). Constructed layers of tissues using a modified desktop printer (B) (from Boland *et. al.*). Images of commercially available microfluidic chips: Micronit micromixers (C) and Agilent CE-chip (D) (Courtesy of Agilent Technologies, Inc. and Micronit Microfluidics BV.).

Compared to industrial laboratory equipment, microsystems offer reduced reagent consumption, high sample throughput and rapid chemical reactions. The ability to create highly integrated addressable channel networks with various functionalities on stamp-sized devices has pushed unprecedented automation [11–14]. Their reduced size makes them suitable for mobile field laboratories, point of care (POC) testing, while at mass production scale their reduced cost allows them to be disposable after sensitive applications. The design of microfluidic systems often requires unusual geometries and the interplay of multiple physical effects such as pressure gradients and capillarity lead to interesting variants of well-studied fluid dynamical problems and some new fluid responses [15].

1.2 Research Goals

Given an ever-increasing demand to understand heterogeneity in suspended cell populations or tissues [16–18], the analyses of the heterogeneity of biological and biochemical samples can significantly advance the comprehension of cellular processes and responses as well as cell-cell interactions. It provides a significant key towards understanding fundamentals of life building blocks, which is an essential issue in bioanalytical research. The

acquisition of data for biological samples, for instance live cells and in many cases at the single cell or molecule level, often relies on fluorescence imaging techniques [19–21]. The rapid development of new fluorescent probes and advances on microscope systems has led to access to elaborate imaging technology - counting, localising and tracking individual molecules. The challenge currently faced, however, is the inability to specifically identify and to distinguish the diverse properties and characteristics of cellular systems within organs, tissues and membranes. Normally via traditional biochemical assays, cells are analysed in bulk fashion and the plentiful information otherwise attainable at single cell studies are often unfortunately disguised. Although fast techniques such as flow cytometry devices are available for suspended single cell analysis, analytical instrumental techniques are often slow and time-consuming in processing high-throughput data if single cells within a tissue or in cell colonies are addressed. For instance, the current available methods such as laser capture and single cell pipetting are non-automated and non-parallel manual techniques [22]. The singly captured samples are non-invasively handled in series, which are however, labour intensive and tedious processes. Thus to mitigate these problem zones, a practical and a logical approach would be the incorporation of the μ TAS concept that efficiently separate, transport and analyse small amounts of sample in an automated manner.

The μ TAS concept and its ability to provide more precise spatial control over samples and reagents handled, to attune and integrate exactly to the experimental requirements, and to fabricate biocompatible microenvironments, have driven many bioanalytical scientists towards Lab-on-a-Chip (LOC) technology [23, 24]. Analyses of single cells with microfluidics have eminently advanced in the last couple of years [25, 26], and benefits for single cell analysis [27], parallel and automated cell handling and analyses [28] and cell culture have been demonstrated.

It is this unique and practical but sophisticated features of microfluidics that provoked an endeavour to establish a novel concept called “microfluidic imaging”. The research combines two diverse integrable applications of microfluidic techniques, namely, sample droplet based pressure driven (or segmented) flow system and pre-concentration. While these subjects compose distinct studies, the handling of small sample volume is a common theme. The marriage between these subjects is anticipated because although segmented flow systems can produce droplets with minute internal volume that provide a discrete and distinct environment (such as a platform for small scale biochemical reactions), reduced volumes can pose a problem for detection and analysis of dilute analytes. Thus sample pre-concentration serves particular importance in microfluidics.

The research was divided into three stages: (i) pixelation, (ii) pre-concentration, (iii) analysis and image re-assembly. The flow diagram in Figure 1.2 represents the outline and the segmentation of the entire research.

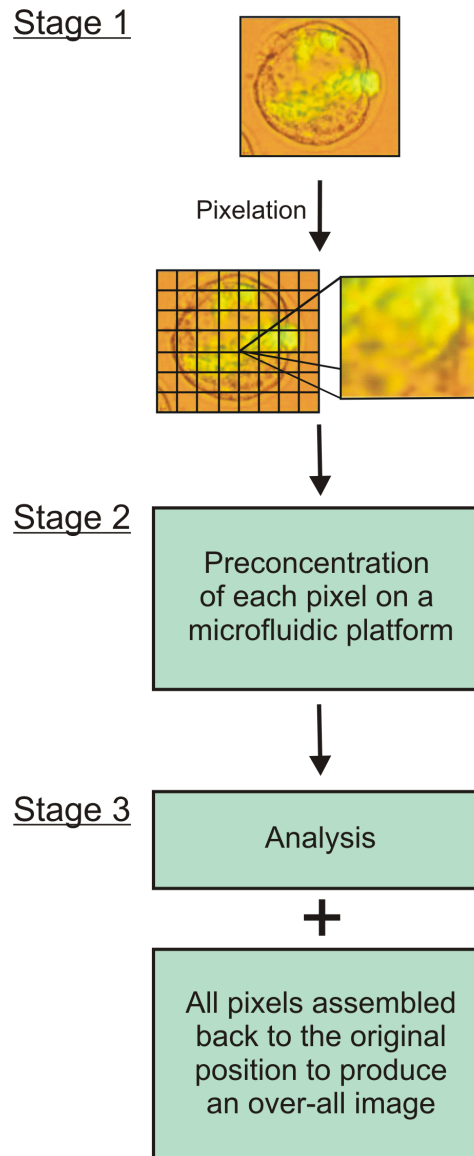


Figure 1.2: A flow chart depicting the research outline of “microfluidic imaging”. Initial step is the pixelation of the sample into addressable units (Stage 1). Second is the pre-concentration of low abundant samples (Stage 2), followed by the analysis and re-assembly of the pixels for generating the final image (Stage 3).

The proposed is a novel concept to image heterogeneous planar samples like tissues and colonies of cells based on a microchip platform. The ultimate purpose is to reduce and automate the labour intensive steps and thus to eventually vastly increase the scope of understanding of stochastic behaviour expected by biosystems at microscale. The device

designed and fabricated has similar functions and operating modes to an electronic charge-coupled device (CCD) chip to compose an image, yet relies on a microfluidic platform. The analogy of parallel to serial pixel readout of an image plane used by a conventional CCD camera is applied to biological samples and heterogeneous constituents (tissues and colonies of cells). It stores the information that can be read out after acquisition of the full image.

Initially, the whole sample is partitioned into addressable units (pixels), which can be analysed individually (Stage 1). Each of these separated volumes represents a μ TAS in its own, and can be processed and analysed along a fluidic network afterwards. The key element of the fabricated device relies on pressure-driven segmented flow to separate the individual sample volumes and store the information of each pixel. The device is capable in handling small sample volumes with a high degree of control over the experimental conditions, providing the ability to manipulate the content of each compartment while avoiding diffusion or coalescence. By basing on the idea of 1ms to 1s data readout rate of a conventional capillary electrophoresis (CE), 1 mega pixela image is produceable in 17 min using the device developed here.

The correspondingly small number of molecules present per droplet, however, would result in a considerable loss of detection sensitivity. For analysis of dilute analytes that are compartmentalised as droplet forms, sample pre-concentration serves particular importance (Stage 2). A pre-concentration method based on the presence of a gel-buffer interface, which generate differing values of electroosmotic flow (EOF) in a microfluidic system, was adapted. When a biased voltage is applied, a mixture of amino acids with different electrophoretic mobilities should give rise to separate signals that focus at different points along their migration path. For sample analysis, the pre-concentration band is separated by reversing the electrical field.

After the sample analysis, the information obtained from each pixel is used to re-assemble an image of the original sample (Stage 3). The data is read out in serial from the samples that were collected in parallel fashion, which is intended to to simplify the requirements of the microchip design, *i.e.*, a planar microchip is suitable for integration of further process steps.

In this research, the first and the third stages were coupled for the investigation of the droplet based microfluidics, while the second stage is a stand alone pre-concentration research. Although each of the aforementioned technologies has its own set of unique potential applications, the aim is to combine these two realms so to help disclose the benefits of microfluidics and to realise the true goal of the μ TAS concept.

1.3 Thesis Outline

This thesis divides the derivation and the application research of microfluidic imaging concept for chemical and biological samples into five chapters.

Chapter 2 gives an overview of the μ TAS concept and examples of fascinating advancements that have been published in the recent years. Some of physical laws relevant in this particular work are also mentioned.

Chapter 3 describes the general fabrication methods and considerations made when fabricating microfluidic chips for materials used, i.e., glass and polymers, throughout this research project. Their properties, fabrication and chip preparative methods are also mentioned in detail.

Chapter 4 introduces pixelation, analysis and re-assembly of planar samples (Stage 1 and 3). A novel concept to spatially resolve the chemical composition of large and complex biological samples by pixelation within an automated droplet based μ TAS platform is described. The device images samples of interest by discretising targeted areas into voxels suspended in a two-phase microflow. These voxels are transferred from parallel to serial mode for data readout in a similar fashion to a CCD camera, thus referred as “microfluidic imaging”. The proof-of-principle experimentations are accomplished with fluorescent dyes and yeast cells.

Chapter 5, which the experiment was carried out before the content of Chapter 4, reflects on the interface pre-concentration method and its design adaptation for analyses of minute volume samples (Stage 2). Glycine was used for testing purposes. At the design level, several chip designs were analysed in order to investigate its suitability for pre-concentrating small sample volumes. Reasons for the results obtained are interpreted and discussed.

This thesis is summarised in Chapter 6, where interpretation of all modules are discussed and recommendations for the future research are proposed.

Micro Total Analysis Systems (μ TAS) Concept

2.1 Overview

In a traditional chemical analysis, all the stages - sampling, sample pre-treatment (dilution, pre-concentration, filtration, etc.), analyte separation and purification, detection and analysis - normally sandwich transfer steps. During the last couple of decades, the demand to invent low-cost instruments capable of rapidly analysing small sample volumes with a high level precision yet with automation has triggered scientists to miniaturise many possible processes. It is this movement that awakened the concept of the micro total analysis system (μ TAS), which especially found its wide use in fluidic systems in the early 1990's [29–31]. It aims to engineer miniature devices to carry out lab-scale analytical sciences for chemical and biological processes. In another words, as the term indicates, the approach is dedicated to significantly downscale all the traditional transfer steps in chemical analyses and integrate them in a compact and efficient manner on one microdevice. Due to this reason, the concept of μ TAS is also commonly referred as “Lab-on-a-Chip” (LOC). A big boost in research and commercial interest came in the mid 1990's, when μ TAS technologies turned out to provide interesting tooling for genomics applications, like capillary electrophoresis and DNA microarrays. The numerous important developments in μ TAS have been covered in several reviews, which may serve as a very helpful introduction for newcomers to the field [23, 32–34].

2.2 Motivation for Miniaturisation

The concept of “scaling laws” with respect to length, surface area and volume give rise to the basic principle for favourable reaction conditions in miniaturisation. In these systems, the parameter of interest can be viewed as a function of the variables to be miniaturised,

space and time. They stay proportional to each other and thus assuming that a miniaturisation is a simple three-dimensional downscaling process characterised by a typical length parameter d , the behaviour of the relevant physical variables can easily be predicted.

Table 2.1 summarises scaling law and the changes in different parameters with respect to characteristic length, d [35]. Taking the typical length d as the scaling factor, “time, t ” remains as a degree of freedom. Two differing situations where time or diffusion are kept constant are considered:

Time-Constant System

In a time-constant system, the time scale is the same for the miniaturised system as for the macroscale system. Relevant time variable such as analysis, transport and response times remain constant. The pressure drop needed to maintain the desired flow rate would remain the same, but parameters of linear flow rate, volumetric flow rate and the Reynolds number would decrease by factors of d , d^3 and d^2 , respectively. In parallel, diffusion would have an increased role in mass flow. This feature becomes particularly important for simple transportation and analytical systems such as flow injection analysis (FIA). However, the biggest advantage of all in downscaling is the decreased carrier and reagent solutions. A 10-fold decrease in d , for example, would cause a 1000-fold decrease.

Diffusion-Controlled System

The importance of diffusion-controlled system is emphasised when molecular diffusion, heat diffusion or flow characteristics govern the separation efficiency in a given system. In such cases, the time scale is treated as a surface, which is proportional to d^2 . Hydrodynamic diffusion, heat diffusion and molecular diffusion effects in the miniaturised system behave in exactly the same manner as in the macroscale system, leaving all dimensionless parameters constant regardless of the size. This means decreasing the diameter of a tube to 1/10 would reduce related time variables, *e.g.*, analysis time and response time, to 1/100 of their original magnitudes. The pressure requirements increase by a factor of 100, but the voltage requirements (for electrophoresis/electroosmosis) remain constant. In such miniaturised systems, faster separations can be achieved while maintaining comparable separation efficiency.

From the above statements, it is apparent that the surface-to-volume ratio is higher in miniaturised systems. Under this condition, reduced heat production and faster heat dissipation are observed that would, for instance, be beneficial to electrophoresis, where the use of higher electric field strengths are permitted. Electroosmotic propulsion can, therefore, aid the demands of separation systems better than a pressure-driven flow, given that aqueous electrolyte solutions are the subject of analysis. In a similar manner, diffusion

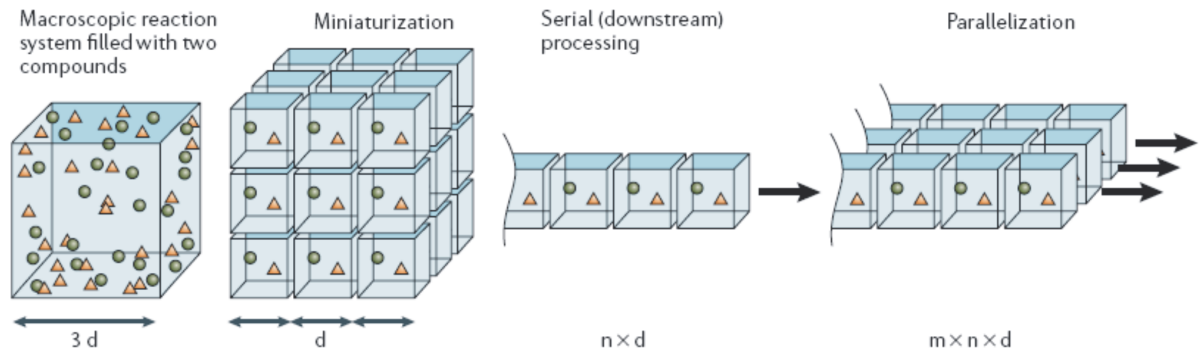
Table 2.1: Scaling law for some mechanical parameters (top) and variance in diffusion time- and information density (middle) with respect to characteristic length d . The flow chart illustrates various advantages gained by the miniaturisation of a system [24] (bottom).

Parameter	Time-constant system	Diffusion-controlled system
Space, x	d	d
Time, t	constant	d^2
Linear flow rate, u	d	$1/d$
Volume flow rate, F	d^3	d
Pressure drop (laminar flow), Δu	constant	$1/d^2$
Voltage (electroosmotic flow), ΔU	d^2	constant
Electric field, U/L	d	$1/d$
Reynolds number, Re	d^2	constant

Parameter	Unit	Length, d		
Length	d	1 mm	100 μm	10 μm
Surface	d^2	1 mm^2	0.01 mm^2	100 μm^2
Volume	d^3	1 μL	1 nL	1 pL
No. of molecules at 1 μM		6×10^{11}	6×10^8	6×10^5
Diffusion time	$t_d = Dd^2$	17 min	10 s	100 ms
No. of volumes	volumes/ cm^2	$5 \times 5 = 25$	$50 \times 50 = 2,500$	$500 \times 500 = 250,000$

Diffusion coefficient $D = 10^{-9} \text{m}^2 \text{s}^{-1}$.

d , length of edge; n and m , numbers of reaction systems serial and parallel, respectively.



time of molecules is increased because the time taken to travel distance d is decreased to $1/d^2$. In a reaction where two molecules meet by Brownian motion that depends solely on the diffusion coefficient, shorter diffusion times mean faster mixing. As can be seen, reaction parameters are dependent on the size of the system, thus, experimental conditions such as compound concentration, temperature, electric field can be adjusted beforehand accordingly.

The relationship between the signal output and the size of a detection system also cannot be neglected. For fluorescence detector, signal is proportional to d^3 . In miniaturised system, fluorophores can be excited and detected selectively. The reduced detection volume enhances the sensitivity of fluorescence spectroscopy, because the background signal generated by impurities of the sample decreases proportional to the volume. High signal-to-noise ratio is obtainable as the fluorescence signal of a single molecule is independent of the dimensions of the detection volume.

Perhaps the most important feature of miniaturisation is its possibility for parallel or sequential processing, which is the underlying principle of the “microfluidic imaging” concept. Because of the small reaction volumes, microfluidic devices are the ideal platform to analyse micro- and nano-scale objects in a high-throughput, highly parallel fashion and are easily automated. With a length of $10\mu\text{m}$, 250,000 devices can be arranged per cm^2 . Moreover, shorter diffusion times increase the exchange of molecular information on the device, thus, the rate of information generation.

2.3 μ TAS: Latest Advancements and Trends

During the last several of years, a steady expansion in the number of publications associated with this research field was witnessed. Simultaneously, there was an obvious increase in the overall quality of the study performances, as numerous arduous obstacles have been overcome and microfluidic devices are, nowadays, considered as a common aid to various applications in natural and life sciences. Many examples of integrated, all-in-one microfluidic chips capable of separation, reaction, and detection have also been observed, all of which realise the principal of μ TAS or LOC. These integrated chips actively adopt the scaling law concepts, while utilising the highly developed fabrication techniques. Their aim is to multi-functionalise and fully automate devices that are believed to assist the future advancements of point-of-care (POC) testing, clinical and medical diagnostics. Herein, some selected examples for every distinct method or device are presented to give a perspective of the recent developments in μ TAS, especially those related to the theme

presented in the research work. However, works on droplet handling and pre-concentration will be referred later in the relevant chapters. For ease of understanding, the categories are divided into “analytical standard operations” and “applications” of the miniaturised systems.

Analytical Standard Operations

Sample Preparation

An online desalting of macromolecule solutions within tens of milliseconds by utilising a two-layered laminar flow geometry that exploits the differential diffusion of macromolecular analytes and low molecular weight contaminants was studied by Wilson and Konermann [36]. A microchip for liquid-liquid extraction was presented by Chen *et al.* Organic solvent droplets were trapped in recesses fabricated in the channel walls. By delivering an aqueous solution containing analytes (here *e.g.*, butyl rhodamine B), the analytes were enriched within the organic solvent droplets with high pre-concentration factors [37].

Fluid and Particle Handling

Takeuchi *et al.* generated nylon coated water droplets in an axisymmetric flow focusing device. They formed droplets of a diamine/water solution in a hexadecane carrier, which were directed into a solution of acid chloride in hexadecane which initiated a polymerisation [38]. Particle filtration and concentration using dielectrophoretic manipulation was presented by Barrett *et al.* Due to ridge-like structures that were fabricated in insulating material, a nonuniform electric field was formed near the ridges when a DC field was applied along the channel, which affected particle motion parallel to the ridges [39].

Gerdtts *et al.* described a microfluidic systems for protein crystallisation [40]. The two general stages of protein crystallisation - crystal nucleation and crystal growth - normally have differing optimal conditions. In an ideal case, the protein forms crystal nuclei at a supersaturation, where ordered growth is possible. For some proteins, however, a supersaturation gap exists, where there is no overlap between nucleation and growth conditions. Thus, by controlling the flow rates and channel length used for the nucleation stage (stage 1) (Figure 2.1A), time control of seconds, minutes, hours, or even days is achievable. Nucleation conditions are combined with growth conditions, at the growth stage (stage 2) to low supersaturation under time control. The model proteins thaumain, SARS protein and oligoendopeptidase were used to test the standard and single crystal formation, displaying the practical use of time-controlled microfluidic seeding.

Detection

An effective observation volume that is approx. 100 times smaller than the observation volume using conventional confocal optics was realised by Foquet *et al.* To achieve this,

microfluidic channels with submicrometer size were fabricated. Single fluorescent analytes were detected and the flow velocity was characterised by fluorescence correlation spectroscopy [41]. Bowden *et al.* used a fiberoptic microarray consisting of 49,777 individually addressable light pathways that was implemented on a microfluidic platform to study DNA hybridisation [42].

Applications

Cell handling and Analysis

To analyse the content of single cells, Wu *et al.* developed a new kind of three-state valve that allows for liquid metering and flow control. A reaction volume of approx. 70 pL is achieved for chemical lysis and derivatisation of the contents of single Jurkat T cells. Separation by electrophoresis and detection by laser-induced fluorescence was additionally performed on the same chip [43]. Ling *et al.* described the simultaneous determination of reactive oxygen species and reduced glutathione in individual erythrocyte cells by conducting all necessary steps (single-cell loading, electrical lysis and capillary electrophoresis) on a microchip [44]. Dynamic gene expression profiling was demonstrated in a gradient producing device by Thompson *et al.* In these experiments, reporter cells (HeLa S3 cells) were stimulated, each containing a green fluorescence reporter plasmid for the gene of interest (here NF- κ B) [45]. The cells were exposed to varying doses of the inflammatory cytokine TNF- α and cellular response (i.e. fluorescence intensity) was continuously monitored. Such devices were also used to study cell behavior in dependence of the mechanical compliance of the substrates.

DNA Analysis and PCR

Upon genome and proteome analysis, quantification of DNA and mRNA from a single cell is an indispensable method in order to grasp accurate cell conditions and responses. For micro- and nano- litre samples, however, problems such as non-specific adhesion to the reaction vessels, degradation due to RNase or damage and incomplete reverse transcription are often encountered [46–48]. Marcus *et al.* have presented an integrated microchip that implement cell capture, cell lysis, mRNA isolation and cDNA synthesis, which allows quantitative measurement of mRNA from a single cell at pico and sub-picogram levels [49].

With respect to PCR, a microfluidic genetic analysis system integrating solid-phase extraction (SPE), static type PCR chamber, and capillary electrophoresis was described by Easley *et al.* (Figure 2.1B) [50]. For clinical diagnostics and forensic genetic profiling, extraction of *Bacillus anthracis* from only a volume of 750 nL of whole blood from mice was achieved, completing the entire process analysis within 24 min.

Comparably, Liu and co-workers developed a portable PCR for (forensic) on-site analysis [51]. The instrument comprises static type PCR and CE and, contains a diode laser as an optical system for detection to accomplish an authentically miniaturised device design. The dimension of the portable device is only $12 \times 10 \times 4$ inches and 10 kg in weight (Figure 2.1C). The capability of the system was tested by the analysis of Y-chromosome STR (short tandem repeat) typing and 20 copies of male standard DNA was successfully extracted.

Immunoassay

A “POCKET (*portable and cost-effective*)” immunoassay for enzyme-linked immunosorbent assays (ELISA) was presented by Sia *et al.* [52]. Reduction of silver ions to silver atoms based on immunochromatographic assay and gold-labelled antibodies was carried out, which was then detected by an InGaAlP red semiconductor laser diode. The developed immunoassay in a microfluidic format was able to quantify anti-HIV-1 antibodies in the sera of HIV-1-infected patients with comparative results to the conventional 96-well microplate, demonstrating its reliability. Incubation times required were 10min, which is a 6- to 18-fold reduction, compared to that in the microwells.

Herr and co-workers presented a microchip electrophoretic immunoassay (μ CEI) to allow direct, automated measurement of the total salivary matrix metalloproteinase-8 (MMP-8) content for use at the clinical point-of-care (POC) [53]. Three specific functional regions with different concentrations of polyacrylamide gel was fabricated in the microfluidic channel by multistep photopolymerisation process. The microchip comprises integrating sample pre-treatment for filtering, enrichment, and mixing, as well as immunoreaction and CE separation compartments (Figure 2.1D). Using 20 μ L of saliva, MMP-8 could be measured in less than 10 min.

Chemical and Enzymatic Reaction

Kobayashi and co-workers devised an efficient gas-liquid-solid tri-phase reactions using a microchannel reactor, a reaction normally considered to be very inefficient [54]. High interfacial area per unit of volume of the microchannel was facilitated by the immobilised active Pd catalyst and hydrogenation reaction was carried out. The flow rate balance between H_2 and solution of a substrate was controlled carefully to obtain the most efficient environment for hydrogenation. The mean residence time of the starting materials was found to be only 2 min. This approach could be applied also to O_2 , CO, CO_2 and other gas-phase molecules.

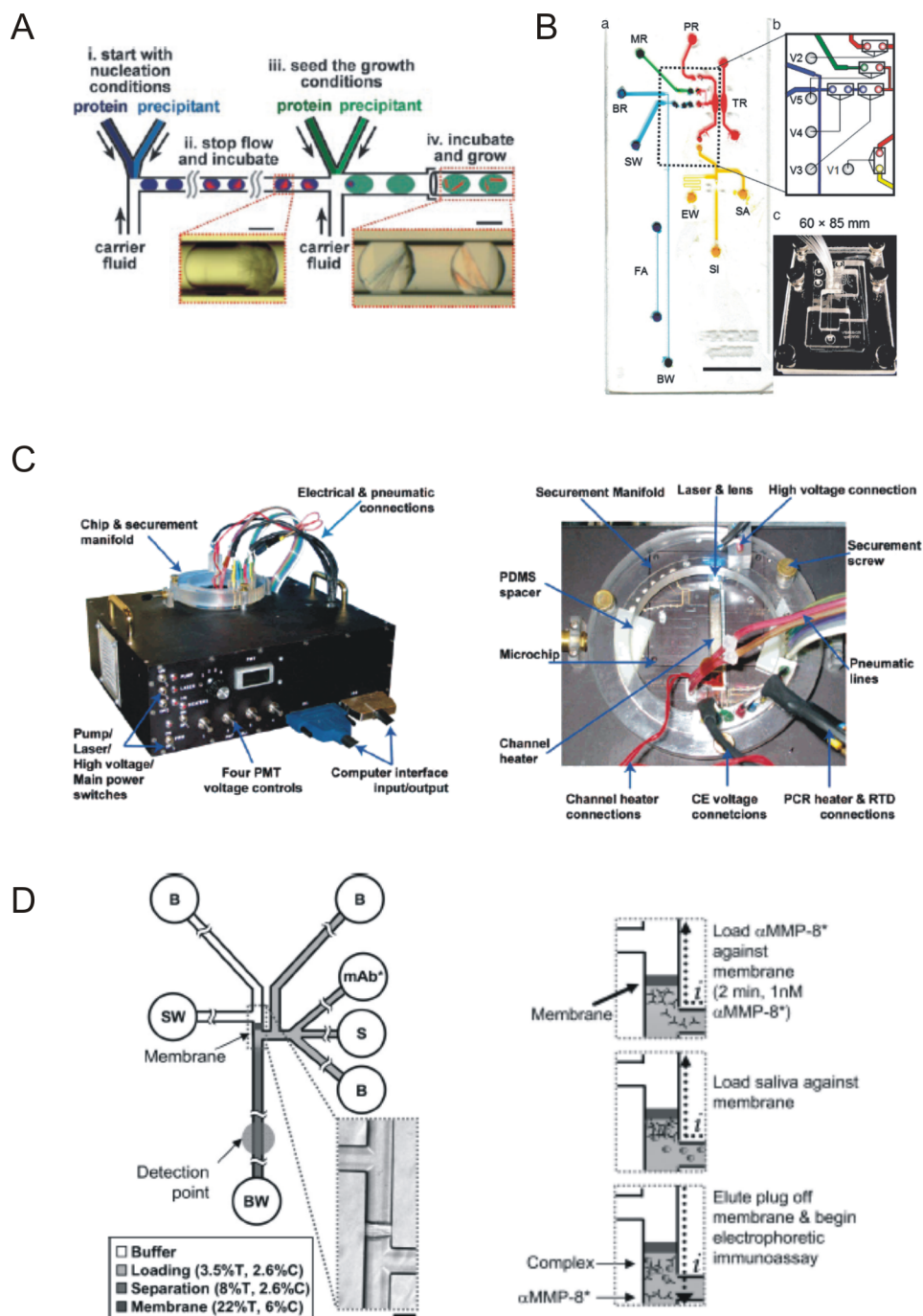


Figure 2.1: Scheme for separating the stages of nucleation and growth in the protein crystallisation (A). Images of the microfluidic genetic analysis (MGA) device with exploded scheme of flow control region (B). Photograph of the portable PCR-CE system (left) and close-up of the microchip and the manifold (right) (C). Schematic illustration of μ CEI device layout (left) and its operation sequence (right) (D).

2.4 Summary

In this chapter, recent advancements in applications of microfluidic systems in chemistry and biochemistry were exploited. In the field of μ TAS, especially at its beginning, the focus was set to develop a thorough understanding in the fundamentals of fluidic control and separation sciences. However, more recently, developments of POC instruments for PCR and immunoassay and their fully integrated portable systems are in demand particularly in the medical sectors [13] and other fieldworks. Nevertheless, the result of miniaturisation and its influence on integrated circuit (IC) chip in semiconductor and computer science industries is evident. Daily encounter with portable cash or credit cards is one of the outcomes of this innovation. Similarly, in the case of incorporated IC chip in laptops and PCs, safety and convenience aspect of the devices have immensely been amplified, enhancing the quality of life served to us directly and indirectly. Despite these efforts, many works still depend on optical analysis systems or electrical power supply systems, making these devices still large and bulky, and inhibiting their use from real practical applications. One of the criteria to be fulfilled to achieve this is to possess the ability for multitudinous interface - a real ubiquitous instrument that is available not only for scientists but also for the public that are especially easy to handle. Hence, the hope is to envision the further realisation of microfluidic applications in the life sciences that contribute to daily lives, health, and society on the whole, in the next the nearing decades.

Fabrication of Microfluidic Chips

3.1 Producing Microstructured channels

Historically, the development of chips is a consequence of the success on microelectronics, which led to a wide range of microfabrication techniques for silicon. In 1979, Terry *et al.* presented a miniaturised gas chromatographic air analyser that was fabricated on a silicon wafer [55]. Currently, there exists various methods for fabricating microfluidic chips. However, a careful attention should be paid to the material and design aspect, with respect to the chosen techniques or vice versa. In this section, those which particularly were used in this research work are discussed. Once the specifications of the chip are firmly established, there are considerations to be made on:

- (1) The choice of materials,
- (2) The design of the masks and the channels, and
- (3) The choice of lithographic techniques.



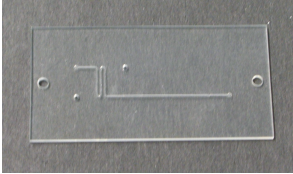

3.1.1 Choice of Materials

The choice of material for microfluidic chips depends on the physical and chemical properties of and the compatibility with the analytes of interest. Some of these aspects are:

- mechanical and chemical stability towards acids, organic solvents and reagents,
- optical transparency,
- design suitability to the rest of the experimental setup, and
- economical factors, *i.e.*, availability, reusability and cost of production.

There are two main types of materials used for fabricating microfluidic chips, namely glass and polymers (Table 3.1).

Table 3.1: Different types of materials used for fabricating microfluidic chips within this research project. CNC stands for Computer numerical control.

Material	Sample Image	Fabrication Technique
Glass		Isotropic etching (HF)
PDMS		Cast from a master
PMMA		Drilling (CNC machining)
Metal		Filing (CNC machining)

Glass

Glass is one of the most commonly used materials for device fabrication for μ TAS. Its advantages are its high mechanical and chemical stability, ability for surface modification to make it biocompatible, non-flexible nature making them easy to adapt to tubing and connection systems. For these reasons, many different techniques for manipulating glass and glass-compatible materials have been developed. Its fabrication, however, requires a cleanroom and is time-consuming, thus considered a more costly technique.

Polymer

In some situations, polymers are better suited for fabricating μ TAS than glass. Many types of polymers show good resistance to chemical treatment and are often biocompatible. Furthermore, polymer microstructures can be mass produced at significantly lower costs than glass microstructures. It is often possible to find a polymer that has the optical qualities desired for a given application.

a) Poly(dimethyl)siloxane (PDMS)

PDMS are elastomer and transparent in the UV region of the electromagnetic spectrum. They form hermetic, reversible seals to smooth surfaces *i.e.*, glass and silicon by adhesion.

It adheres very well to another sheet of the same material by cohesion. The temporary seal of PDMS can be made permanent by chemical treatments such as plasma activation (see Section 3.3.2).

b) Poly(methyl) methacrylate (PMMA) Thermoplastic polymers are transparent in the visible region. Two major ways of machining polymers are replication from a master and direct machining. The latter is used for the experiments in this project (see Section 4.1.2), which removes small amounts of polymer in places where microstructures should be located.

3.1.2 Mask Design

To make photolithographic masks, a mask design is created using computer-aided design (CAD) software. The mask design should fit the chosen mask production process. For example, for a lithographic process, attention to the balance between large and small features should be paid, as by the time large features developed, small features maybe over developed. When designing channels, taking PDMS as an example, the aspect ratio of the channel design needs to be taken into consideration. An aspect ratio of 1:10 is workable, but anything exceeding 1:20 usually results in collapse with PDMS, unless there are pillars to hold the channel up.

3.1.3 Lithography Techniques

Lithography is a printing method for producing an image using chemical processes. Such techniques are capable of structuring material on a fine scale.

Photolithography

A film of photoresist is applied to the substrate and the photoresist is exposed to light through a photolithographic mask. After exposure, the photoresist is developed, which transfers the desired pattern to the photoresist (Figure 3.1). The substrate is subjected to a chemical treatment only in places where no photoresist protects the surface, thus the pattern on the mask is transferred to the substrate. The photoresist is removed by dissolution of the photoresist.

Soft lithography

This technique refers to a set of methods for fabricating or replicating structures using “elastomeric stamps, molds, and conformable photomasks”. The term “soft” derives from

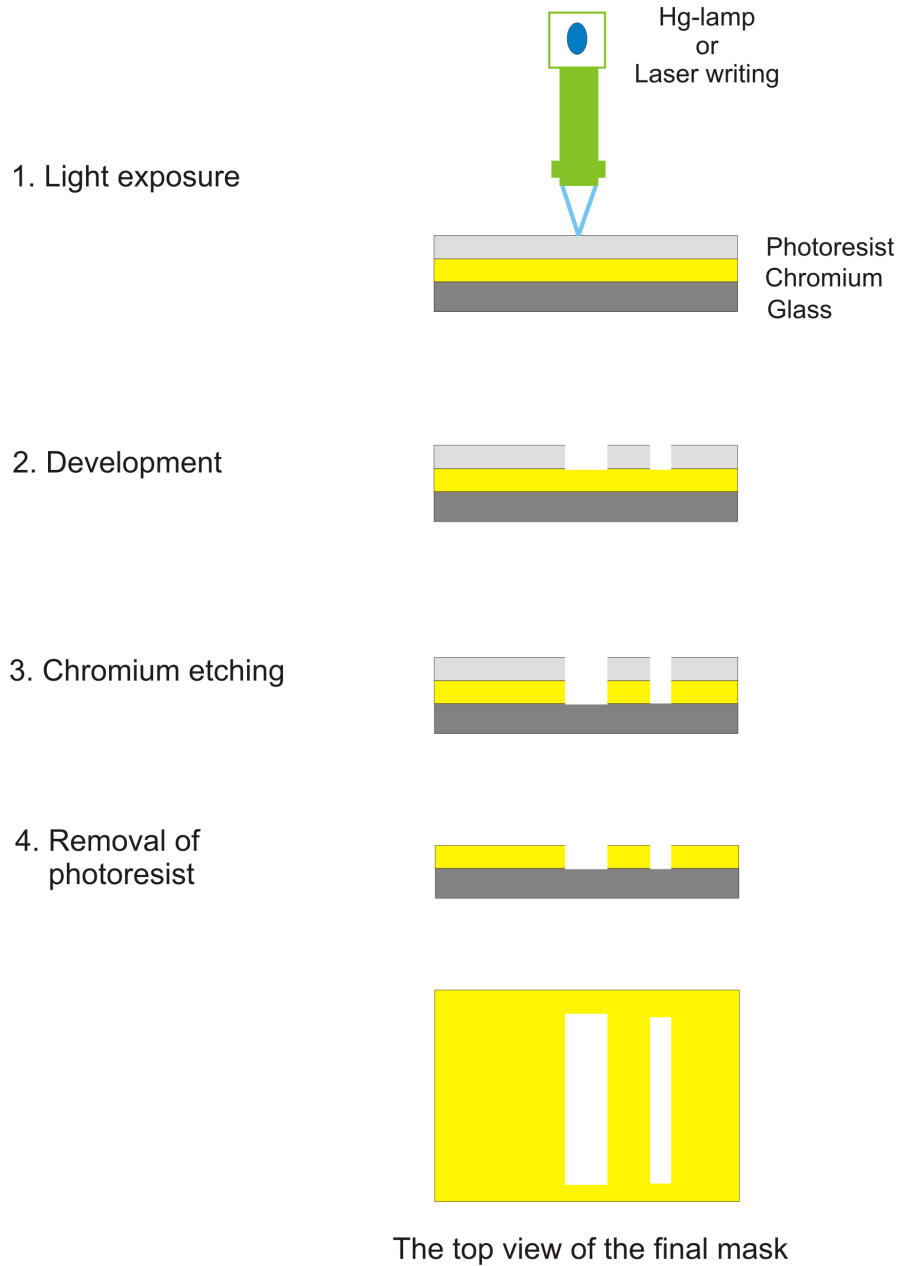


Figure 3.1: Schematic illustration of a photolithography mask fabrication.

its use of elastomeric materials most notably PDMS. Soft lithography is generally used to construct features measured up to the nanometer scale.

Using different combinations of the above described materials, various types of chips can be fabricated, depending on the experimental conditions and setup, as well as by taking material compatibility with analytes of interest into account. The following section introduces the repeatedly used chip preparation methods throughout this work. Various materials and methods commonly used in chip fabrication techniques are described in detail. Other sections of this thesis will refer to the methods explained here.

3.2 Glass/Glass Chip Fabrication

The chips for pre-concentration experiments were made from commercially available soda lime glass substrates, obtained from Nanofilm (Westlake Village, CA, USA, 3" × 3" (76.2 mm) wide and 0.6" (1.5 mm) thick). It is precoated with a 530 nm thick layer of positive photoresist (AZ 1518) on top of a 100 nm chromium layer. The fabrication process consisted of three main steps: i) exposure with UV light and subsequent development, ii) isotropic etching using diluted hydrofluoric acid (HF), and iii) thermal bonding. The process is illustrated in Figure 3.2. Channel designs were drawn using AutoCAD 2004, (Autodesk Inc., San Rafael, CA, USA).

3.2.1 Exposure using Direct Write Laser (DWL)

A direct write laser (DWL) lithography system (Heidelberg Instruments, Heidelberg, Germany), employing a blue HeCd-laser ($\lambda = 442$ nm) was used to transfer the design onto the photoresist. The exposed substrate was developed for approximately 60 s using a standard developer solution, which consisted of a 1:5 dilution of Microposit 351 Developer (Shipley Europe Ltd., Coventry, UK) in ultra pure water. After rinsing with ultra pure water and drying with compressed nitrogen, a chromium etching solution (Lodyne, Microchem Systems Ltd., Coventry, UK) was utilised to remove the chrome layer where the photoresist had been developed. Whilst the substrate was immersed in the solution, the container was gently shaken to facilitate the process. Once the chromium had been completely removed, the substrate was rinsed once more with ultra pure water and dried. On completion, the structures were checked visually for imperfections under a microscope. The chip could now be used as a mask for replication using a UV lamp or etched directly with HF.

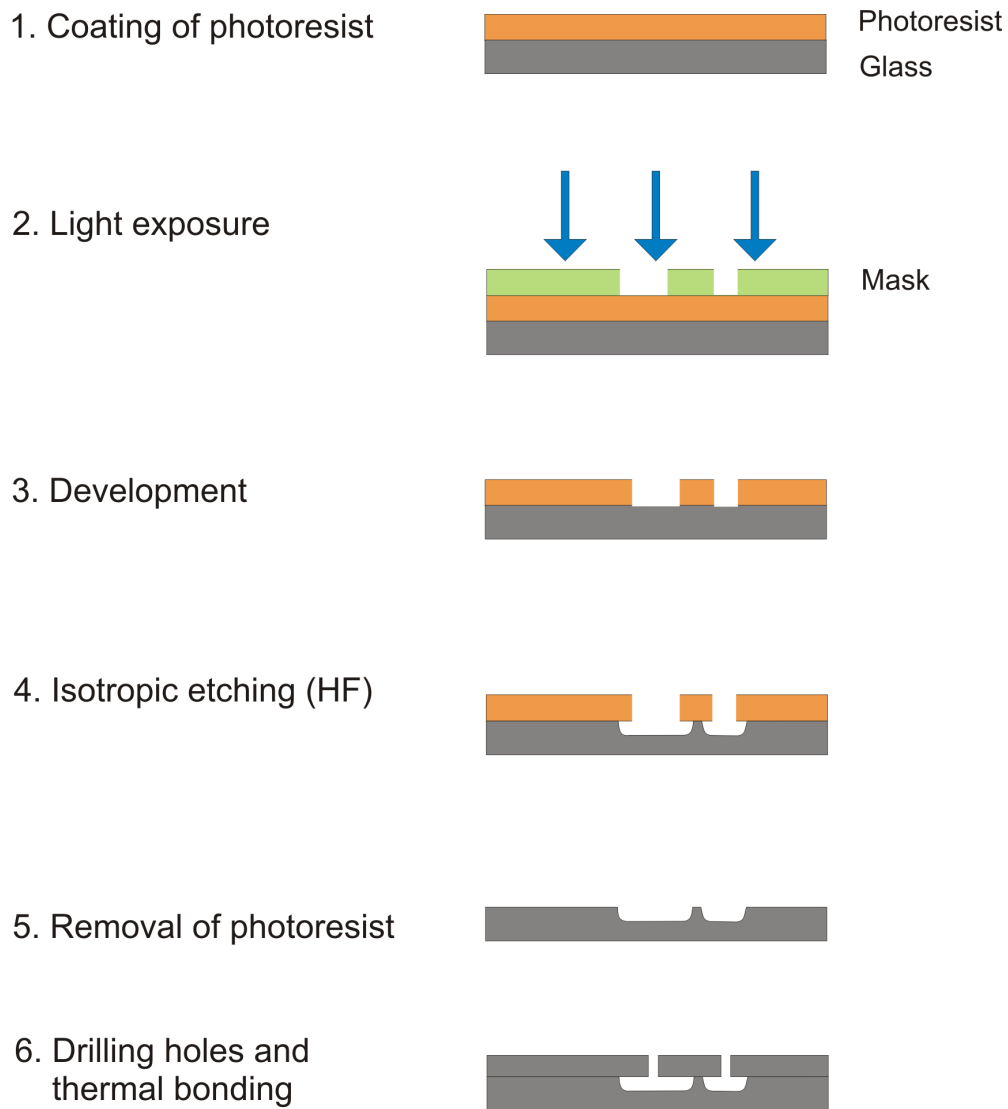


Figure 3.2: Schematic illustration of a glass/glass chip fabrication. Commercially available glass substrates were coated with a photoresist layer (1). A mask is overlaid and was exposed to UV-light (2), resulting in a developed photoresist, exposing the areas of the glass to be etched (3). Isotropic etch of the glass employing a diluted solution of HF was carried out (4). After removal of photoresist (5), the chip fabrication was completed by drilling of access holes and thermal bonding at 581°C (6).

It was considered very useful to keep important original designs as a mask on a separate wafer. For this purpose, it was necessary to produce a duplicate of the original with a second substrate. The production of replica of the substrate was achieved by utilising a flat, closable UV lamp (UV exposure unit, RS, Corby, UK). The original was flushed against a blank substrate in such a manner to prevent any light scattering that would have led to creating blurred edges. On closing the lamp, UV light was exposed through the original onto a blank substrate for 45 s to yield a mirrored structure. The substrate was developed as previously described and then kept in a light-tight box for storage.

3.2.2 Design Etching using Hydrofluoric Acid (HF)

The non-removed chromium and photoresist layer from the DWL step acted as a mask for the etching process. The substrate was isotropically etched by a diluted solution of HF consisting of the following solution ratio (Table 3.2).

Table 3.2: Etching solutions.

Solution	HF	NH ₄ F	HCl _{conc}	H ₂ O
10% for faster etching (%)	1.25	8.75	20	70
5% for slow etching (%)	0.625	4.375	10	85

As the etch rate of HF depends on its concentration and the solution could be reused until the rate deteriorates, the rate was recorded after each use so that the etched depths could be anticipated accordingly. Upon acquiring the desired channel depth, the remaining photoresist and chromium were removed with DMF and chromium etching solution, respectively, to obtain a clear glass wafer with etched channels.

Isotropic etching produces features in the wafer, which are narrower than those etched in the photoresist/chromium layer, *i.e.*, the photoresist/chromium layer is undercut by the etchant. The degree of undercutting (U) is equal to the depth of the feature (D), hence, to produce a channel structure of width W_{chip} in the wafer, the width W_{CAD} in the initial AutoCAD drawing must be $W_{CAD} = W_{chip} - 2D$ (Figure 3.3).

3.2.3 Preparative Steps before Bonding

Drilling of access holes

To avoid introducing small drilled glass debris into the channels, the drilling step of access

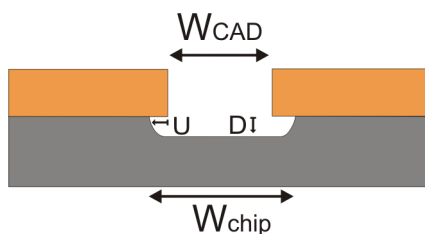


Figure 3.3: Schematic illustration of under-etching in a glass master. U = degree of under-cutting, D = depth. The result of isotropic etching is $U = D$.

holes was performed prior to the bonding step. A miniature, high precision drill and drill press (Micro Miller MF 70, Proxxon, Germany) were used to drill the access holes for in- and outlet reservoirs. Tungsten coated grinding bit (Proxxon, Germany) with diameter of 1.0 mm was employed to drill the reservoirs. The glass plate was laid onto another glass that acted as a support and shock absorber against the pressure and the vibration of the drill. During the milling process, the setup was facilitated with water bath as cooling system to avoid overheating of the drill heads and breaking of the glass wafer.

Sawing

As more than one AutoCAD chip designs were drawn on a 3" \times 3" wafer, it was necessary to cut the glass plates into appropriate sizes. This was carried out with a water cooled, circular diamond saw. The plate had to be pushed gently at a slow constant speed against the rotating blade to prevent breaking of the glass. Afterward, the edges were smoothed with a rotating grinder.

3.2.4 Bonding

To clean and hydrophilise the glass surfaces to facilitate the bonding process, the substrates - one plate with the channel design and the other without, for the countering part to produce an enclosed chip - were treated with different solutions (Table 3.3). After each step, they were rinsed with distilled water and dried with nitrogen.

Table 3.3: Solutions used for glass/glass bonding.

Solution	Acetone	DMF	Methanol	Conc. H ₂ SO ₄
Time (min)	5	5	30 - 60	Overnight

The prepared glass plates were aligned under the microscope and a small drop of ultra pure water was placed between the two plates to increase adhesion through surface tension. The

substrates were placed in between two clean flat ceramic plates, which acted as weights to sustain the flatness of the upper and lower surfaces of the glass chip. This sandwich was then placed in the bonding oven (Model K114, Heraeus, Hanau, Germany). Steel plates were evenly arranged over the upper ceramic plate as weights to maintain the contact between the glass plates, during the bonding process. A pre-defined temperature gradient programme was carried out (Table 3.4 and Figure 3.4).

Table 3.4: Pre-defined temperature gradient for the glass chip bonding.

Duration (h)	ΔT	Temperature ($^{\circ}\text{C}$)
0	\longleftrightarrow	25
1	\uparrow	400
3	\rightarrow	400
1	\uparrow	581
4	\rightarrow	581
2	\downarrow	400
3	\rightarrow	400
6	\downarrow	25
20	in total	-

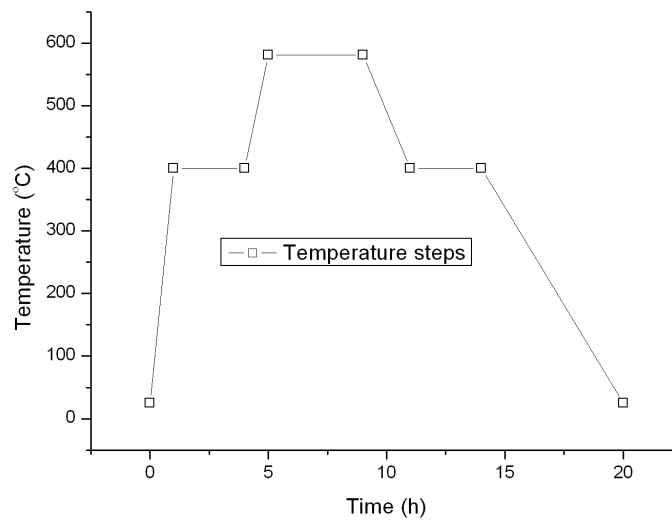


Figure 3.4: Graph of pre-defined temperature gradient for the glass chip bonding (400 $^{\circ}\text{C}$ - glass transition temperature, 581 $^{\circ}\text{C}$ - softening point)

At 400°C, the glass transition point, the morphology of the glass became less crystalline, at which point internal stresses that are present were alleviated. The actual bonding took place over the 4 h period at 581°C, the softening point of glass, where the layers were fused together. The cooling stage with a slow temperature decrease via the glass transition point allowed the crystal structure to equilibrate and removed any existing stresses that might have led to cracking during the process.

On completion of all the above stages, the chip was checked for the presence of Newton's rings between the glass layers, which is an indication for existence of non-bonded areas. This usually means that the bonding process would have to be repeated, if the rings affected any of the functioning areas of the chip.

3.3 PDMS/Glass Chip Fabrication

The disposable and easy-to-make PDMS/glass chips were fabricated by the bondage between plastic formed PDMS (Sylgard 184, Dow Corning), and a standard microscopic cover glass either of size 60×24 mm or 40×24 mm (Menzel-Gläser, Germany). Prior to the bondage, PDMS structures were cast over a master with the channel designs drawn using AutoCAD. The actual fabrication process consisted of three main steps: i) formation of PDMS via mixing of pre-polymer with the curing agent, ii) casting of the PDMS over NiV₇ wafer, followed by iii) plasma bonding. The entire process involved is illustrated in Figure 3.5.

3.3.1 Formation and Casting of PDMS

PDMS, with the chemical formula $(\text{H}_3\text{C})_3[(\text{Si}(\text{CH}_3)_2\text{O}]_n\text{Si}(\text{CH}_3)_3$, where n is the number of repeating monomer $[\text{SiO}(\text{CH}_3)_2]$ units, belongs to a family of siloxane. In the purchased PDMS kit is a mixture of siloxane oligomers that has vinyl groups, and the cross-linking oligomers containing at least 3 silicon hydride bonds each. Typically, this pre-polymer is mixed with the curing agent, containing a proprietary Pt-based catalyst that promotes an organo-metallic cross-linking reaction. It catalyses the addition of the SiH bond across the vinyl groups, forming Si-CH₂-CH₂-Si linkages. The multiple reaction sites on both the base and cross-linking oligomers allow for 3D cross-linking. One advantage of this type of addition reaction is that no waste products such as water are generated (Figure 3.6).

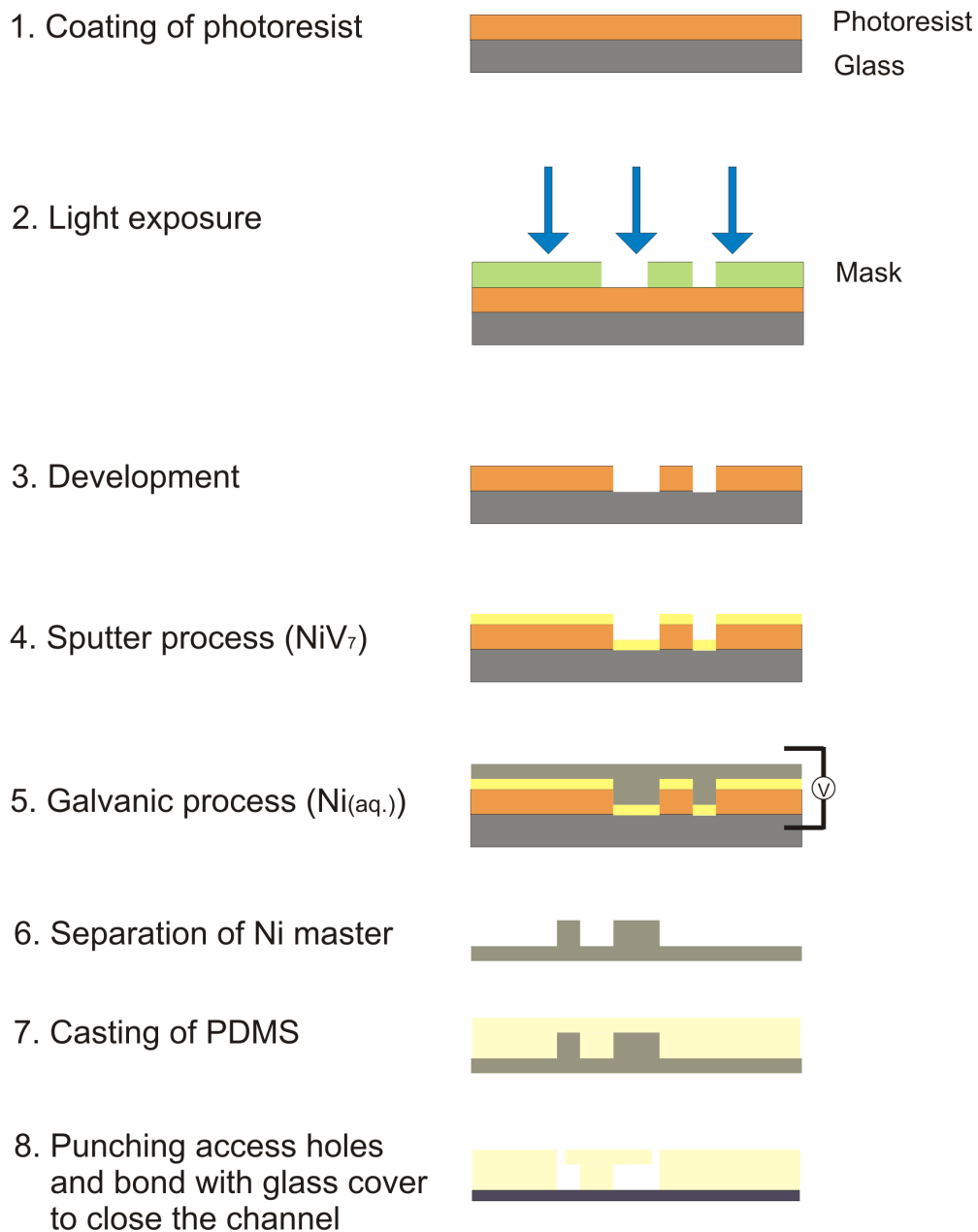


Figure 3.5: Schematic illustration of a PDMS/glass fabrication procedure. Commercially available glass substrates were coated with a photoresist layer (1). Mask is overlaid and was exposed to UV-light (2), resulting in a developed photoresist, exposing the areas of the glass to be coated (3). Sputtering of NiV_7 over the resist (4), followed by application of aq. Ni galvanic process (5). On the separated Ni master (6), PDMS was cast (7). After the removal of the PDMS structure, holes were punched in appropriate places and it was bonded to a cover glass (8).

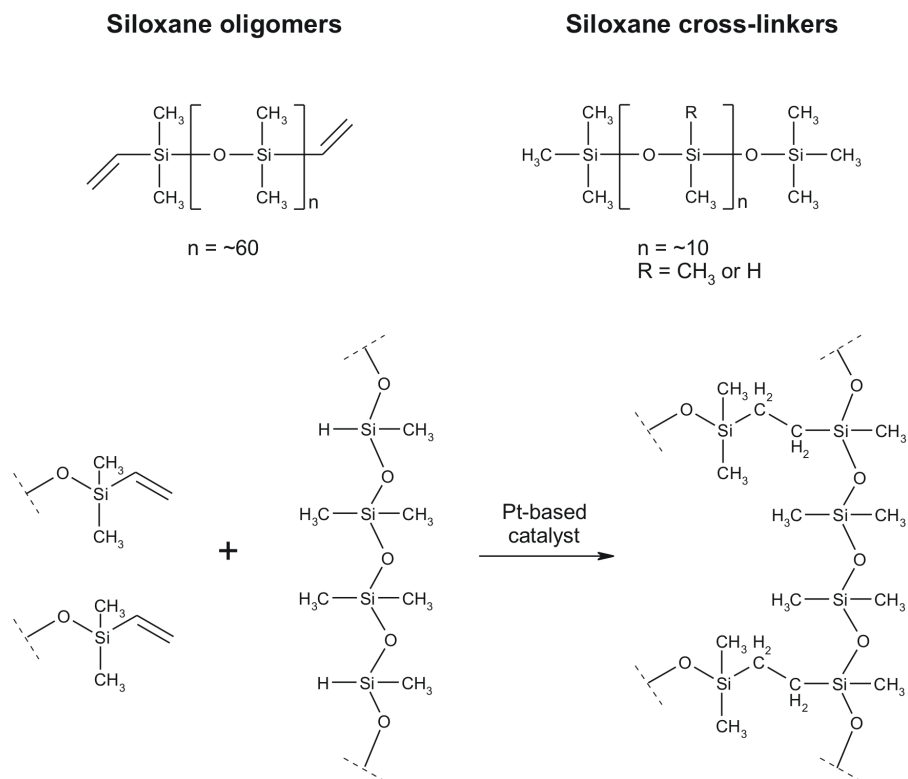


Figure 3.6: The reaction mechanism for PDMS formation.

In brief, the pre-polymer and the curing agent are mixed in the ratio of 10:1 (or accordingly to the experiments). The mixture is degassed in the desiccator for approximately 30 min. to remove any air bubbles. Once removed, it is poured over the mask with features that is gently pre-heated on the hot plate that accelates the corss-linking reaction. The low energy viscous fluid of siloxane covered the pattern of relieves on the surface of the mask, thus forming a precise replica of the surface. By adjusting the ratio, the hardness of the product can be controlled, *i.e.*, more curing agent, the harder the polymer.

3.3.2 Plasma Bonding

After polymerisation and cross-linking, solid PDMS will present an external hydrophobic surface. This surface chemistry usually makes it difficult for polar solvents to wet the PDMS surface, and may lead to adsorption of hydrophobic contaminants. For the two surfaces of PDMS and glass to permanently bond, O_2 plasma treatment is used to alter the surfaces, adding silanol (SiOH) groups to the surface. This treatment renders the PDMS surface hydrophilic, allowing water to wet (this is frequently required for, e.g. water-based microfluidics). The oxidised surface resists adsorption of hydrophobic and

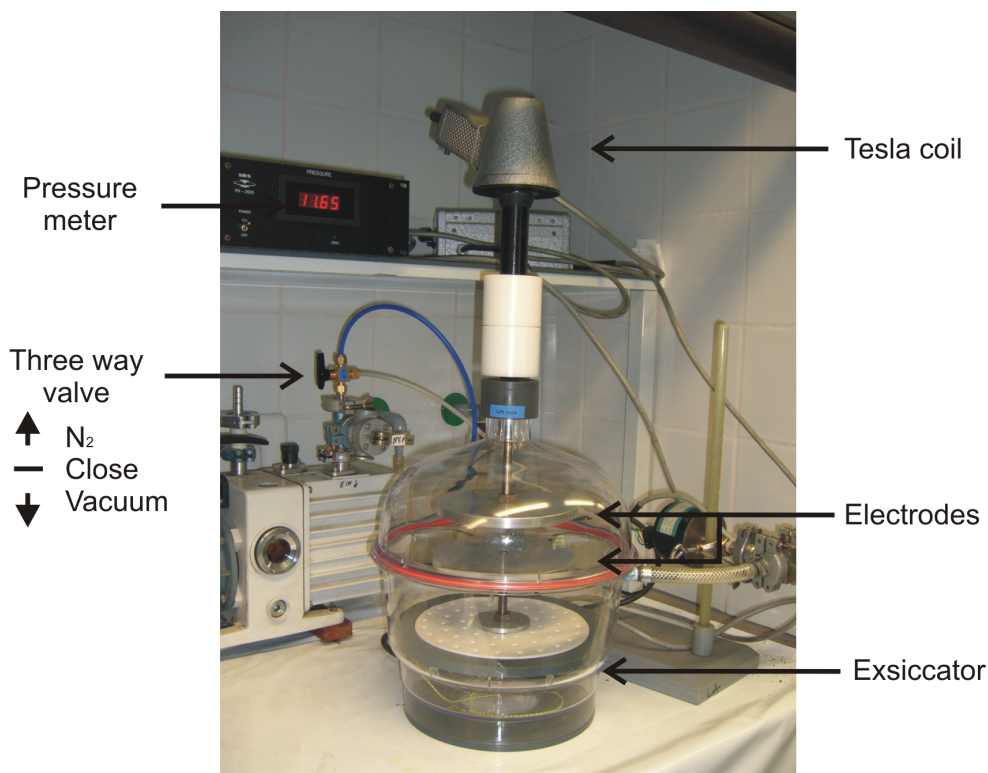


Figure 3.7: A photo of O₂ plasma cleaner.

negatively charged species. The oxidized surface can be further functionalised by reaction with trichlorosilanes. Oxidized surfaces are stable for approx. 30 min in air, after a certain time hydrophobic recovery of the surface is inevitable independent of the surrounding medium whether it is vacuum, air or water.

3.4 PMMA Chip Fabrication

The plastic reusable chips for pixelation experiments were fabricated from poly(methyl methacrylate), PMMA, a solid and transparent polymer of high mechanical stability. They were manufactured in house by computer numerical control (CNC) machining system using a universal milling machine (Model UWF 721H, Hermle AG, Gosheim, Germany). The AutoCAD designed data for the channel shapes were output by a control computer, which defines the path for a drilling head to mill channels into the material. A technical drawing of the channel design was translated into a machine-readable programme code and manually entered into the control computer. Examples of technical drawings can be found in Appendix A.2. Using an appropriate drill head, the design was milled into the chip at a rotational speed of 4500 rpm (approx. 30 mm/min.). The width of the channel

was determined by the diameter of the drill bit and the number of adjoined lines. Channel depths were altered by the height of the xyz-stage.

3.5 Summary

As illustrated in this chapter, fabrication of microstructured channel systems can be achieved via multiple methods, using different materials and varied fabrication techniques. Suitable materials and methods must be carefully chosen depending on the overall experimental conditions. The diverse properties possessed by different materials make them an interesting target for developing devices that are capable of carrying out analyses of chemical and biological samples. These advantages should be utilised fully to fabricate microfluidic chips that would help investigate pre-concentration techniques and especially help understand physio-chemical and cellular behaviours at microscale.

Pixelation of Planar Biological and Chemical Samples

Microfluidics bears the potential to create, handle and meter defined small liquid volumes. Among the possibilities to create such microvolumes, segmented or two-phase flow is one of the most intriguing approaches [56]. Aqueous droplets with high homogeneity formed in a stream of hydrophobic or gaseous carrier provide a high degree of control over the experimental conditions. As a result, the idea of forming droplets to carry out chemical and biological reactions in compartmentalised manner has brought forth enormous benefits for various applications such as enzyme kinetics [1], protein crystallisation [57] and cell treatment [58], and improvements in mimicking reaction conditions comparable to that of cells [59].

In this study, an automated droplet based microfluidic approach was developed to spatially resolve the composition of large and complex biological and chemical samples by pixelation. Incorporation of the droplet approach makes it possible to cope with high-throughput assays while offering the ability to handle multiple samples both in serial and parallel fashion. One such example has been presented by Manz and co-workers before [60,61] for a microfluidic chip design, where a conversion of serial to parallel sample analysis takes place by using up to 80 separation channels, all of which were filled at once for simultaneous homogeneous sample separation. The device developed here can be applied to isolating and analysing cells or specific areas from tissue, biofilms or cell colonies, allowing systematic studies of cellular responses in the mentioned specimen simultaneously. It could serve as an alternative to the existing microarray approaches [62] which are commonly utilised to reduce the time needed to screen large library in the field of drug discovery, biomedical research [63] and protein analysis [2,3].

Detection methods used in microfluidics should have high-sensitivity to cope with the demand at the decreased dimensions and low concentrations of the analyte of interest. Fluorescence imaging technique [19–21] is often relied on for the acquisition of data from

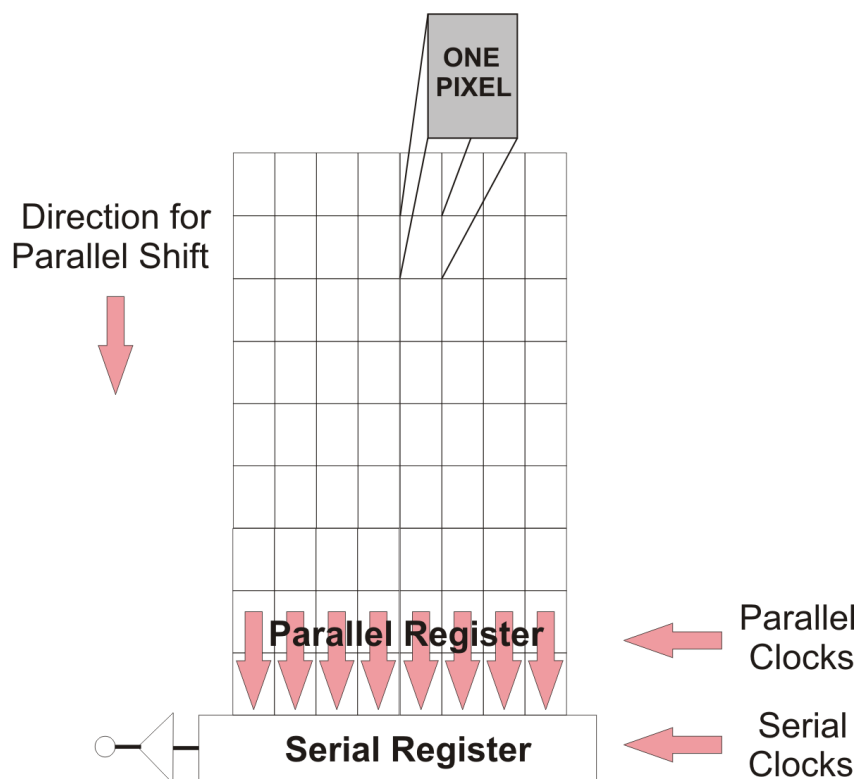


Figure 4.1: Schematic drawing of a CCD device. The sketch places a special emphasis on the data conversion from parallel to serial.

biological samples like living cells or even at single cell or molecule level. It is non-invasive and provide high temporal and spatial resolution for a suitable experimental setup.

The device presented here is a modular system that provides flexible solutions for integration to other reactions as well as to varying detection methods such as mass spectrometry [64], high-resolution microscopy [65,66] and various other detection methods [67]. Its ultimate purpose is to reduce and automate the labour intensive steps and thus to vastly increase the scope of understanding of stochastic behaviour expected by biosystems at microscale.

As briefly described in Section 1.2, the device realised here has similar functions and operating modes to an electronic CCD chip to compose an image, yet relies on a microfluidic platform. In a standard CCD chip, images are optically projected onto the parallel array that acts as the image plane (Figure 4.1). The device takes the scene information and partitions the image into discrete elements that are defined by the number of “pixels”. The resulting rows of scene information are then shifted in a parallel fashion to the serial register that subsequently shifts the row of information to the output as a serial stream of data. The image is then reconstructed as dictated by the system. Applying this analogy

to biological samples on a chip-based device and substitute heterogeneous constituents, *e.g.*, tissues and membranes, as the image plane, the first microfluidic imaging concept was established.

Figure 4.2 depicts the concept and the microfluidic realisation as a flow chart for easier understanding. The procedure of imaging consists of three steps, *i.e.*, (i) sample capture, (ii) transfer and analysis steps, and (iii) reassembling of the image. First, the sample is pixelated and discretised into smaller addressable units (pixels). Second, after parallel injection, the segmented sample is transferred into a microchannel for individual analysis. The emerged droplets can be transported afterwards along the channel in a stream of hydrophobic or gaseous carrier. Sample treatment steps can be implemented before the droplets are delivered to a stationary detection window, for data readout and serial collection. Finally, the information obtained from each pixel is assembled as an image of the sample. By mapping the data obtained to the original position, the image of the sample is generated, allowing recognition and visualisation of the spatially heterogeneous sample.

Herein, a brief introduction to already existing droplet based techniques and their utilisation are initially given. The progressive development of the chip designs and their results are explained and discussed thoroughly with respect to some of the typical physical phenomena that occur in microdomain. Finally, the results obtained from the chip application test are reported that was accomplished by using the final design of the pixelation chip.

4.1 Droplet Based Microfluidic Platforms

The principal idea behind droplet based systems is the use of single droplets as reaction confinements for biological assays or chemical reactions. The precise generation and spatial stabilisation of these droplets are accredited to dominant interfacial and surface tensional forces in the microdimension. Lateral dispersion (Taylor dispersion) that occurs in the direction of the flow can be avoided during mobilisation of the droplets to different locations as the droplets are kept isolated within an immiscible surrounding carrier like air or oil. A multitude of parallel screening reactions, each consuming only a minute amount of reagent, is achieved inside several small sized droplets on the platform that are generated under selected flow conditions, geometry, and fluid properties.

In the pressure driven realm of droplet based microfluidics, two immiscible phases dispersed in one another flow through the microchannels forming a flow scheme called segmented flow. It is referred so since the size of the inner phase droplet (d) exceeds the

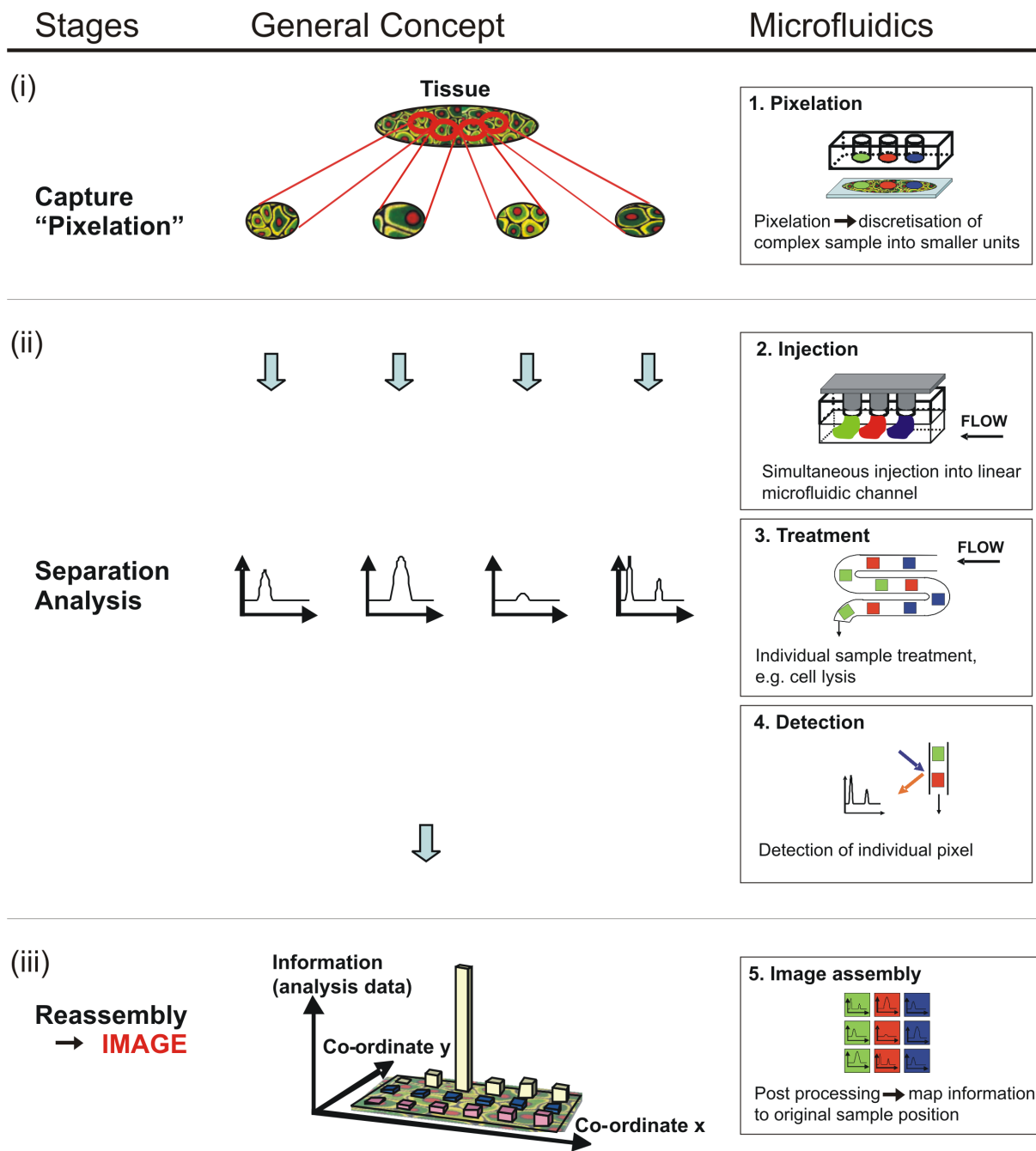


Figure 4.2: A conceptual flow diagram depicting the concept of sample pixelation and imaging. The procedure is divided into three distinct stages: capture, separation and reassembly, as can be seen under the heading "General Concept". On the left-hand side, under "Microfluidics", is the specific steps taken to realise these stages.

cross-sectional dimensions (R) of the channel leading to squeezed fluid plugs. An example being a sample fluid (*e.g.*, aqueous solution) forming plugs of a certain length separated by the carrier fluid (*e.g.*, oil) by injecting the aqueous phase into the stream of the carrier medium at a T-junction or by applying focusing techniques (Figure 4.3). The two phase flow is driven throughout the channels by an externally applied pressure.

In this manner, droplets are generated with an exceptional reproducible size with a volume of femtolitre to nanolitre. They can form small reaction containers that can be filled with (various) compounds at the very moment of formation. Thus, droplets are used to study chemical reaction kinetics because reagents are not dispersed beyond the boundary of the drop.

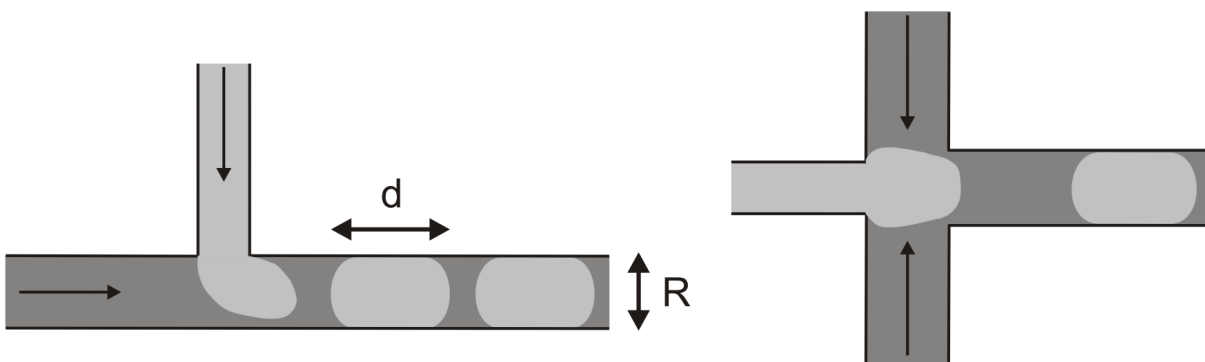


Figure 4.3: Sketches of droplet formation in a channel by T-junction (left) and co-flowing streams (right). For squeezed fluid plugs, $R < d$.

Sophisticated and interesting features rendered by the pressure driven, droplet based devices have provoked many publications in this field with the focus on the underlying physics, droplet manipulation techniques and their applications in multidisciplinary field [58, 68–81]. An excellent review on reactions in droplets is given by Ref. [82].

For controlled droplet generation, or metering of liquid volumes, the flow focussing structure [68, 69] and T-junction [70, 81] have been reported. The channel dimensions and the strength of the shear forces at the channel junction determine both the size of the droplet and droplet formation mechanisms. Ismagilov and co-workers have adapted a cross-flow device design as the basis for almost all droplet based research performed to combine multiple fluid reagents relying on a sheath flow arrangement into single droplets for use as microreactor [71, 72]. The formation of double emulsions, *e.g.*, water-in-oil-in-water (W/O/W), has also been shown in a serial arrangement of T-junctions, which require selective modification of hydrophobic channel surfaces [73].

Mixing is another fascinating feature of the droplet based devices as the rate of mixing inside the droplet can be controlled by a recirculating flow due to shear forces induced by the motion along the stationary channel wall [74]. For bubbles or drops, the shear stress on the surface induces an internal motion, which results in a decrease of the drag coefficient [75]. Since each droplet functions as a batch reactor moving along a channel, the reaction time corresponds to the length traveled by the droplet. Consequently, sampling of droplets at different spatial locations can be used to deduce chemical kinetics, provided that the local micromixing is faster than the chemical reaction rate. The effect is enhanced for two liquids with different viscosities (Figure 4.4) [76].

Applications of the produced droplets have also been studied extensively. Short, for the investigation of the kinetics of chemical reactions in the order of some milliseconds [72], and long, for storing applications in the order of a week [77], incubation times are reported that show results comparative to the conventional systems. Protein crystallisation [78, 79] and introduction of cell suspension (Figure 4.4) [80] to treat single cells [58] have also been demonstrated that bring benefits and improvements in mimicking reaction conditions comparable to that of surrounding biological cells.

Electrohydrodynamics can also be used to manipulate droplets as an alternative to the pressure driven or flow rate controlled systems. Microelectrode arrays with programmed electric fields create electrohydrodynamic (EHD) forces, namely electrowetting [83–86], dielectrophoresis [87–89] for transporting, merging and splitting droplets in microfluidic equivalents of microprocessors [90].

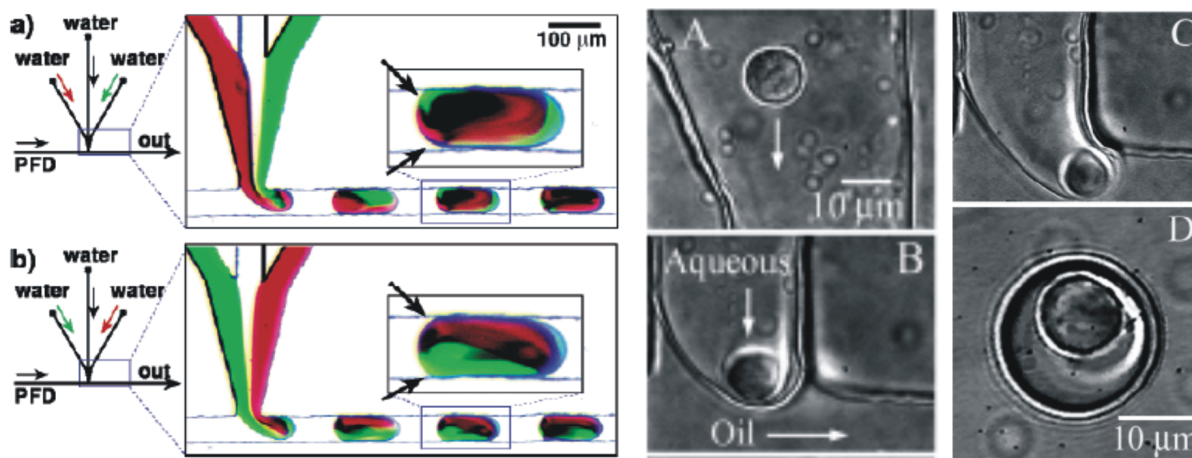


Figure 4.4: Works presenting applications of droplets. Two liquids with different viscosities mixing in a droplet (Ref. [76]). Encapsulation of single cell (Ref. [80]).

4.1.1 Experimental Outline

Different chip designs and pixelation methods were explored in order to derive an optimal chip design in terms of effective sample uptake/pixelation, injection, droplet transfer, droplet production success rate and ease of operation. Several different approaches were evaluated, including the surface condition for pixelation, channel design features and chip materials, which are discussed in the coming sections.

Initially, the sample uptake stage to observe the sample behaviour against pixelation method was tested. The method should capture the sample from the target by avoiding sample mixing with the neighbouring areas to assure the preservation of the spatial heterogeneity. Cells cultured on hard and soft surfaces were compared using different materials for sample uptake efficiency.

In parallel, the injection stage was investigated. Total fluidic chip design was first utilised, which solely relied on the fluidic pressure to inject the captured samples. The bottom and the top layers embedding serpentine channels sandwiched the perforation layer. With a controlled fluidic pressure, an attempt was made to inject the captured samples in the perforations. The weakness in this design led to the introduction of the micropillar manifolds.

The above trial-and-error experiments revealed certain conditions necessary for the pixelation and the injection stages; a soft surface for sample capture and the micropillar manifolds for the injection. The chip design was finalised accordingly, in which the proof-of-principle studies were carried out using a flexible microchip comprising three layers. The PDMS microchannels are reversibly bonded on to the PMMA perforation layer for easy cleaning.

4.1.2 General Experimental Setup

Commonly utilised chemicals, biological cells with their handling procedures and devices throughout this work are described here. Any adjustments made are mentioned in the relevant sections.

Chemicals

The source, the properties and, where necessary, the preparative methods for the chemicals, reagents, solvents, dyes and solutions are given below.

Agarose (Fluka)

It is a highly purified polysaccharide derived from agar at high purity grade with low Electroendosmosis (EEO)¹ for molecular biology. A varying concentration of gel was prepared for different test purposes (0.05 to 2 % (w/v)). In brief, agarose powder is added to deionised water and brought to boil, the hot solution is poured into a Petri dish and was allowed to cool and set. Although the pore size and sieving characteristics of a gel is determined by adjusting the concentration of agarose in the gel, this property was not used in this work, as agarose gel was used to provide a soft sample pixelating surface.

0.7% (w/v) Alginate solution (Sigma)

It is an alginic acid sodium salt from brown algae with viscosity 2% solution at 25°C. 0.7 g was added to 100 ml deionised water and stirred over-night with a magnetic stirrer. The solution was used to form polymerised alginate gel upon in contact with CaCl₂.

CaCl₂(MERCCK)

The solid was dissolved in deionised water to form 20 mM solution. The solution was used for the polymerisation of the alginate solution: *e.g.*, 2 ml alginate solution was pipetted into a Petri dish. 5 ml 20 mM CaCl₂ is added slowly and left for 30 min to allow polymerisation to form alginate gel.

Fluorescein (Sigma-Aldrich)

2.5 μL fluorescein of a 10 mM aqueous solution was added to 500 μL alginate solution and mixed well under vortex.

Fluorescent beads(Molecular Probe, The Netherlands)

1 μL of 1 μm sized fluorescent bead suspension is added to 500 μL alginate solution or deionised water. Vortex is applied to the new suspension before every use. An appropriate amount is pipetted and used as model samples.

Erythrosine B (Applichem GmbH, Germany)

2',4',5',7'-Tetraiodofluorescein disodium salt, C₂₀H₆I₄Na₂O₅; λAbs. max = 525 nm, spectral range : 900-190 nm

Food colouring (McCormick France SAS)

A commercially available food colouring was bought from a supermarket. 2 μL of pure food colouring was added to 500 μL 0.7% alginate solution and vortexed before use.

¹EEO is a movement of liquid through the gel. Anionic groups in an agarose gel are affixed to the matrix and cannot move, but dissociable counter cations can migrate toward the cathode in the matrix, giving rise to EEO. Since electrophoretic movement of biopolymers is usually toward the anode, EEO can disrupt separations because of internal convection.

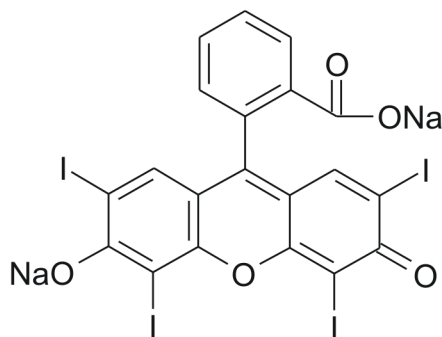


Figure 4.5: The chemical structure of erythrosine B.

Cell Handling

Two types of cells were used in the experiments. Colon cancer cells were used for the trial-and-error test of pixelation method. *Saccharomyces cerevisiae* was used for the final chip application test. They will be explained in detail at relevant sections.

Colon cancer cells (SW 480)

Colon cancer cells were cultivated in the mixture of Dulbecco's Modified Eagle's Medium and nutrient mixture F-12 Ham (DMEM/F-12), supplemented with 10% foetal bovine serum (FCS) at 37°C in a humidified atmosphere with 5.5% CO₂ (v/v). All chemicals were purchased from PAA.

Cells are detached by an EDTA-Trypsin solution (0.02 gL⁻¹ and 0.05 gL⁻¹ respectively) and are filled into the poly-D-lysine covered microchips with fresh DMEM/F-12 medium. Cells are incubated for one day on the surface of the glass cover slide under the same conditions as described above. Prior to the experiments, the medium was removed and colourless DMEM/F-12 medium (3 μL) and 0.1% erythrosine B in PBS (0.25 μL) was added.

Saccharomyces cerevisiae Cen PK (pAH56)

The yeast *Saccharomyces cerevisiae* is recognized as a model system representing a simple eukaryote, whose genome can be easily manipulated. Yeast has only a slightly greater genetic complexity than bacteria and they share many of the technical advantages that permitted rapid progress in the molecular genetics of prokaryotes and viruses. Some of the properties that make yeast particularly suitable for biological studies include rapid growth, dispersed cells, the ease of replica plating and mutant isolation. Being non-pathogenic, yeast can be handled with little precautions and can be cheaply obtained from supermarkets.

In this study, strain *Saccharomyces cerevisiae* Cen PK was transformed and the plasmid pAH56 was introduced to produce recombinant yeast. It expresses the enhanced green fluorescent protein (eGFP) gene controlled by a lac promoter, hence it is induced in the absence of glucose. The cells were cultured either in YPD (glucose) or YPG (galactose) medium, as cell suspension or on agar plate. Long term storage was prepared by taking cultured cells in a 500mL solution of an equal volume of YPD medium and 50% glycerol and kept at -80°C.

YPD/YPG medium preparation:

For a 1 L final medium, mix 10 g yeast extract and 20 g peptone (if agarose plate, then 20 g agar was added) in 950 mL distilled water. Autoclave the solution and add autoclaved 50mL 40% (w/v) glucose solution. Mix well.

Devices and Materials

PMMA (Roehm GmbH or ICI GmbH, Germany)

Large piece of PMMA was ordered and was cut to the size appropriated, according to the design produced by computer numerical control (CNC) machining system.

Panasil (Kettenbach GmbH, Germany)

Panasil is a curing, elastomeric precision impression material based on polyvinyl siloxane with an especially short oral setting time.

For chips made of PMMA, the inlet holes for the plastic tubing were fabricated by mechanical drilling. A drill head with a diameter of 0.8 mm was used. The tubing fitted the produced holes tightly, however to ensure a leakage free environment, epoxy glue, Panasil was placed around the interface of the tubing and the hole.

Mikroglas (mikroglas chemtech GmbH, Germany)

FOTURAN glass (25 × 60 × 0.5 mm) was cut into a small piece with approx. 10 × 10mm for the pixelation purpose.

Microscope

Olympus XI 71 or Leica DM IRB equipped with 100W or 50W Hg-Arc lamp, respectively. Blue light (450-500 nm) or green light (510-550 nm) from a 100W Hg-arc lamp of Olympus microscope was used for fluorescence excitation, and emitted light (> 500 nm or > 590 nm, respectively) was detected by a camera (EMCCD iXON DV887, Andor technology, Germany), or from Leica microscope with 50W Hg-Arc (CCD EHD12V5H, EHD Imaging GmbH, Germany). The optical filter sets are purchased from AHF, Germany. Online free

software VirtualDub (Version 1.26) or in-built function from iXon camera were used for image capturing.

neMESYS pump (centoni GmbH, Germany)

1mL syringes were placed in the in-house manufactured holders to secure the syringes in place. The pump was operated at varied flow rate from 20nL s^{-1} to $1\ \mu\text{L s}^{-1}$.

4.2 Pixelating and Capturing Samples

The importance was emphasised on investigating the pixelation method and the respective behaviour of the targeted samples. Key features that the pixelation method should fulfill were:

1. To capture and fix the sample within a given space.
2. Avoid neighbouring sample mixing, preserving their spatial heterogeneity.

Two different materials were subjected to the experiment for a comparison (Figure 4.6). The first was the in-house mechanical workshop fabricated, 5 by 5 PMMA perforation stamp. At the trial-and-error stage, flexibility in terms of chip implementation was considered important. Prior to material optimisation, the perforation dimension of $500\ \mu\text{m}$ in diameter, interspacing of $300\ \mu\text{m}$ with $1.5\ \text{mm}$ in depth was mechanistically possible for the production. The second was the commercially available FOTURAN hole plate from mikroglas. Sample pieces were obtained that had the dimensions of $200\ \mu\text{m}$ in diameter, interspacing $100\ \mu\text{m}$ and $800\ \mu\text{m}$ thickness with spherical and square perforation shapes. Compared to the PMMA stamp, FOTURAN can be photolithographically fabricated, which would enable the future miniaturisation and integration of the design, if this method proves to function.

4.2.1 Pixelation from the Hard Surface

In this experiment, the properties of the in-house fabricated PMMA stamp and the commercially available FOTURAN stamp were compared for the SW 480 cell pixelation ability from a hard surface.

Experimental

On the surface of an autoclaved cover glass, an area restricted by a PDMS frame, was cultured SW 480 cells, using the method described in Section 4.1.2. Prior to the actual

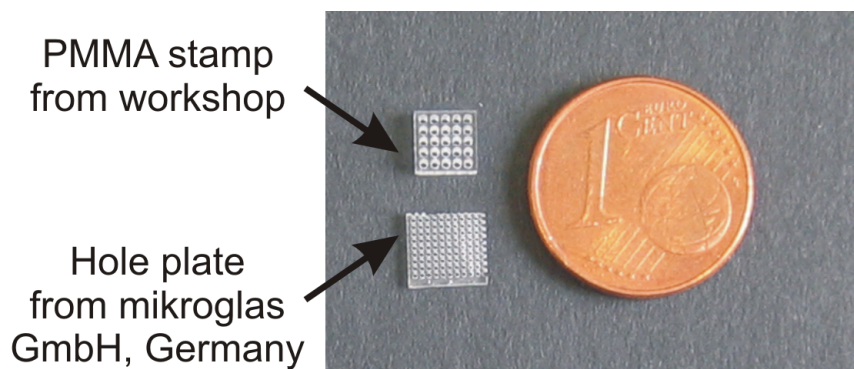


Figure 4.6: A comparison of mikroglas hole plate to PMMA stamp made by the workshop.

PMMA: Hole diameter = 500 μm , Thickness = 1500 μm .

mikroglas: Hole diameter = 200 μm , Thickness = 800 μm .

pixelation step, the medium was removed to visualise under fluorescence, erythrosine B was pipetted. A direct pixelation of the cells grown on the cover glass surface was conducted by employing the two stamps made of the materials *i.e.*, PMMA and FOTURAN, and the sample behavioural comparisons were made. The images of the perforations and the surrounding areas were taken to observe the effect of the pixelation method.

Results and Discussion

The observation revealed similar results for both the PMMA stamp and the FOTURAN hole plate with the thickness 1500 μm and 800 μm respectively, for the pixelation of the SW 480 cells from a hard surface.

In the first experiment, the observations was made after the direct placing of the perforation layer on the cells cultured on the cover glass (Figure 4.7B and C). It was shown that for both the PMMA stamp and the FOTURAN hole plate, pixelation of the cells from a hard surface was impractical, as the glass surface is inelastic. The small space existing between the surface of the glass and the stamp causes difficulty in fixing the sample in a given perforation, allowing minute sample flow and mixing between the perforations, thus leading to a loss of spatial information.

What was witnessed was that the FOTURAN hole plate withstood the hand applied pressure, despite having almost half the thickness of the PMMA stamp. This showed that FOTURAN can be a potential material for the perforation layer when the microchip is to be photolithographically produced.

In the second experiment, to mimic the sample transfer conditions that would later be implemented, the perforation layer was moved to a clean cover glass surface to test the

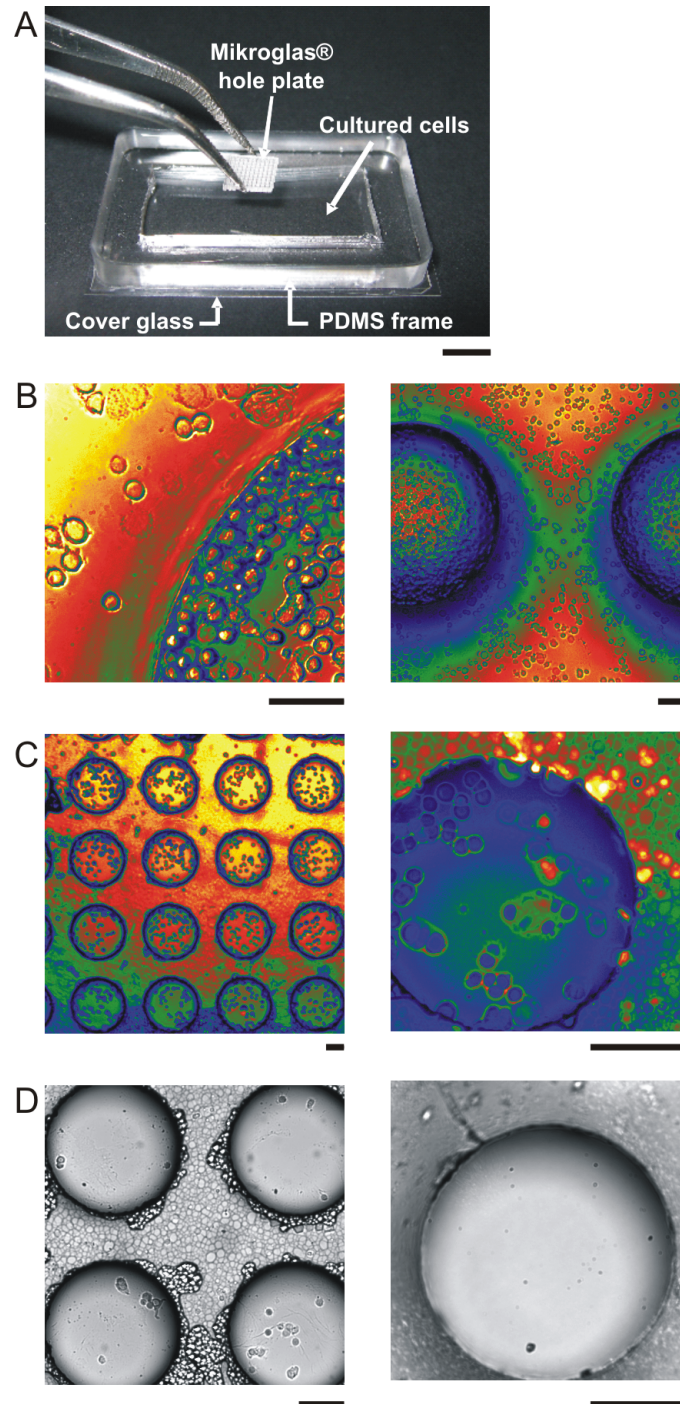


Figure 4.7: The procedure used to pixelate and capture the SW480 cells cultured on cover glass surface. The SW480 cells were cultured on a cover glass restricted by a PDMS frame, before they were pixelated by the careful placing of PMMA stamp or FOTURAN hole plate (A). The images of SW 480 cells in and around the individual holes, after placing the PMMA stamp (B) or hole plate (C). Images taken after the perforation layer was transferred to a new surface. No cells were contained in the perforations (D). Scale bar: 1 cm (A), 100 μm (B-D).

viability of the hard material as the sample capturing surface. As an additional experimental condition, vacuum suction was applied to test its effect on the sample capturing enhancement.

The results showed that the capturing of the sample in the perforation layer from the hard surface is not simple (Figure 4.7D). Special attention had to be paid to the aqueous based samples during the microscopic observation due to the heat produced by the microscopic lamp that tend to dry the surface. When the sample surface was too dry, it was not possible to capture the cells as they would be strongly adhered to the glass. Despite a constant supply of the medium, under these conditions, the spatial information was not represented by the majority of the perforations. In addition, a comparison was also made on the capturing ability by the addition of suction using a peristaltic pump. A gentle suction applied by the pump was thought to aid the sample capturing after pixelation. Although it was shown that in general more number of cells were observed in the perforations where the suction was applied, the problem with surface dehydration over-rode the efficient sample uptake condition.

These experiments showed that the samples need to be kept in the liquid or gel phase: once the sample extracting surface was dried, the chances of sample capturing success was greatly reduced. It was, therefore, suggested that the pixelation stage should take place on a soft rather than a hard surface, as its surface is more prone to dehydration. At the same time, with a soft surface, the stamp can be pressed avoiding sample leakages between holes, as the flexibility of the gel allows the stamp to enter the soft phase (Figure 4.8). With enough pressure, it can also behave like a cutter which separates the sample by going through completely.

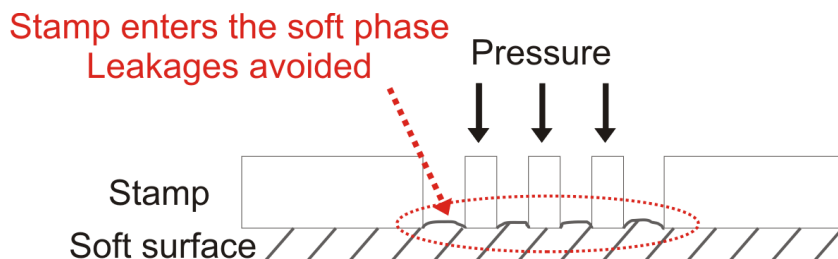


Figure 4.8: A predicted side view of the soft surface when a pressure is applied from the top to pixelate samples, using a stamp. The red dotted circle emphasises the region of interest.

4.2.2 Pixelation from the Soft Surface

From the above observation, an attempt was made to pixelate the sample from a soft surface. Agarose and alginate gels were utilised to suffice the material conditions and SW 480 and yeast cells were the chosen pixelation targets.

Experimental

Saccharomyces cerevisiae was cultured on a 10% agarose gel plate (based on YPD medium). A small piece (1×1cm) where a colony resided was cut out and was subjected to the pixelation test.

As an alternative to the agarose gel soft surface, alginate gel was polymerised upon bringing an equal volume (600 μL) of 0.7% alginate solution and 20 mM CaCl_2 in contact for 30 min. SW480 cells were cultured on the surface of an autoclaved cover glass before being detached by the pipett tip. 10 μL of the cell suspension was pipetted onto the surface of the polymerised alginate surface.

After the gel pieces were prepared, the PMMA stamp was used to pixelate the cells residing on the surface of the gel and the captured sample was transferred to a clean surface (Figure 4.9). The images of the perforations and the surrounding areas were taken to visualise the results of the pixelation method.

Results and Discussion

An attempt was made to keep the sample in the gel phase. This could be feasible as the gel surface provide cell-friendly environment. A pressure was applied from the top on the PMMA stamp to try and capture the yeast cell grown on the agarose gel. Under this particular experimental condition, agarose gel split before the sample capture was successful. The problem was enhanced by the small size the gel was cut into, providing an unstable surface to pixelate the sample from. If the gel is fixed in an area or had a larger surface area, it would withstand a larger pressure. As an alternative, alginate gel was utilised to test its compatibility as the surface material. The result showed that there is a greater number of cells transferred to the new surface compared to the agarose gel, especially with the vacuum application, however, still proved to be difficult to reflect the true spatial information of the given sample (Figure 4.10).

A general conclusion drawn from the above experiments is that the pixelation of a sample is better conducted on the surface having a soft consistency. As can be seen, the pixelation of SW 480 cells from agarose or alginate gel surface proved to be more successful compared

to those cultured on the hard glass surface. It is, however, not ideal to capture the sample together with the gel matrix as it makes the sample analysis under microscope difficult.

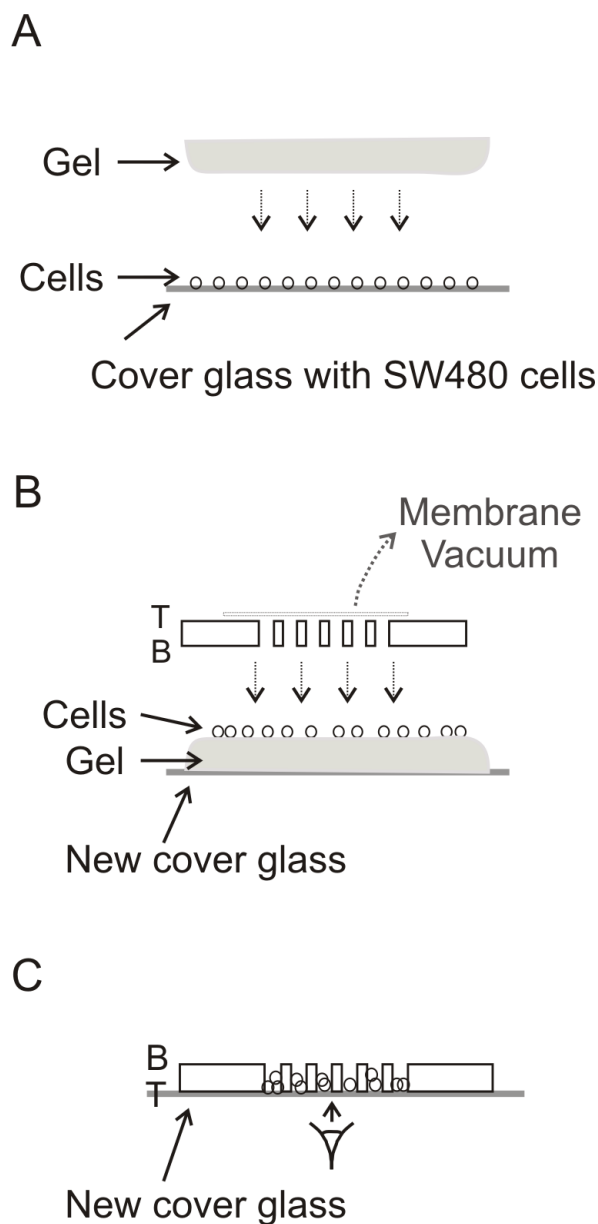


Figure 4.9: A sketch showing the procedure used to pixelate and capture the SW 480 cell suspension or the yeast cells from the surface of material with a soft consistency, *i.e.*, alginate or agarose gel. An appropriate sized gel was cut or polymerised (A). The perforation layer was placed from the top either with or without vacuum application at this stage (B) and then placed on a clean cover glass surface with cells facing down (C).

In the current experimental condition, the target sample is in a liquid state; cell suspensions in PBS medium. An improvement to the sample capturing ability would be to increase the viscosity of the sample suspending medium, so to enhance the surface retention power to keep the once pixelated samples in the perforations, without using the vacuum, which avoids an extra complication to the experiment. This suggestion was investigated and the results are reported in Section 4.5.

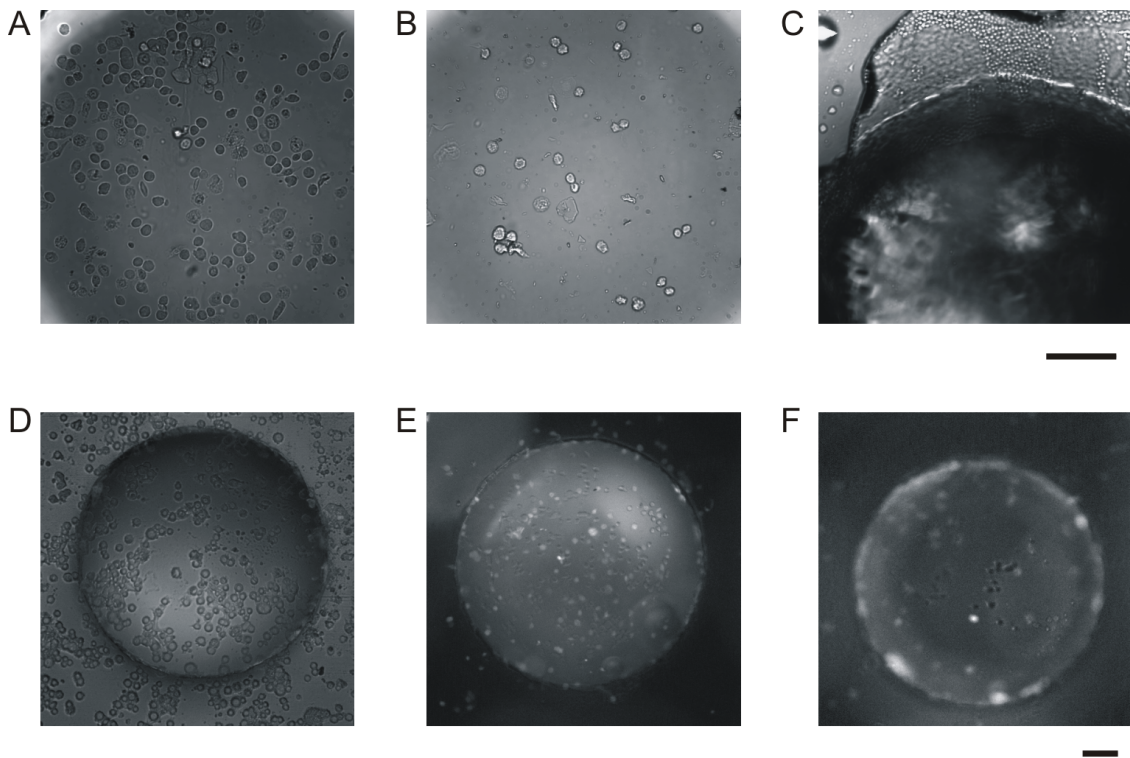


Figure 4.10: The images of perforations and the surrounding areas after pixelation and transfer of the PMMA stamp on to a new glass surface. Images without vacuum application (A-C). The cells inside the perforation directly after the stamp placement (A). The cells after the stamp transfer to a new glass surface (B). A perforation containing cells and the gel matrix which reflects difficulty encountered when observed under microscope (C). In the second experiment, vacuum was applied to some of the perforations before the transfer for a comparison. Perforation before the transfer (D). After the transfer with (E) and without (F) vacuum application. In general, images show an improvement compared to a hard surface but still with a poor sample pixelation ability. The scale bars represent 100 μm .

4.3 Total Fluidic Approach

In parallel with the pixelation technique (Section 4.2), in the preliminary experiments, a total fluidic/hydraulic approach was utilised to inject and transfer the pixelated samples into the microchannel.

4.3.1 Chip Design

Out of several chip designs proposed to accommodate for various sample types as well as sample capturing and delivering situations, the serpentine channel design was chosen for the investigation (Figure 4.11). The simplest yet the most interesting design that provide several experimental opportunities was tested for its fundamental applicability to simultaneously inject pixelated samples into the microchannel. Two chip material compositions were considered to test the design suitability, *i.e.*, three PMMA and PDMS-PMMA-PDMS compositions.

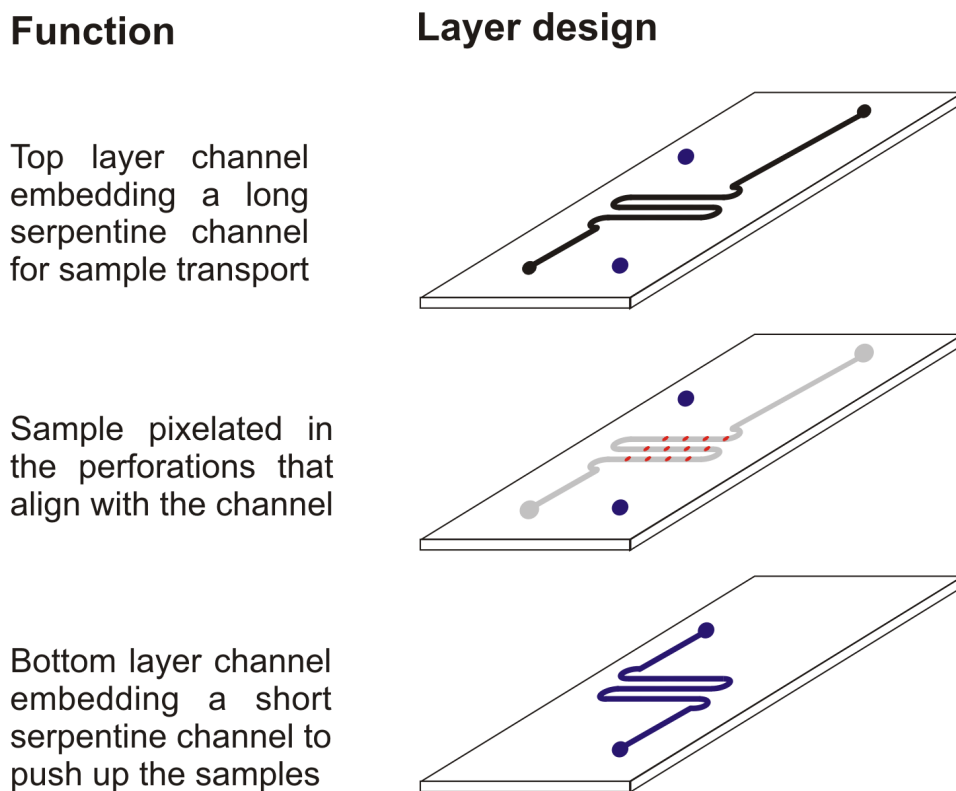


Figure 4.11: The chip design chosen for the total fluidic approach. Serpentine channel design having only one channel that allows for parallel sample droplet injection and serial data read-out.

4.3.2 Three PMMA Layer Chip

This particular experiment was aimed to testing the leakage of the three PMMA layer chip from the material and the design suitability point of view.

Experimental

The chip consisted of three PMMA layers with the dimension $2.4 \times 4.8 \times 0.1$ cm. In this particular design, the top layer could slide side-ways above the perforation and the bottom layer embedding the serpentine channel (Figure 4.12).

The three PMMA layers were overlapped while the top layer was in misalignment with respect to the bottom two layers. Mineral oil was introduced as the carrier fluid into the top serpentine channel, using a peristaltic pump.

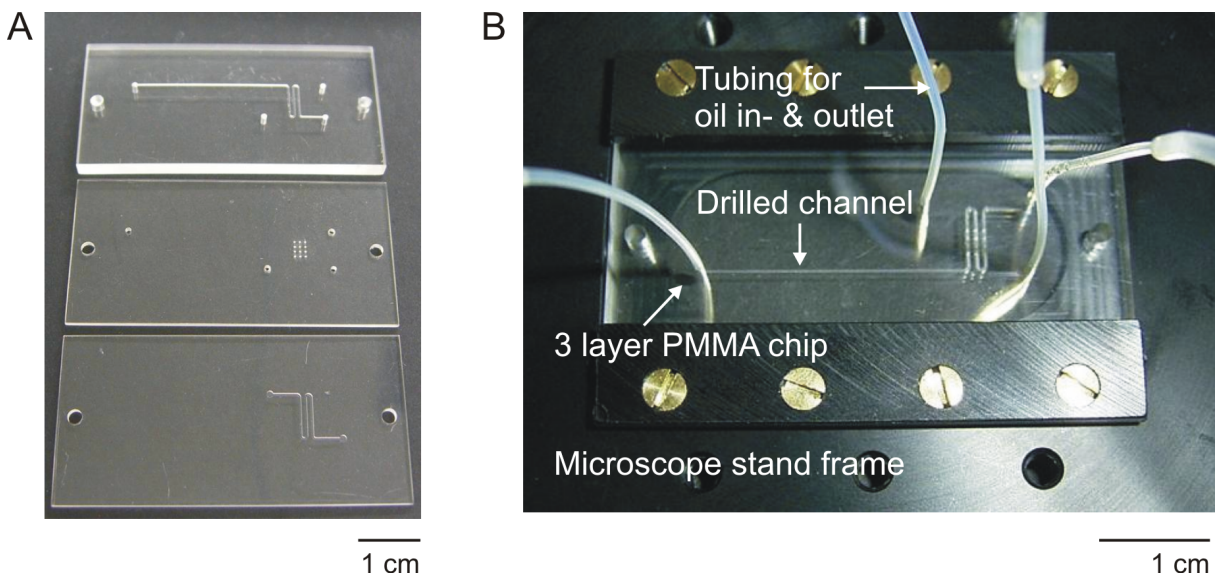


Figure 4.12: Three PMMA layer chip design used to realise the parallel sample injection via total fluidic approach. Picture (A) shows the individual layers. From the top: 3mm thick, channel $300 \mu\text{m}$ wide and deep (top layer); 1 mm thick, perforations $300 \mu\text{m}$ diameter with 300, 500 and $800 \mu\text{m}$ interspacing (middle layer); 1mm thick, channel $300 \mu\text{m}$ wide and deep (bottom layer). The assembled chip with the tubings for the oil in- and outlets (B).

Results and Discussion

First the quality of alignment of the produced chip was checked for the perforation layers having three different inter-spacings. The result showed that upon misalignment, the top

serpentine channel sits between the bottom serpentine channel, which should provide a sufficient environment to independently fill the channels (Figure 4.13A-C).

At a low speed, mineral oil was injected into the top serpentine channel to test the ability to independently fill the top and the bottom channels which would finally create an opposing flow direction. It was possible to fill the channel but with a low reproducibility. On successful occasions, the top layer was moved to be aligned with the rest of the layers. Upon further oil injection, it entered the bottom channel which proved that this approach would be appropriate for the sample injection (Figure 4.13D and E). Majority of the times, however, it was observed that even with a careful control of the oil injection, this approach was thought impractical having a low reproducibility, as there was no tight sealing between the layers of the PMMA, which led to the oil leakage during the channel fill (Figure 4.13F).

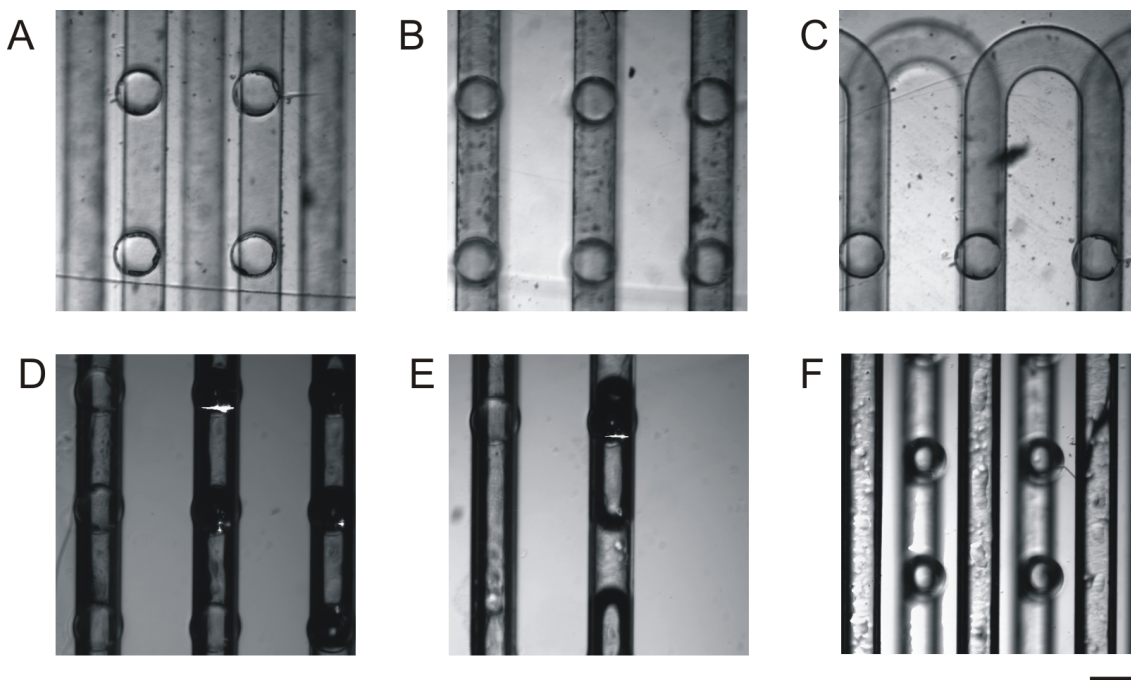


Figure 4.13: Images of different alignments produced by the three PMMA layer chip: Layers is aligned (A); in alignment, straight section of the channel (B) and curved section of the channel (C). Upon injection and filling the top layer with the oil, it was moved in alignment with the rest of the chip. Oil entered the bottom layer without leakage (D) with the oil plug front shown (E). Majority of the cases, oil leakage and spread was observed (F). Scale represent $300 \mu\text{m}$.

4.3.3 PDMS-PMMA-PDMS Chip

Due to the leakage caused during the channel filling step, an effort was made to circumvent this problem by utilising PDMS while using the same channel design.

Experimental

The channel and the perforation design and the chip dimension were kept the same as in the previous experiment. The top and the bottom layers embedding the serpentine were cast out of a mask (a negative produced from NanoFlame² coated PDMS).

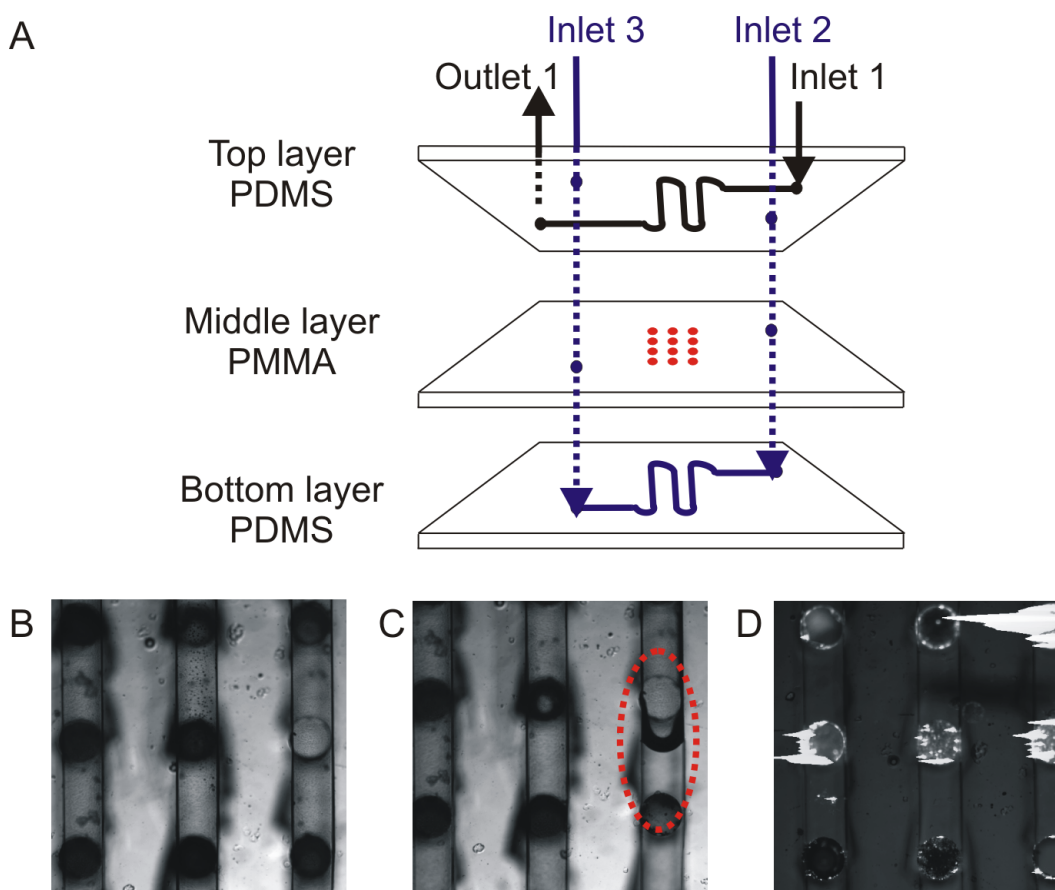


Figure 4.14: Sketch of the composed PDMS-PMMA-PDMS chip and the tubing positions (A). Inlet 1 and outlet 1 belong to the top layer while inlet 2 and inlet 3 belong to the bottom layer. The mineral oil is introduced at a flow rate of 20 nL s^{-1} from inlet 1 and 2. Images showing a good alignment of the PDMS-PMMA-PDMS chip (B). Oil injection with its front running in the channel marked with dotted red (C). The filled channel without disturbing the samples residing in the perforations (D).

²A flame pre-treatment device that generate a very thin (5 to 40 nm) but very dense silicate layer by flame-pyrolytic deposition of an organosilicone compound.

Sealing ability and the pressure resistivity of the chip were tested using the neMESYS pump. 20 μL 1 μm sized fluorescent beads suspension was pipetted into the perforations of the PMMA layer. The three layer chip was composed by the adhesion of the top and the bottom PDMS layers, at which stage the alignment was checked under the microscope. Mineral oil was introduced at a flow rate of 20 nL s^{-1} into the channels from the inlet 1 and 2 (Figure 4.14A). Once the channels were filled, the flow rate was increased at inlet 2 and 3, while at inlet 1 was kept constant.

Results and Discussion

PDMS-PMMA-PDMS chip composition showed a good and an easy alignment whilst providing sufficient sealing around the channel for the injection of the mineral oil (Figure 4.14). As shown in Figure 4.14D, when the oil was injected from inlet 1, the channel was filled without disturbing the sample plugs residing in the perforations.

Following the successful results obtained from the preliminary tests on the PDMS-PMMA-PDMS chip, the oil flow rate, thus the pressure, at inlet 2 and 3 were increased slowly from 20 to 80 nL s^{-1} to test the sample injection ability of the chip design. In doing so, the pressure in the bottom channel should be increased, which results in the injection of the sample plugs residing in the perforations. In general, it was concluded that the chip design is successful in retaining the samples in the perforations. However, due to the uneven volume of the captured sample volume per perforation, it was not possible to perform a concurrent sample injection.

Pascal's principle states:

“A change in the applied pressure on a fluid is transmitted undiminished to every point of the fluid and the walls of the container.”.

Based on this principle, once the sample with the least volume, hence, the pressure, is released from one of the perforations, the force distribution on the sample plugs becomes unequal and the fluid will move in the direction of the resulting force. The serpentine channel of the bottom layer was designed in such a way that the channel lengths were equi-distance from the two ends. However, to satisfy Pascal's law, the depth of the channel also needs to be altered so the pressure applied on each sample plugs would also be equal (shown by the distances **a** and **b** and angled channel depth in Figure 4.15C).

It should be stated that to fabricate the channel floor at an angle is a difficult task. In the current design, the channel floor was kept leveled, thus, subsequent to the pressure release from the first perforation, the injection of the rest of the sample plugs was inhibited. For this reason, the sample injection procedure attempted here that relies especially on the

principle of applying an equal force could not further be used. Therefore, a method that did not rely on a fluidic approach was sought.

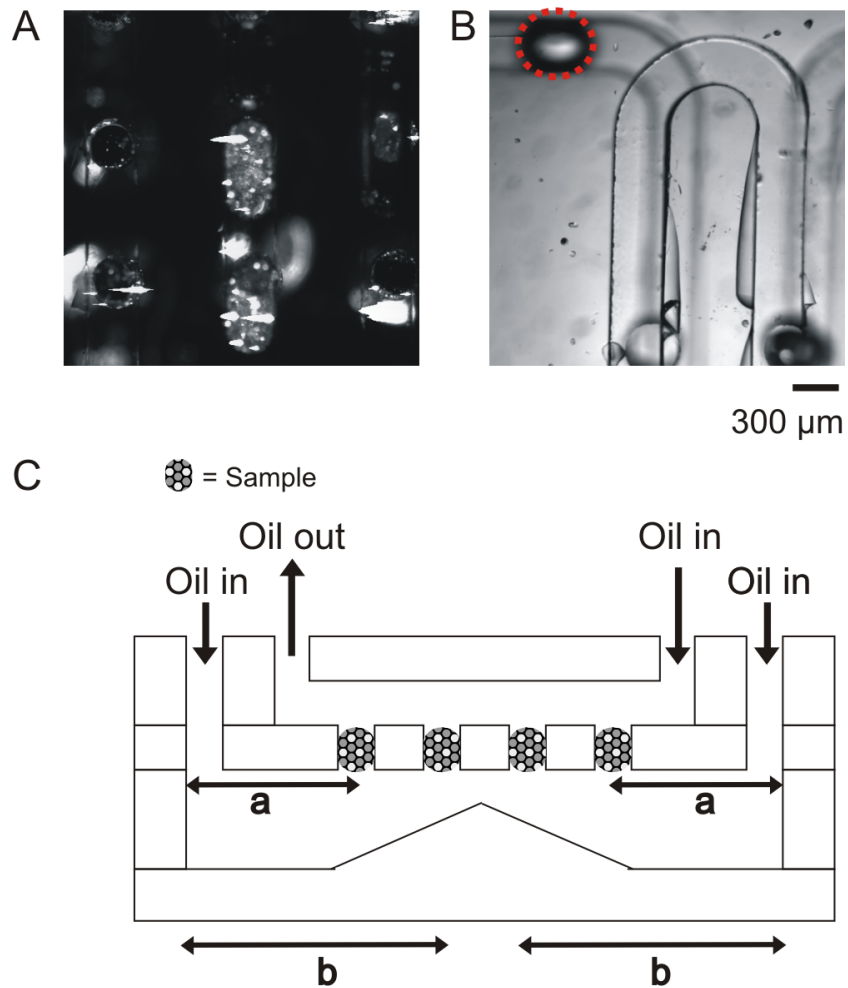


Figure 4.15: Images showing injection of the sample (fluorescent beads) using PDMS-PMMA-PDMS chip. On filling the channels, sample plugs were injected into the channel, depicted by the oval shapes in the middle (A). The travelling sample plug from the first perforation at the top left corner circled with dotted red (B). In this image, misalignment of the top and the bottom channels is observed and the focus was set to the top channel. A scheme showing the ideal conditions for the functioning of Pascal's principle (C).

4.4 Micropillar Manifolds Approach

The results from the total fluidic approach showed that the uneven sample volume instigated non-simultaneous injection of the samples from the individual perforations. The new approach employed pillars that would force out the samples independent of the captured sample volumes. Several experiments were conducted using different readily available materials to test the functionality of the pillars for the purpose of injection.

4.4.1 Experimental

Materials used as pillars were glass capillaries (OD = 200 μm), fibre optics, Panasil. The PMMA layer, in which the perforations are filled with fluorescent beads and the PDMS channel layer (with the long channel) were aligned and adhered together. Mineral oil was pumped into the channel. For capillaries and fibre optics pillars, 12 \times 3 mm pieces were cut and were individually placed in the PMMA perforations through a layer of Parafilm. PDMS was cast in a small frame and upon polymerisation, the pillars embedded in the PDMS holder were removed from the frame.

Once the channel was filled, the pillars were manually aligned and pushed downwards to inject out the samples in the perforation. A thin layer of PDMS was placed between the pillars and the PMMA layer to create a better adhesion. For Panasil, the same procedure was used to prepare the chip. Instead of the rigid pillars, a small amount of freshly mixed Panasil was placed using the tip of a small spatula for the sample injection. It was ensured, by a repeated application, that the siloxane would fully enter the perforations. The results were observed under the microscope.

4.4.2 Results and Discussion

The results from the use of pillars demonstrated a great improvement on the performance of the simultaneous injection compared to the total fluidic approach. The injection of the samples employing capillary and fibre optics functioned well (Figure 4.16A and B), resulting in the production of droplets, although sometimes coagulation of the neighbouring sample plugs occurred. The gap existing between the pillar (200 μm) and the perforation (300 μm) allowed for the oil leakage. The PDMS layer was, hence, placed in between the PMMA layer and the pillars to create a better sealing. In the majority of the cases, however, leakage was not alleviated and air bubbles were produced when the pillars were

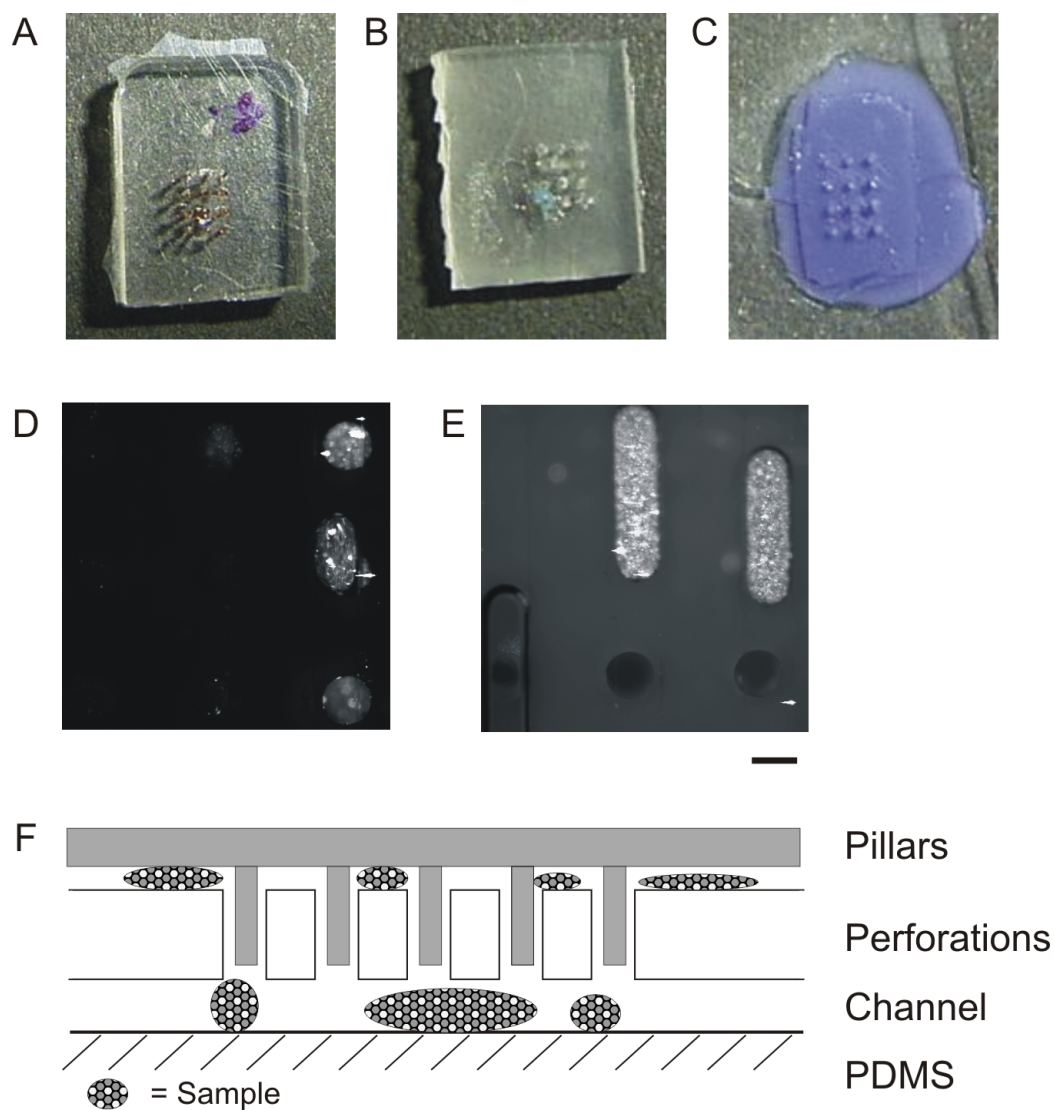


Figure 4.16: Images of the pillars made out of capillaries (A), fibre optics (B) and Panasil (C). Injected sample droplets in the channel (D) and those that coalesced (E). A cross-sectional sketch of the microchip showing the conditions after the pillar injection (F). The scale bar represent $300 \mu\text{m}$.

inserted. This was found to be problematic as it will prevent exertion of enough pressure on transport of the sample droplets injected into the channel. The fabrication method with these materials was also found to be laborious. The pillar insertion was difficult due to the need for alignment of the pillars.

A successful sample injection was observed with a more flexible material, Panasil, where an increased sealing and an air-tight condition was created (Figure 4.16C). Compared to the more rigid pillars, the formation of the air bubbles were avoided. Despite the advantage, further use of this material was discontinued. Under the current experimental condition, the method lacked in reproducibility as the amount of Panasil applied cannot be controlled nor can it be simultaneously applied over the 12 perforations. It was inevitable that the sample from one side out of the total 12 perforations was injected first on manual application of Panasil.

From the observations made by the use of different materials, it was concluded that rigid pillars serve a better concurrent sample injection condition, despite the carrier fluid leakage. To solve the problem, it was necessary to fabricate reusable pillars made of a sturdier material with similar design with a smaller gap between the perforation and the pillars.

4.5 Sample Pixelation, Injection, Transport and Stability

The final chip design was decided on the basis of the above tests on sample capturing conditions and the material for the micropillar manifolds. In all the following experiments, a multi-layered reversible microfluidic chip bonded by adhesion was used.

The final composition of the microchip was:

- (i) A PMMA slide (Figure 4.17B) with microarrayed perforations, used to “pixelate” or capture sample analyte from the surface into discrete microsized perforations simply by imprinting the PMMA slide onto the sample.
- (ii) A layer with microsized pillars (Figure 4.17A) matching precisely the sizes and the patterns of the pixelation holes, employed to mechanically inject the captured sample as arrayed droplets into a microchannel positioned below as a third layer.
- (iii) By the serpentine-like design of the microchannel (Figure 4.17C) the individual pixels are collected and can be transported linearly along the microchannel for a serial analytical processing, independent post-treatments, separation steps and analyses.

As defined here, each layer contributes to a specific role. The device design and realisation of microfluidic imaging is shown in Figure 4.17. Figure 4.17D shows the representative approach for the microfluidic imaging. Subsequent read-out is executed by fluorescence detection techniques as demonstrated in this study, or by coupling to any suitable analytical device. Reassembly by preserving the initial positions of the pixels finally enables the creation of an image. Along with an increased pixel number, the resolution of the image will enhance accordingly.

4.5.1 Experimental

Microfluidic device

The microfluidic chip comprises of three layers. A slide of PMMA, $24 \times 48 \times 1$ mm was cut out and $12 \times 300 \mu\text{m}$ diameter perforations were drilled with $800 \mu\text{m}$ spacing horizontal to the channel direction between the adjacent perforations. Two additional holes ($800 \mu\text{m}$) were drilled for the insertion of the tubes for the in- and outlet of the carrier fluid. Microfluidic serpentine-shaped channel of width and height of $300 \mu\text{m}$ were produced by moulding premixed polydimethylsiloxane (PDMS; Sylgard 184 Silicone Elastomer kit, Dow Corning) against the “master” frame, made out of drilled and filed aluminium block. For PDMS, monomer and curing agent were mixed at a ratio of 9:1 (w/w), degassed for half an hour, poured into the moulding structure and cured at ca. 60°C for an hour. Micropillar manifolds with dimension of $290 \mu\text{m}$ diameter and 1mm high, which are in perfect alignment with the perforations, were mechanically filed out of a block aluminium. The alignment of the adhered PMMA and PDMS layers against the micropillar manifolds was achieved by the aid of the two pins that pierce through the two layers, located at each end of the chip, when assembled. The PDMS microchannel layer is reversibly bonded onto the PMMA perforation layer, and can be readily removed for cleaning, changing of analytes or to allow different microfluidic channels. This chip design was used for all the following experiments.

Reagents

Agarose gel with different consistency varying from 0.05 to 1% (w/v) was cast in a Petri dish to test the viability of the pixelation technique to uptake samples from a surface of a soft material. In all the experiments, the samples are dissolved in an aqueous solution that contained 0.7% alginate to increase the viscosity of the sample. For visualisation of the concept in the first experiments, we used commercially available red food colour ($2 \mu\text{L}$ pure stock solution) and fluorescein ($2.5 \mu\text{L}$ fluorescein of a 10 mM aqueous solu-

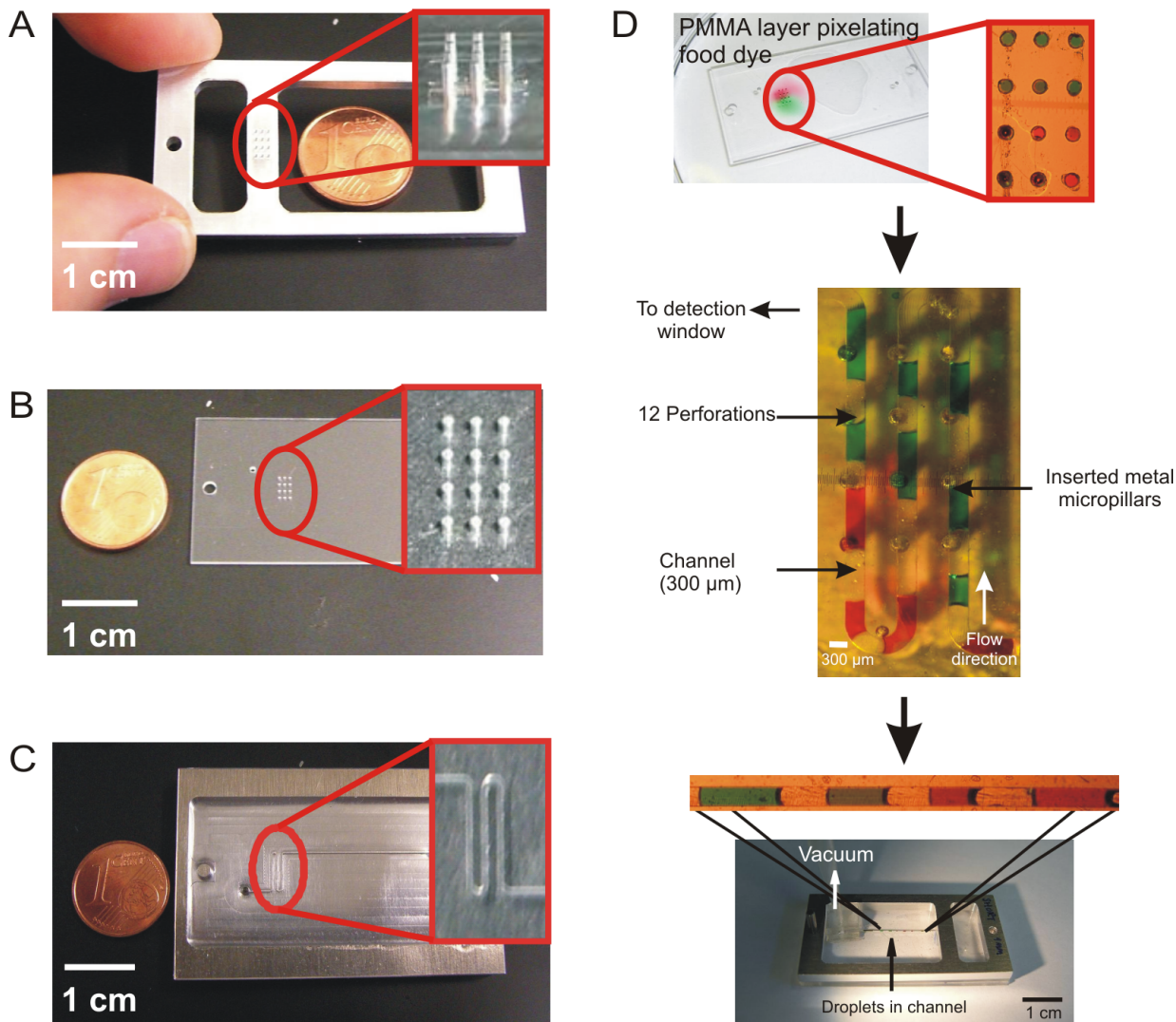


Figure 4.17: Exploded view of the microdevice. Micropillar manifold made of aluminium acts like pistons for parallel sample injection (A); perforations from PMMA sheet used to pixelate analyte (B), serpentine shaped microchannel cast from PDMS (C). The respective approach for microfluidic imaging (D). The sequence shows an example of the pixelated food dyes (red and green) from an agarose gel plate, followed by the injection of the captured samples into the 300 μm wide serpentine channel with 290 μm metal micropillars. Formed droplets are transferred to the detection window under vacuum. The blow-up shows the travelling droplets in the long channel.

tion), which were added respectively to 500 μL alginate solution and mixed well under vortex. For aqueous-in-oil experiments, 0.1% (v/v) Tween 20 (Sigma-Aldrich, Germany) was added to the fluorescein/alginate solution. For the first chip application test, an equal volume (1.5 μL) of 0.1 mM rhodamine B (Radiant Dyes Laser and Accessories GmbH, Germany) and 0.1 mM fluorescein in alginate solution was pipetted onto agarose gel. In the second application test, a heterogeneous sample was artificially created by spreading suspensions of wild type yeast cells and recombinant yeast cells expressing the enhanced Green Fluorescent Protein (eGFP) gene next to each other on the surface of 0.75% (w/v) agarose gel. The recombinant yeast cells contained the plasmid pAH56 and the protein synthesis was induced by galactose in absence of glucose.

Experimental setup

The freshly cured PDMS channel layer was adhered to an either 5min oxygen plasma treated (for aqueous-in-oil experiments) or non-treated (for aqueous-in-gas) PMMA perforation layer. The sample pixelation was carried out by direct placement of the PMMA perforation layer over the sample residing on the surface of 0.75% (w/v) agarose gel. Once the samples were captured in the perforations, PMMA layer was slowly lifted off from the agarose gel surface and any excess samples were carefully removed. The assembled device was mounted on a home-made microscope stage and positioned on an inverted microscope. Blue light (450-500 nm) or green light (510-550 nm) from a 100 W Hg-arc lamp was used for fluorescence excitation, and emitted light (>500 nm or >590 nm, respectively) was detected by a camera.

For the aqueous-in-oil experiment, mineral oil (Sigma-Aldrich, Germany) was supplied into the channel at the flow rate 20 nL s^{-1} using syringe pumps (neMESYS, Cetoni GmbH, Germany). To the channel completely filled either with oil or to the empty channel, the micropillar manifolds were inserted into the perforations, with the aid of two pins for alignment.

To realise the microfluidic imaging approach as described above, two challenges had to be addressed, which are discussed in detail in the following. Firstly, a procedure for sample loading and pixelation had to be developed and optimised, and secondly, the transfer of pixels into a serial droplet-based system had to be realised. In these experiments, the sample was food dye dissolved in an aqueous 0.7% alginate solution. Finally, we have shown the applicability of our concept by imaging heterogeneous samples, which was created on the surface of an agarose gel. As a model for a biological sample, recombinant enhanced green fluorescent protein (eGFP) expressing yeast cells (*Saccharomyces cerevisiae* Cen

PK (pAH56)) were used to test and prove the viability of the chip for the microfluidic imaging technique in terms of the fluorescent intensity measurement.

4.5.2 Sample Pixelation

Pixelation and upload of sample into the microdevice is a single-step process realised by stamping the PMMA layer with the integrated microholes onto the sample. After our first attempts, it turned out that this was not a straightforward process, and the hydrophobicity of the surfaces as well as the undersurface of the sample determined how efficient the pixelation step could be realised.

In order to decide the most suitable method for pixelation, a study investigating the viability of the pixelation technique for a sample was conducted and a comparison between manual direct pipetting, pixelation from a cover glass surface and agarose gel was made (Table 4.1). In all experiments, the transfer of the aqueous sample into the perforations was supported by oxygen plasma treatment of the PMMA layer for 5 min, which was rendering a hydrophilic surface.

Table 4.1: Comparison of suitable methods for pixelation from different surfaces. A method is considered “suitable” when creating least air spaces and bubbles in the 1mm deep perforations upon sample capture.

Surface material for pixelation	Manual pipetting	Cover glass	0.05% agarose gel	0.5% agarose gel	1% agarose gel	2% agarose gel
Suitable?	No	No	No	Yes	Yes	No
Reason	Uneven filling with air bubbles	Too high surface tension	Too fragile and watery, sample too diluted	Successful capture	Successful capture	Rigid and sticky

The sample used in this study was commercially available red food colouring dye mixed in unpolymerised 0.7% alginate solution. This was a suitable choice of sample as it is biocompatible especially for later applications and has a higher viscosity than an ordinary water based sample. As a consequence the surface retention power to keep the once pixelated samples in the perforations was higher in these samples.

Testing the pixelation efficiency of the PMMA perforation layer against rigid cover glass and soft agarose gel of different viscosities was investigated by the direct placement of the perforation layer over the sample. The PMMA layer placed over a cover glass forms more

air bubbles during the lift off of the chip, as the surface tension is higher between these two layers (Figure 4.18B), compared to PMMA against agarose gel (Figure 4.18A). The results showed that the best surface to capture the sample analyte was off from a soft surface, *i.e.*, agarose gel. Following this observation, different percentage of agarose gel, varying between 0.05 to 2% (w/v) was prepared to study the most suitable gel consistency. 0.05% is seen to be too fragile and watery for the sample to stay in place, whereas 2% is hard, thus creating a similar environment to the glass surface with an increased surface tension. It, therefore, was revealed that 0.5 to 1% is the most suitable consistency for pixelating the sample. For comparison, manual direct pipetting of sample into the 1mm deep holes was also conducted and turned out to be the least favourable method as it often creates air spaces in an uneven fashion and the filling of the perforations to their maximum volume is rarely achieved (Figure 4.18C).

As the results of the above findings, in the first half of the following experiments, 5min oxygen plasma treated PMMA perforation layer was used for pixelation of samples from 0.75% (a mean value) agarose gel surface.

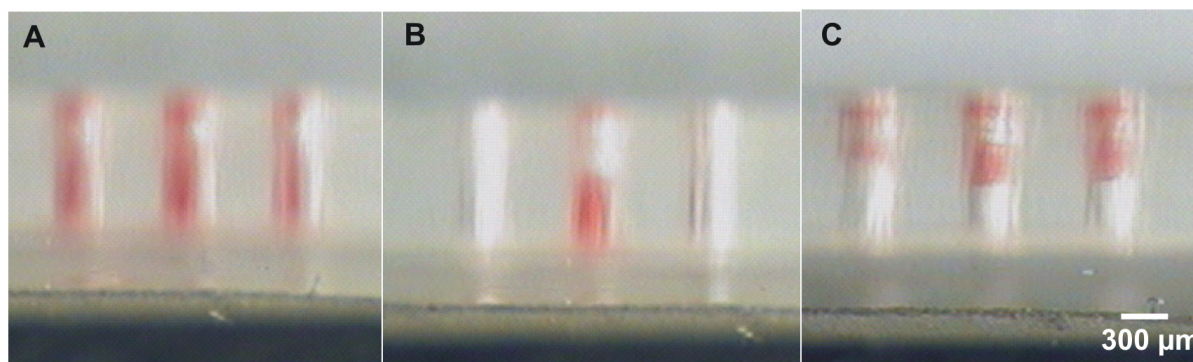


Figure 4.18: Efficiency of sample uptake using different techniques and surfaces. The photographs show the side view of PMMA perforations used for pixelation. The sample (here: 0.7% alginate with dye) was uploaded directly from the soft surface of 1% agarose gel (A), the rigid surface of a glass cover (B), manual pipetting (C). All perforations are filled completely in a one-step stamping process, when the sample is placed on a stable, but soft surface created *e.g.*, by 1% agarose gel.

4.5.3 Segmented Flow System

Once the sample was loaded into the pixelation holes, the whole device was assembled. First, a PDMS layer embedding a 300 μm wide and deep serpentine microchannel, with

the same dimension as the PMMA layer, is aligned with the perforations. The purpose for the serpentine channel shape is to permit concurrent collection and delivery of ordered droplets to the detection window. Second, individual samples pixelated in the 12 PMMA perforations were mechanically forced out, in piston fashion by micropillar manifolds with 290 μm pillar diameter. The micropillars are inserted into the countering holes with the aid of the metal pins positioned at two ends of the chip to help with the alignment. The chip construction allows easy implementation with a conventional inverted microscope, and arduous array preparation steps are avoided.

Aqueous-in-Oil Flow System

In the first experiments, the microchannels was initially filled with mineral oil as carrier fluid, at a flow rate of 20 nL s^{-1} , followed by non-flow condition during the injection step and an increased constant flow rate of 40 nL s^{-1} was applied for the transport step. Preliminary studies proved that upon insertion of micropillars into the perforations, injection of 12 consecutive droplets with an average volume of 50nL into the microchannel was possible and they were transported within the mineral oil carrier fluid, while conserving the same spacing as the perforations (800 μm), without coalescence in the channel (Figure 4.19). The average sample volume in aqueous-in-oil system was found to be smaller than the theoretical maximum possible volume per perforation, which is calculated to be 70 nL. This discrepancy can be explained by the loss of samples due to the surface tension that is created when the PMMA layer is pulled away from the gel surface.

The total flow rate of the mineral oil was varied between the lowest achievable 20 nL s^{-1} to 1 $\mu\text{L s}^{-1}$ for the sample transport, to confirm the reversibly bonded chip resistivity against the carrier fluid pressure.

The bottleneck in this setup is the introduction of a volume into an occupied space, *i.e.*, the injection of sample droplets into oil-filled channel. The law for the conservation of mass is disobeyed by the presence of incompressible oil. In order to lessen the interfacial energies between hydrophilic aqueous samples and hydrophobic carrier fluid during the injection step, experiments with 0.1% Tween 20 added to the aqueous sample was conducted. As surfactant is absorbed at the interfaces, it stabilises the flow against coalescence and obviates the sample leakage upwards. Despite the effort, the attempt to stabilise the interfaces seem to have resulted in the tailing and adhesion of the sample droplets to the walls made of PMMA. By the insertion of the micropillar manifolds, creation of

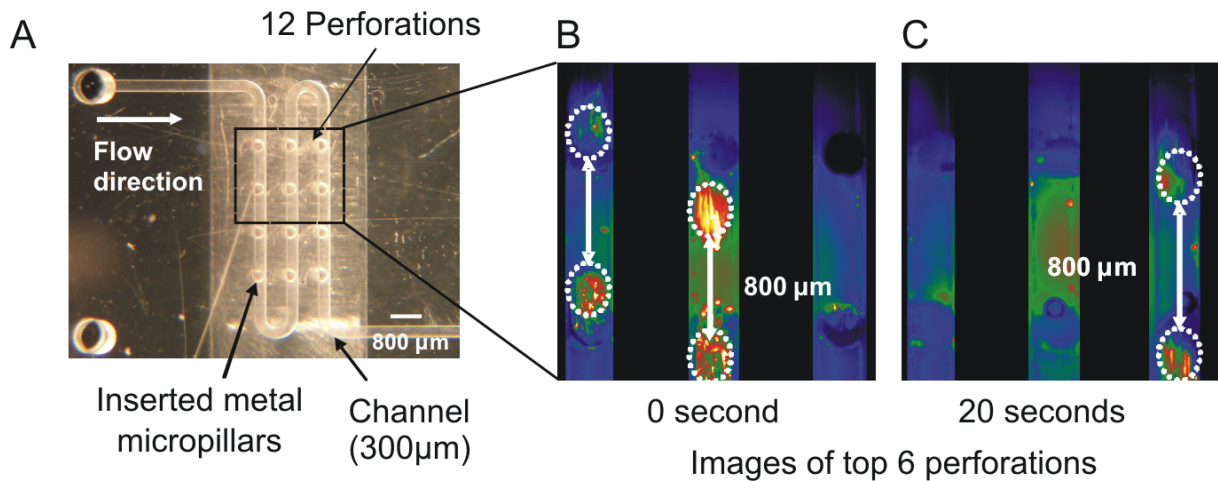


Figure 4.19: (A) Image of the perforation area design, (B) and (C) show pixelated fluorescent beads transported within the flow of a hydrophobe carrier fluid for subsequent analysis with the retention of droplet interspacing ($800\ \mu\text{m}$) at 0 and 20 seconds, respectively. Diffusion or coalescence of droplets could be avoided in the channel. Images have been masked for clarity.

air bubbles between the droplets and sometimes fission of the sample plugs into smaller droplets were also observed. Three-phase flow with gas bubbles placed between aqueous droplets in a carrier fluid has been proposed and demonstrated previously, especially to prevent the coalescence of plugs during flow [91, 92]. Gas bubbles can be effectively introduced as spacers between plugs to (1) minimise the relative motion of plugs and (2) to act as a physical barrier to prevent the coalescence of adjacent plugs during flow. While, in majority of the cases, droplet plugs (droplets that are large enough to conform to the cross-sectional area of the channel) moved at approximately the same velocity as the carrier fluid [74], the small, spherical droplets generated in these channels are expected to be moving much slower due to drag. Although recirculation within viscous droplets due to external surface shear reduces the Stoke's drag on droplet in comparison to a solid sphere [75], the droplet will be moving slower than the carrier fluid in the microchannel. Thus, small droplets have the capacity to move past gas bubbles in three-phase flow by travelling between the air bubble and the wall of the channel. In these scenario, adjacent plugs could contaminate one another despite the presence of gas spacers.

Aqueous-in-Gas Flow System

An alternative experimental condition was tested, where pixelated aqueous samples were delivered in the channel and gas was used as the carrier. The compressible nature of air as well as the permeability of PDMS for gas was thought to alleviate the leakage or fission of the sample droplets, otherwise expected to occur during the insertion of the micropillars. The injected droplets are transported along the serpentine microchannel by applying a vacuum at the end of the channel. Under this condition, successful injections of aqueous samples with a good reproducibility are observed. The injected sample volume follows a Gaussian distribution with 41.1 ± 10.5 nL per droplet (Figure 4.20) and the success rate for injection was found to be at an average of 95%, with a concave plug shape.

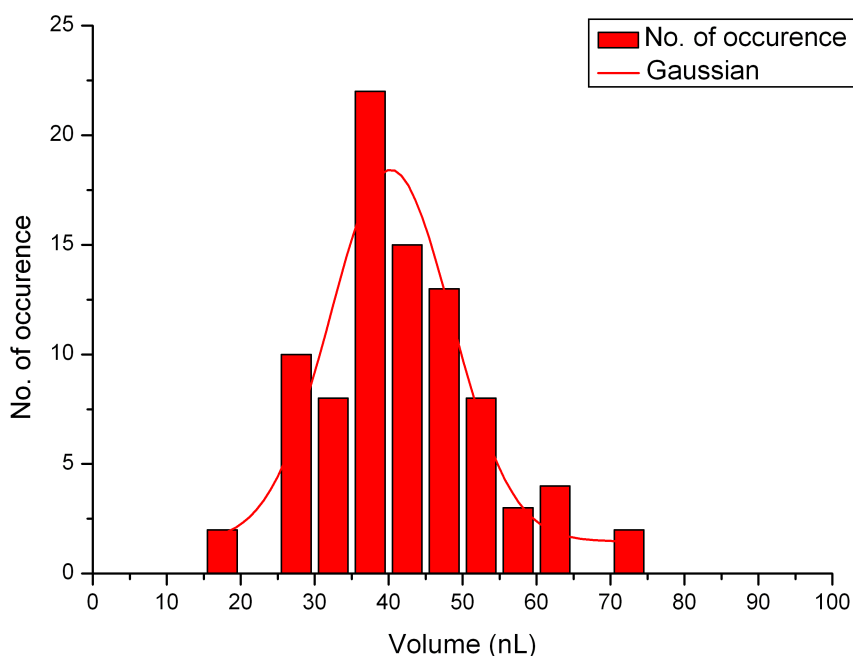


Figure 4.20: Distribution of the injected sample droplet size in the aqueous-in-gas approach with the average droplet size of 41.1 ± 10.5 nL.

What was noticeable from a series of measurements taken, however, was the decrease in the contact angle of the PMMA over repeated usage, which leads to an increased captured sample volume (Figure 4.21). In theory, from the dimension of the channel, for fully filled perforations (70 nL), an inter-spacing of $20 \mu\text{m}$ between two droplets is left, however, in practice there was more likelihood of the sample droplets fusing together. Moreover,

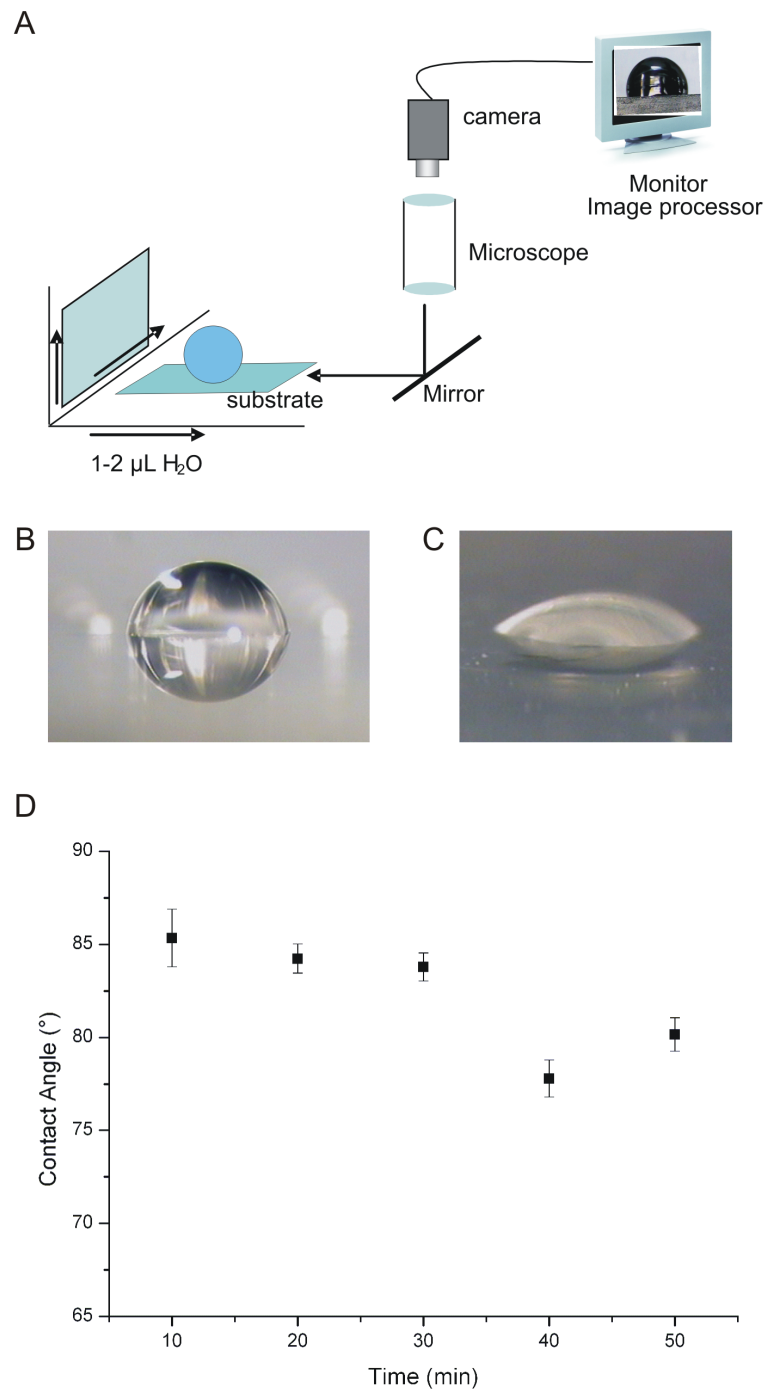


Figure 4.21: The contact angle measurements of a water droplet on the PMMA layer were taken on the same spot over five consecutive experiments, using the set-up (A). Typical contact angle profile of a water droplet on a hydrophobic (B) and hydrophilic (C) surfaces. The trend in the decrease of the contact angle is shown in the plotted graph (D). The reason for the fourth measurement being lower than the fifth can be due to the difficulty encountered during taking the images and the angle at which the image was taken.

this change in the contact angle is expected to have an affect on the flow profile of the sample droplets during the transportation step, as from the chip design, one side of the channel inner wall is composed of PMMA and the rest with PDMS. To avoid this problem, the consecutive use of one single PMMA chip was limited to twice and oxygen plasma treatment was avoided. This supports the observation that the injected sample volume per droplet in aqueous-in-gas system (41.1 ± 10.5 nL) is smaller compared to that of aqueous-in-oil system (ca. 50 nL), where plasma treatment was used. To prove the above statement, three sets of experiments were carried out. In the first, a series of measurements of the contact angle of a water droplet pipetted on the same spot of one PMMA layer over five consecutive experiments was taken. In between each run, the PMMA chip was subjected to exactly the same chip preparative method and the experimental condition as in one standard set of experiment. The results obtained was the decrease in the water droplet contact angle; it was understood that the surface hydrophobicity of PMMA decreases with time when left in constant contact with an aqueous environment or due to biofouling.

It is likely that with prolonged exposure to air, the surface hydrophobicity will return. To confirm this, a set of experiments where the contact angle measurements were taken every 30 min: at $t=0$ min, PMMA is at the normal state then for 30 min immersed in water. At $t=30$ min, measurements are taken, followed by 30 min exposure to air. The sequence was repeated until $t=12$ min. The time in between allowed for the expected surface condition recovery. A third set of experiment was carried out as a control test to examine whether the contact angle measured from different pieces of PMMA layers would fall within a reasonable margin. As the water droplet volume pipetted onto the PMMA surface had a volume of $3 \mu\text{L}$, evaporation by the lamp on the microscopy was rapid. The measurement from each droplet was taken as quickly as possible after being placed in the right position and the microscope focus was adjusted. The result showed that there is a significant change in hydrophobicity on the PMMA surface (Figure 4.22). As can be seen from the step feature of the graph, 30 min immersing in water alters the angle between 3 to 8 degrees. However, the hydrophobicity returns half as much the normal extent after exposing the surface to the ambient air. With an extended air exposure period, it is expected to recover fully. The average water droplet contact angle on a PMMA surface was calculated to be $86.67 \pm 1.93^\circ$. This proved that the initial measurements for the graph to show the decrease in the contact angle over repeated use fall in a reasonable region.

Attention should, however, be paid in aqueous-in-gas two-phase flow system as when motion is induced, contact angle disturbance increases the complexity of the system. In

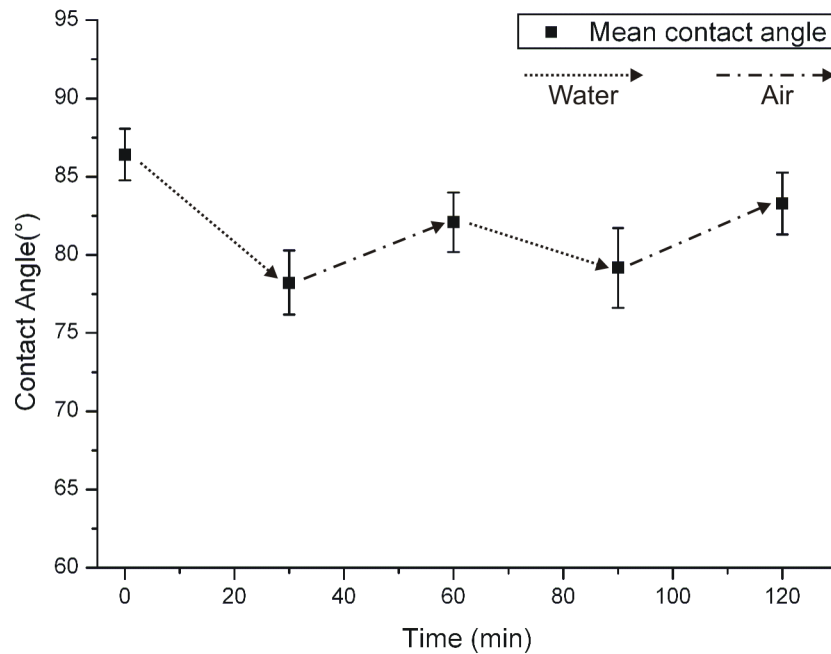


Figure 4.22: Average water droplet contact angle at $t=0, 30, 60, 90$ and 120 min after immersed in water or exposed to air. The variance in the surface hydrophobicity is reflected by the step feature of the plot. In 30 min, the surface regains more than half as much the original hydrophobicity. An average of a water droplet contact angle on a PMMA surface from different pieces was $86.67 \pm 1.93^\circ$.

a polygonal channel composed of N sides, the shape of a droplet depends on N and the contact angle θ [93]. When $\theta < \pi/N$, liquid fills the channel walls, and when $\theta > \pi/N$, liquid fills the entire channel cross-section. In a hydrophobic square channel ($N = 4$), a droplet is typically shaped concave as shown in Figure 4.23. The contact angle θ is the boundary condition that sets the shape of the liquid/gas interface. The contact angle is defined with respect to the liquid; the advancing contact angle is at the rear of the droplet and the receding contact angle is at the front of the droplet. As velocity increases, the advancing contact angle increases and the receding contact angle decreases. Thus, the droplet shape loses symmetry with respect to the direction of the flow. Since contact angles are influenced by roughness and heterogeneities of the channel wall [94], moving droplets may lose their symmetry with respect to the center axis of the channel. The complexity may further be amplified by the fact that three of the four sided walls are made of PDMS and one with PMMA. They have differing hydrophobicity, thus, could lead to difference in solid-liquid interfacial energy. In either material, as they are both hydrophobic with

respect to the sample, if too great a velocity is applied, droplet break-up is induced, which result in the loss of spatial information.

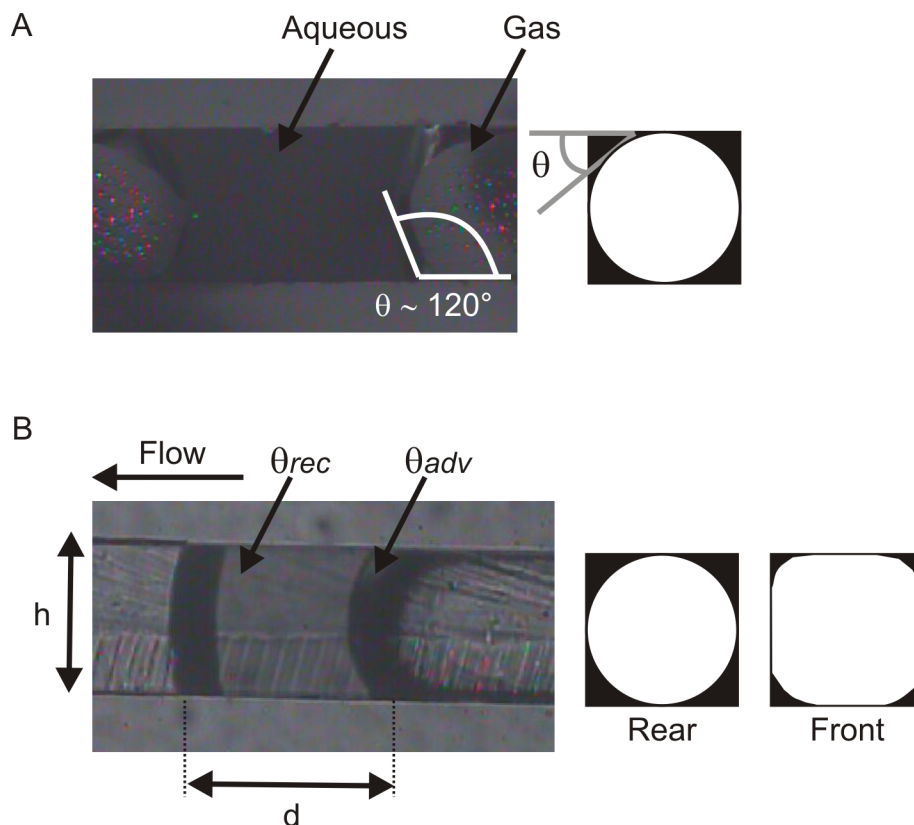


Figure 4.23: Contact angle of a typical droplet in the microchannel (A). Sample plug under vacuum (B). Next to the photos are the sketch of the corresponding front view of the contact angles, especially showing the difference between advancing and receding contact angles.

Despite a couple of points to bare in mind, the observations made showed that the aqueous-in-gas segmented flow serves a suitable environment for the simultaneous injection of the samples, while satisfying the purpose of retaining spatial orientation and heterogeneity of the planar samples.

4.6 Testing the Chip Application

In order to realise the functionality of the chip for microfluidic imaging purposes, a heterogeneous environment was manually created on a fixed area of an agarose gel plate, by pipetting an equal volume of two target analytes next to each other. At three different

steps throughout the experiment, *i.e.*, pixelation, injection and detection, appropriate images from every perforation or produced sample droplet were taken. The detection window was set at a fixed position along the straight channel.

4.6.1 Aqueous Dye Manipulation

As the first test model, solutions of rhodamine B (red fluorescent) and fluorescein (green fluorescent) were used. Two fluorescent dyes having different excitation and emission wavelengths created a heterogeneous condition, whereby the fluorescence intensity ratio (red/green) at each step was measured and plotted as a graph (Figure 5A). Droplet 1, 2, 7, 8, 9 and 10 correspond to perforations originally pixelating fluorescein having lower values of ratio and 3, 4, 5, 6, 11 and 12 rhodamine B with higher values of ratio. In the lower set of six perforations, however, a bigger deviation of the intensity ratio occurs between the pixelation and the injection steps. This tendency in loss of rhodamine B intensity was most probably caused by adsorption of the fluorophore to the PMMA layer. Once the samples were injected and droplets formed in the channel, no significant loss was observed neither in the fluorescence intensity nor in the ratio of intensities. The final reassembled image reflects the gradient of rhodamine B and fluorescein concentrations that have initially been created on the agarose gel plate.

4.6.2 Yeast Cell Manipulation

Bioanalytical application of the microfluidic system was tested on recombinant yeast expressing the enhanced Green Fluorescent Protein (eGFP). A population of non-eGFP and eGFP yeast was placed over the agarose gel plate. Droplets 1, 2, 7, 8, 9 and 10 correspond to perforations originally pixelating the area with non-eGFP yeast cells, reflected by the low percentage values. Droplets 3, 4, 5, 6, 11 and 12 correspond to eGFP yeast cell pixelated perforations having high percentage ratios (Figure 4.24B). The result shows that the ratio of the eGFP expressing and non-expressing cells were conserved with only little variation between each step of the experiment, representing the reliability and reproducibility of this microfluidic system in delivering pixelated samples to the detection window for sample analysis without loss of information. The efficient conservation of sample orientation and data acquisition has demonstrated a promising application of the microfluidic imaging chip.

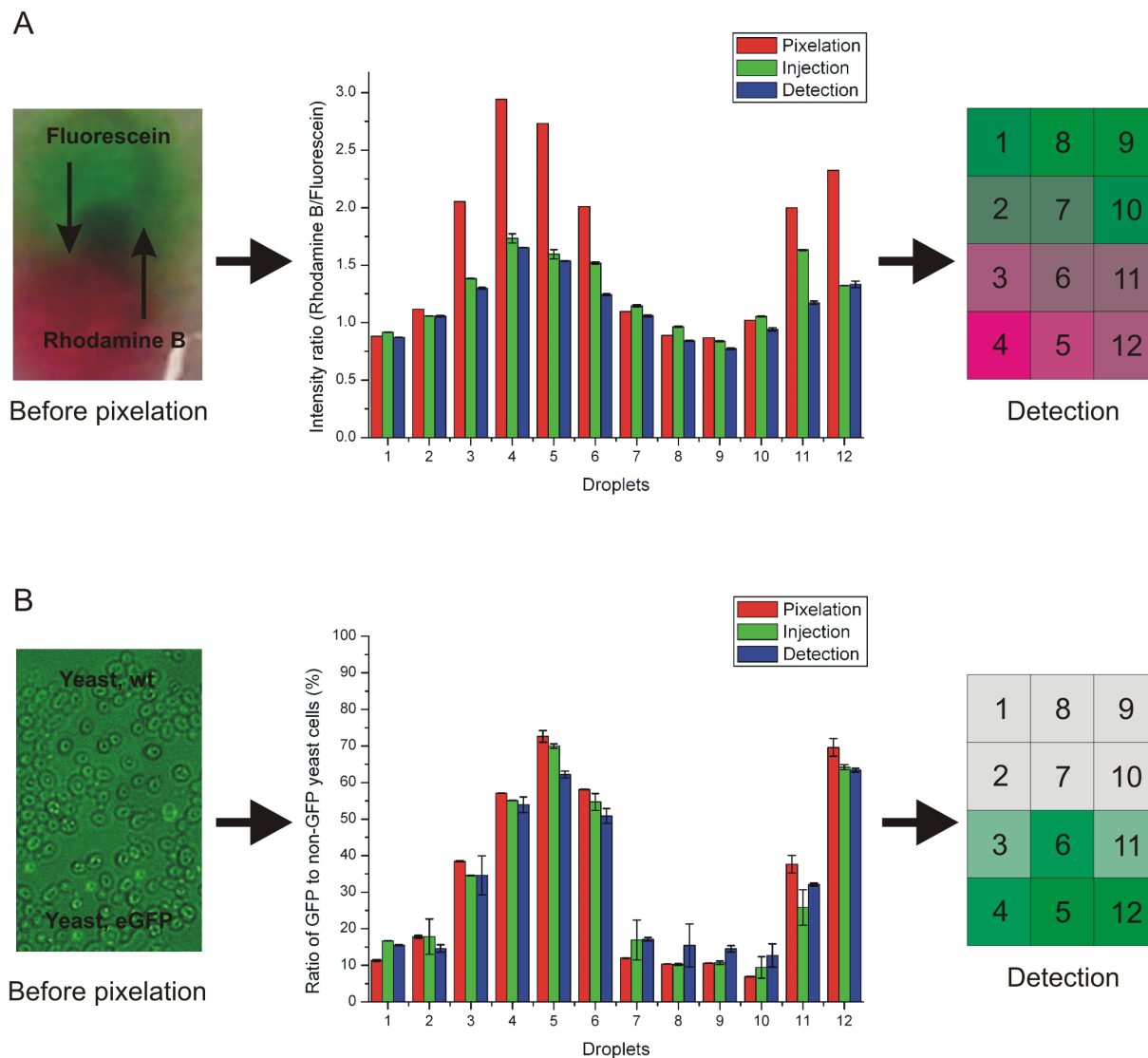


Figure 4.24: Measurement of the fluorescence intensity after the three main process steps pixelation, injection into the microchannel and serial readout at the end of the microchannel (here referred to “detection”). Aqueous dye manipulation (A): A gradient from red (rhodamine B) to green (fluorescein) fluorescence is created on an agarose gel surface. Mixing of the dye solutions occurred at the interface through diffusion. The ratio of the intensities indicates the colour (<1 : green-orange fluorescent, >1 red fluorescent). Yeast cell manipulation (B): The ratio of fluorescent (eGFP expressing) and non-fluorescent yeast cells is determined by counting the number of respective cells in each droplet. The insets show the grid diagrams to represent 12 perforations and their individual pixel ratios after the final detection step, using colour gradient respectively: yellow = fluorescein and magenta = rhodamine B, grey = non-GFP and green = GFP.

4.7 Summary

This research has successfully demonstrated that the multi-layered chip accommodated by micropillar manifolds can spatially resolve the chemical composition of biological samples by pixelation within microfluidic platform. The proof-of-principle experiments accomplished with fluorescent dyes and yeast cells suspended in a two-phase microflow suggest that it is capable of obtaining non-averaged data by distinguishing and conserving the sample spatial heterogeneity in droplet forms. The ability to convert the acquired compartmentalised information from a parallel to serial manner is an advantage this device has allowing to approach closer to automation and to implement preparation, separation and detection steps. The utilisation of agarose gel as a feasible surface material for pixelation opens up possibilities for wider applications for this device, particularly to immobilise and capture cells. Moreover, alginate as the sample analyte solution also holds potential for further biological applications described in several recent publications, as it meets the demands of biocompatibility and long-term integrity [95,96].

While successful proof-of-principle experiments was achieved under aqueous-in-gas condition, the most significant draw back was the low transport velocity of the sample droplets. Flowing the appropriate solvent through the channel can be used to control and modify the channel surface properties. It is, thus, also significant to investigate adequate experimental conditions for aqueous-in-oil, as they possess several advantages depending on the post sample treatments. For instance, the presence of oil in the channel provide an even inner channel wall environment that surround the droplets. This will enable investigations of various samples regardless of sample types. The small internal volume of the droplets would create an ideal platform for carrying out small scale biochemical reactions while offering an isolated condition that alleviate any sample evaporation or contamination. Moreover, the droplets can be flowed under increased velocity. Nevertheless, it is necessary to remove the oil phase prior to the post sample treatment. The advantages and disadvantages of both aqueous-in-oil and aqueous-in-gas systems are outlined in Table 4.2.

Table 4.2: Advantages and disadvantages of the aqueous-in-oil and -gas systems.

	Advantages	Disadvantages
Aqueous-in-oil	<ul style="list-style-type: none"> • Same channel wall environment ; oil creates an even condition in the inner channel wall • Faster flow rate possible 	<ul style="list-style-type: none"> • $V \neq 0$; oil and sample leakage upon injection • Non-moving sample plugs • Post sample separation required
Aqueous-in-gas	<ul style="list-style-type: none"> • No sample leakage • Compressible ; $V = 0$ can be kept • Post sample separation not required 	<ul style="list-style-type: none"> • Inner wall environment control necessary • Slow sample flow ; sample break-up observed at high speed

To realise the goal of μ TAS, further miniaturisation of the system and integration of sample pre-treatment steps are currently underway. It is of particular importance to apply this novel concept not only to already spatially heterogeneous samples but also to a homogeneous sample that have undergone screening assays or different sample pre-treatments, which as a consequence generates a heterogeneous environment. For a brief explanation on the specifics of the experiment, see Appendix A.1.

Towards Electrophoretic Focussing of Amino Acids

The analysis of amino acid is of high importance as they are key elements of living organisms. Derivatisation, separation and detection of amino acids have been accomplished within microfluidic devices while employing many different strategies. Virtually zero-dead volume interconnections and fast mass transfer in small volume microchannels enable dramatic decreases in on-chip derivatisation reaction time, while only minute amounts of sample and reagent are needed. Simple, selective yet sensitive methods to quantify low-abundance materials derived from complex samples are required especially after sample pixelation.

The goal of this study was to implement the described pre-concentration method, sometimes also referred as stacking or focussing, by Valussi [97] as a supporting tool for the “microfluidic imaging” concept. The experiments presented here were conducted before the contents of Chapter 4. In this pre-concentration method, the presence of a gel-buffer interface gives rise to differing values of EOF. This feature was used to investigate on-chip extraction and stacking of amino acids. A mixture of amino acids with different electrophoretic mobilities focus at different points along their migration path. Separate signals are obtained when a reverse biased voltage is applied.

In the original work, the requisite of this method was to perform investigation of finger prints at forensic science scenes. The application of a suitably designed and fabricated microfluidic chip was tested to the analysis of real finger print samples (Figure 5.1). In this study, Valussi’s pre-concentration method was adapted and the new chip design functionality was tested. As a model sample amino acids were used instead of finger prints to determine the conditions for concentrating a small volume sample at a low concentration.

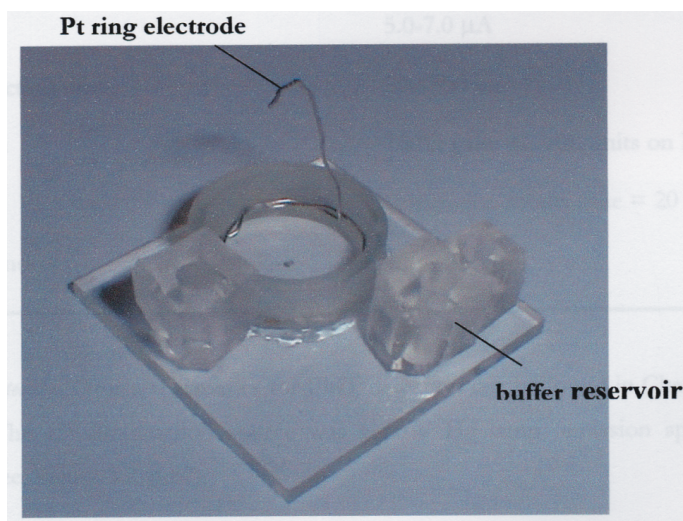


Figure 5.1: A photo of the chip construction. [Courtesy Thesis Valussi [97]]

Herein, a brief introduction to already existing pre-concentration techniques, basic mathematics and a specific theoretical scenario of Valussi's stacking method precedes detailed discussions of the results obtained in the experiments.

5.1 Existing Pre-concentration Techniques

While microfluidic devices have a large number of advantages (see Section 2.2), they tend to suffer from the disadvantage that the sample is usually present at very low concentration in very small volumes. Often, the amount of analyte may fall near or below the detection threshold for the analytical system. In conventional scale operations, material can be provided in much larger volumes and concentrated prior to analysis, using conventional off-line concentration methods, such as filtration, chromatography and evaporation. These methods, however, do not lend themselves to microscale quantities of material. Accordingly, it would be desirable to be able to perform an online sample concentration operation on microfluidic devices to increase the concentration of an analyte of interest above detection sensitivity. Pre-concentration, for this reason, is for instance utilised in capillary electrophoresis and electrochromatography to enhance the detection of analytes [98].

Although there already exist various sample enrichment methods addressing the problem of on-chip detection limits by concentration, a highly reproducible and efficient concentration method with minimal microfabrication complexities has been elusive. One technique that is commonly utilised for focussing DNA, proteins or fluorescent samples is sample

stacking [99, 100] or isotachopheresis [101–104]. It is implemented by applying electrical fields to channels containing plugs of buffers with different conductivities for concentrating analytes with different mobilities. For example, field-amplified sample stacking (FASS) [102, 105–107] is one of the simplest enrichment methods and can achieve up to 1000-fold enrichment of fluorescein and Bodipy with, respectively, 2 μM and 1 μM initial concentrations [102], but requires at least two buffer solutions and a relatively large amount of chip space.

Another method for pre-concentration is dialysis or the use of selectively permeable membrane [108–110]. Non-permeating analytes become concentrated at the interface, and can be subsequently analysed. With this technique, β -galactosidase and ovalbumin were concentrated at 600-fold [111] and proteins with molecular weight larger than the threshold was concentrated up to 10,000-fold [112] have been achieved. They used cover plate bonded with a silicon adhesive and a membrane fabricated by laser-induced polymerisation, respectively. The drawback of this method is the necessity of fabricating specific membranes in microfluidic devices. A microfluidic separation device presented by Zeng *et al.*, on the other hand, incorporates self-assembled colloidal arrays and in situ colloidal crystallisation [110]. Differently sized silica microspheres and polystyrene beads were utilised to form a three-dimensional nano-sieving system, where 100–2000 bp DNA fragments and SDS-denatured proteins were separated (Figure 5.2). This approach reflects simple, fast and economic fabrication of a 3D molecular sieving structure into microfluidic systems, which the performance is comparable to the conventional gel/polymer matrices.

Perhaps the most common pre-concentration technique is solid-phase extraction (SPE), where analytes (*e.g.*, hydrophobic) are adsorbed onto a solid medium, allowing contaminants (*e.g.*, hydrophilic) to be rinsed away [113–116]. Although yielding in concentration factor of more than 1000 for peptides and green fluorescent protein has been reported [114], it involves the complexity of incorporating appropriate capture and release chemistries inside a microchannel. Temperature gradient focussing (TGF) [117] is capable of achieving extremely high enrichment factors ($>10,000$ in 40 min), but it requires special buffers, a high operating voltage (~ 1000 V), and precise temperature control.

Table 5.1 summarises the characteristics of the described pre-concentration techniques as well as other well-known pre-concentration methods, such as micellar electrokinetic chromatography (MEKC) based on micellar solubilization as well as electrophoretic migration [118, 119] and entropic trapping that rely on periodically varying depths of the channel to trap analytes [120].

Table 5.1: A table summarising some of the existing online pre-concentration techniques.

Method	Enrichment Factor	Enrichment Time (min)	Only one buffer?	Small chip space?	Ref.
Isotachopheresis (ITP)	10-560	<1	No	No	[101, 103, 104]
Field-amplified sample stacking (FASS)	10-1000	2	No	No	[102, 105–107]
Dialysis	600-10000	<2	Yes	Yes	[108–112]
Solid-phase extraction (SPE)*	80-500	2	Yes	Yes	[113–116]
Micellar electrokinetic chromatography (MEKC)	450	<1	No	No	[118, 119]
Temperature gradient focussing (TGF)**	10000	40	Yes	Yes	[117]
Entropic trapping	100	4	Yes	Yes	[120]

* Complexities of immobilised phase incorporation, effective eluent needed.

** Careful choice of temperature sensitive buffer, bulky metallic thermostat used.

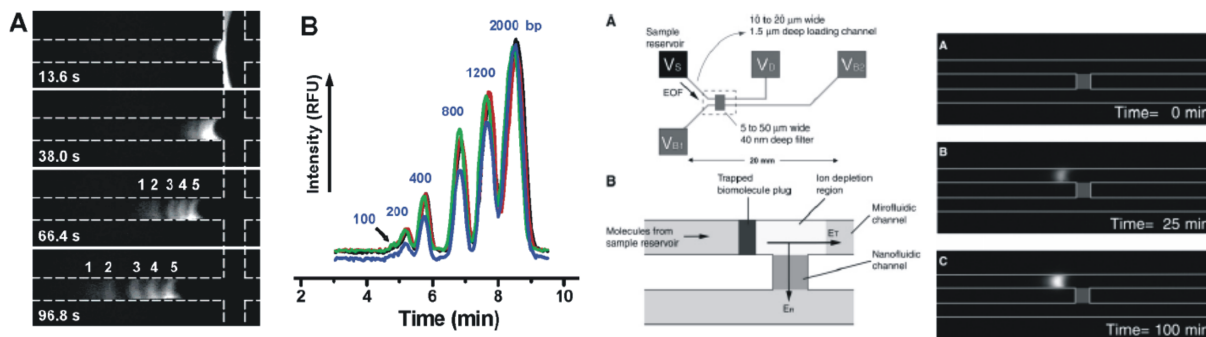


Figure 5.2: Published work on pre-concentration method. Fluorescent images and electropherogram for the electrophoretic separation of DNA fragments (Ref. [110]). Microfluidic sample pre-concentration device based on the electrokinetic trapping mechanism enabled by nanofluidic filters (Ref. [109]).

5.2 Mathematics for Electrophoretic Sample Stacking

To help understand Valussi's pre-concentration theory, some of the fundamentals, common terms and various electrophoretic focussing techniques usually associated with pre-concentration are briefly described.

5.2.1 Electrophoresis and Mobility

Electrophoresis is the process of moving charged molecules in solution under the influence of an electric field. This movement is due to the Coulomb force, which is related to fundamental electrical properties of the analyte and the ambient electrical conditions by the equation given below. F_e is the Coulomb force, q is the charge carried by the analyte, E is the electric field:

$$F_e = qE \quad (5.1)$$

The resulting electrophoretic migration is countered by forces of friction, F_f , such that the rate of migration is constant in a constant and homogeneous electric field:

$$F_f = vf \quad (5.2)$$

where v is the velocity and f is the frictional coefficient.

$$qE = vf \quad (5.3)$$

For a spherical ion, the frictional force can be given by:

$$F_f = -6\pi\eta rv \quad (5.4)$$

where η is the solution viscosity, r is the ion radius and v is the ion velocity.

Separation by electrophoresis is based on differences in solute velocity in an electric field. The velocity of an ion can be given by:

$$v = \mu_e E \quad (5.5)$$

where v is the ion velocity, μ_e is the electrophoretic mobility and E is the applied electric field. The electric field is a function of the applied voltage and capillary length (V cm^{-1}).

The electrophoretic mobility, often called as “mobility”, is a constant which is characteristic for a given ion and medium. The mobility is the proportionality coefficient, which is determined by the electric force that the molecule experiences, balanced by its frictional drag through the medium. That is,

$$\mu_e = \frac{F_e}{F_f} \quad (5.6)$$

During electrophoresis, a steady state defined by the balance of these forces, is attained for a spherical ion. At this point the forces are equal but opposite and thus,

$$0 = qE - 6\pi\eta rv \quad (5.7)$$

For a molecule, a factor, μ_e should be introduced to Eq. 5.7. Solving for velocity and substituting Eq. 5.7 into Eq. 5.5 yields an equation that describes the mobility in terms of physical parameters,

$$\mu_e = \frac{q}{6\pi\eta rv} \quad (5.8)$$

From this equation it is evident that small, highly charged species have high mobilities whereas large, minimally charged species have low mobilities.

Because mobility of molecules depend both on the particle properties (e.g., surface charge density and size) and solution properties (e.g., ionic strength, electric permittivity, and pH), electrophoresis has been extensively developed for molecular separations. As an analytical tool, electrophoresis is simple and relatively rapid. It is used chiefly for analysis and purification of very large molecules such as proteins and nucleic acids, but can also be applied to simpler charged molecules, including charged sugars, amino acids, peptides, nucleotides, and simple ions. Highly sensitive detection methods have been developed to monitor and analyse electrophoretic separations.

5.2.2 Electroosmotic flow (EOF)

The velocity of an ion in capillary electrophoresis (CE) is not only determined by the electrophoretic velocity. Electroosmotic flow (EOF) occurs when an electric field is applied over a silica capillary containing a buffer solution. As shown in Figure 5.3, EOF is caused by the electrical double layer that develops on the capillary surface. The inside wall of the capillary is negatively charged above pH 3, due to ionisation of the silanol groups

(Si-OH) on the silica surface. The cations in the buffer then move and gather adjacent to the negative capillary surface to form an electrical double layer. The cations on the outer layer, which are solvated, are attracted towards the cathode (negative electrode) and drag the bulk buffer solution along with them to form EOF in the capillary.

The EOF velocity in a capillary is given by

$$v_{EOF} = \mu_{EOF} E = \mu_{EOF} \frac{V}{L} \quad (5.9)$$

where v_{EOF} is the EOF velocity, μ_{EOF} is the EOF mobility, E is the applied electric field in $V\text{ cm}^{-1}$, L is the capillary length and V is the applied voltage.

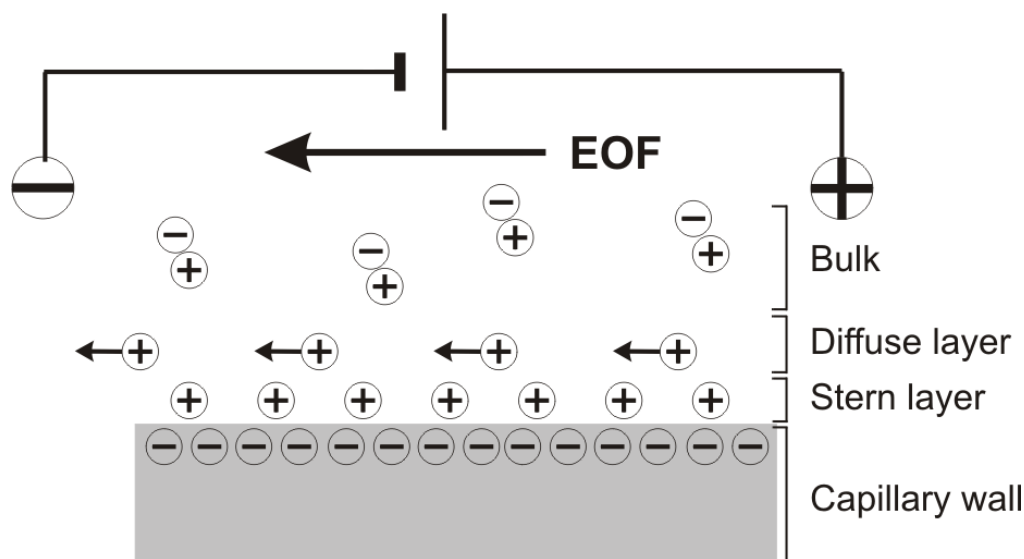


Figure 5.3: Schematic representation of the EOF induced by charge differences in the double layer. The total number of positive and negative charges is exactly the same (electro neutrality). Because of freely moving cations in the diffuse layer the bulk is moving toward the cathode.

5.2.3 Electrophoretic focussing

In miniaturised systems, electrophoretic focussing can be accomplished by balancing the electrophoretic velocity of the analyte against the bulk flow of the buffer in the absence or presence of gradients. In presence of gradients, differently charged analytes seek a unique equilibrium position along the migration path. At the equilibrium point, the net force on the molecule or particles reaches zero. As a consequence, a sharp stationary zone is

formed, at which the analytes are concentrated. Giddings and Dahlgren [121] first provided a general theoretical treatment of an equilibrium-gradient method (Figure 5.4).

An important advantage of equilibrium gradient methods is that on-line focussing and concentration of analytes occur simultaneously during the separation process. Depending on the properties of the analytes, various applied forces/gradients are possible to perform equilibrium gradient focussing.

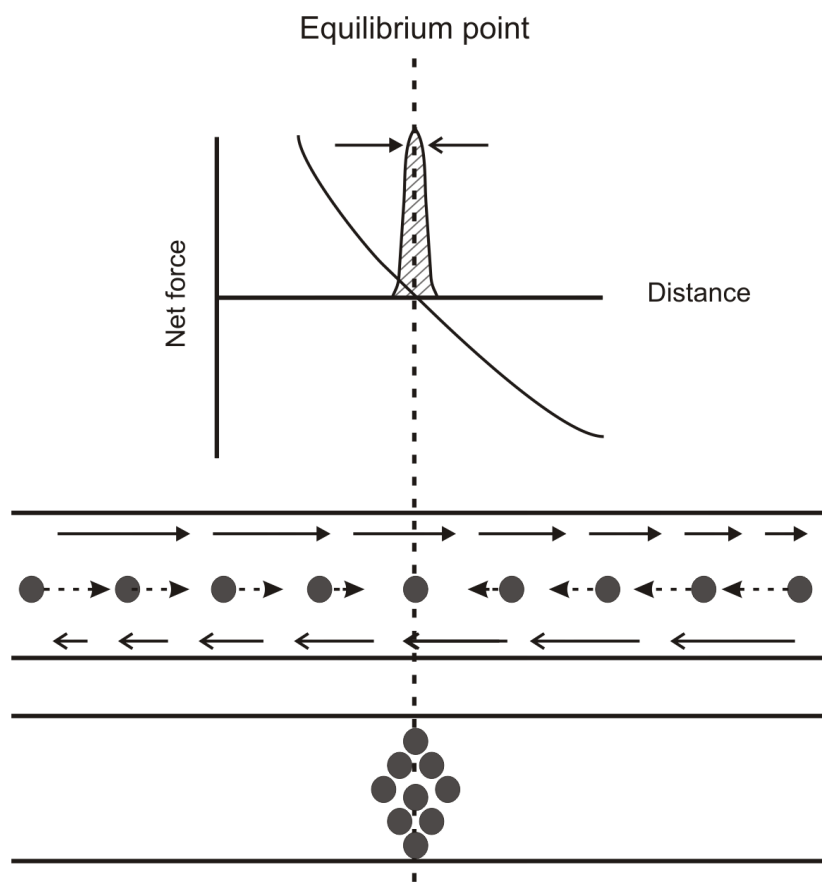


Figure 5.4: Schematic of an equilibrium gradient showing sample analytes focussing as they reach an equilibrium. The solid curve and the dashed arrows represent the net force on an analyte, the solid arrows show the direction and the magnitude of two counteracting forces, the dashed line down the middle represents the position of the equilibrium point, and the dash-filled shape is the profile of the focussed band.

5.2.4 Field-amplified sample stacking (FASS)

FASS uses gradients in electrolyte conductivity to subject sample ions to non-uniform electric fields. As shown in the schematic (Figure 5.5), sample ions are dissolved in a

relatively low conductivity electrolyte which has a high electrical resistance in series with the rest of the background electrolyte. This high resistance results in large electric fields within the sample and, therefore, large local electrophoretic velocities. Sample ions stack as they move from high field, high velocity region to the low field, low velocity regions, near the interface between regions of high and low conductivity. This stacking increases sample concentration and results in an increased signal.

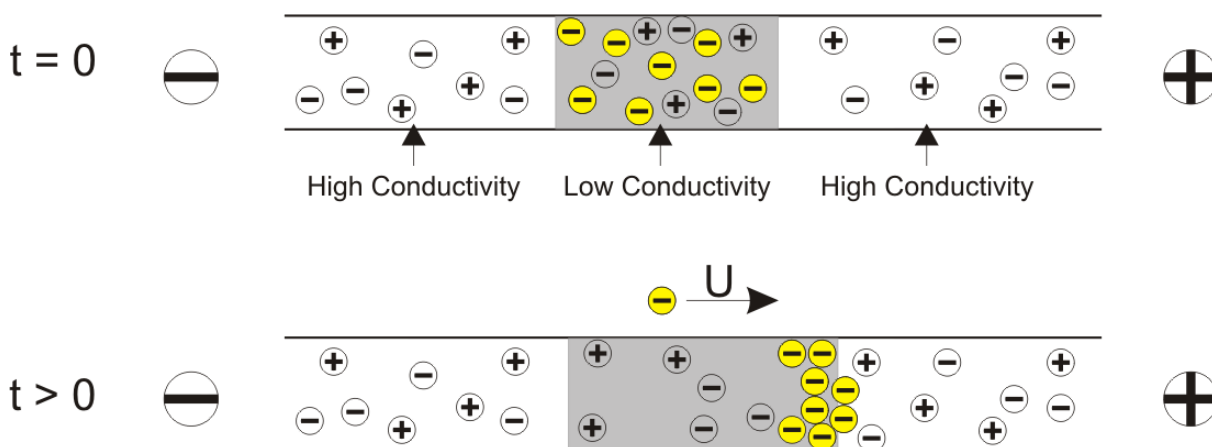


Figure 5.5: Schematic of FASS showing anionic species (in yellow) stacking in the absence of EOF. A gradient in the background electrolyte ion concentration is established with the sample in the low conductivity zone. Upon application of an electric field, the axial gradient in conductivity results in an electric field gradient. As sample ions exit the high field/high electrophoretic velocity region and enter the low velocity region, they locally accumulate and increase in concentration.

5.3 Theory of the Gel-Buffer Interface Pre-concentration Method

The functional component of the pre-concentration method implements an agarose gel plug (zero EOF) at the end of the microfluidic channel to create a gel-buffer interface (Figure 5.6). When an appropriately biased voltage is applied, a mixture of amino acids with different electrophoretic mobilities should give rise to separate signals that focus at different points along their migration path. The forces opposing are dominantly EOF of the buffer and electrophoretic mobility of the analytes. After a successful production of the pre-concentration band, the electrical field is reversed for the mobilisation step. The

focussed band is mobilised to separate and detect the individual analyte component in the pre-concentrated zone.

The pre-concentration is induced by the synergic contribution of the geometry of the field and the counteraction of the bulk flow in the channel, which result in the analyte focussing in proximity of the gel-buffer interface. The combination of the gel-buffer configuration, the electrical properties of the gel and the presence of a disk electrode is expected to give rise to several phenomena, when a potential difference is applied across the disk electrode and the wire electrode in the buffer reservoir.

There are mainly three types of phenomena that can contribute to the production of the sample concentration band, namely, the electric field amplification, the counteraction of the bulk flow at the interfaces and the electric field gradient, which are explained in detail in Ref. [97]. Here, a brief summary will be made.

5.3.1 Effect of the electric field amplification

The gel plug prepared have lower conductivity values than the running buffer (gel:buffer = $\sigma_1 : \sigma_2 \approx 1:10$). This condition satisfies FASS to be created and allows sample stacking to result from the movement of the analyte ions across the stationary boundary between gel and buffer. Due to the difference in conductivity between the gel and the buffer regions, the ions would experience a lower electric field in the buffer in the channel than in the gel. Thus, they would slow down once crossed the boundary and stack, according to the reduced electrophoretic velocity.

In an equilibrium, the region of constant cross-sectional area across the gel-buffer interface has a constant current density, thus,

$$E_1\sigma_1 = E_2\sigma_2 \quad (5.10)$$

which can be rearranged to

$$\frac{E_1}{E_2} = \frac{\sigma_2}{\sigma_1} \quad (5.11)$$

where σ_1 and σ_2 are the conductivities, with $\sigma_2/\sigma_1 = 10$ and E_1 and E_2 are the electric field experienced by the ions in the gel and buffer respectively. E_1 and E_2 can be replaced

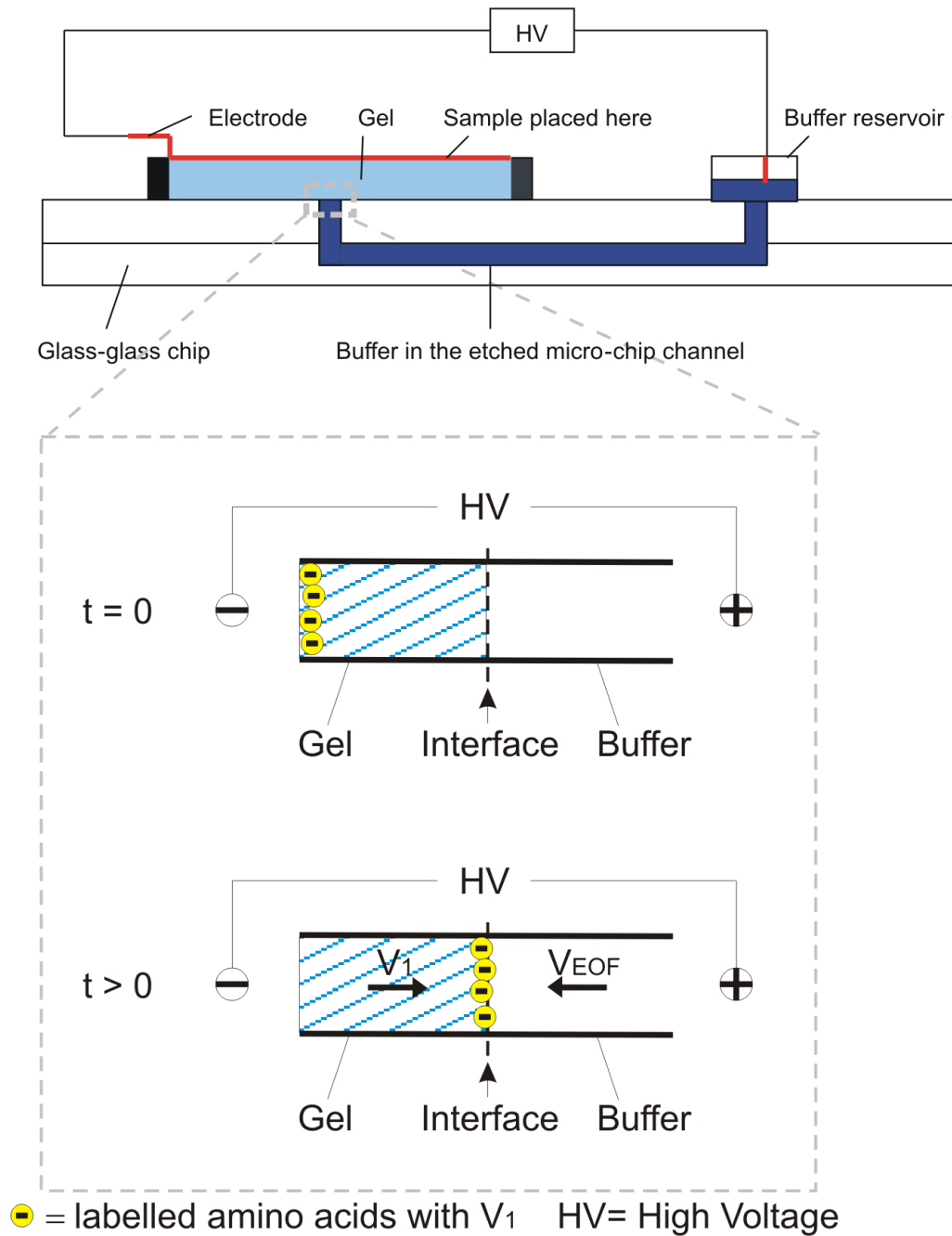


Figure 5.6: Schematic illustration of the side view of the microfluidic chip layout. In the blow-up window is the scheme showing the migration followed by stacking of the labelled amino acid at the gel-buffer interface as the result of the different electrophoretic velocity profiles of the absolute electrophoretic velocity v_1 , v_2 and v_{EOF} .

by v_1 and v_2 , the absolute electrophoretic velocities of the respective component (from Eq. 5.5). Therefore we have

$$\frac{v_1}{v_2} = \frac{\sigma_2}{\sigma_1} \quad (5.12)$$

5.3.2 Effect of the counteraction of the bulk flow at the interface

Presence of EOF in the channel makes the apparent velocity of the analyte ion in the channel v_{app} to be the sum of its absolute electrophoretic velocity in the buffer v_2 and the convective velocity of the buffer, which corresponds to the electroosmotic velocity v_{EOF} (assuming a constant and equal level of fluid in all reservoirs).

For anions, upon the application of the negative potential difference between the disk (cathode) and the wire electrode in the buffer reservoir (anode), the counteraction of the EOF in the channel could result in three different situations (Figure 5.7):

1) $|v_2| > |v_{EOF}|$:

Assuming $(v_2 + |v_{EOF}|)$, v_{app} is strong enough to counter-balance v_1 , the sample ions slow down and are concentrated in the buffer phase. On reversal of the potential difference, all the sample will be transported toward the anode. The concentration efficiency will, however, be decreased and band broadening is observed, if v_{EOF} is too low.

2) $|v_2| = |v_{EOF}|$:

The ions stop at the gel-buffer interface with half of the sample in the gel and the other half in the buffer phase. On reversal of the potential difference, the sample residing in the gel phase will migrate back toward the cathode.

3) $|v_2| < |v_{EOF}|$:

With a high v_{EOF} , the ions are pushed backwards, toward and into the gel until they reach an equilibrium point. Although diffusivity of the ions in the gel is lower than in the buffer, and it can be expected that they remain within a region adjacent to the gel-buffer boundary, upon potential difference reversal, the sample ions in the gel phase will migrate back toward the cathode.

In all the above situations, while assuming v_1 is much greater than v_{EEO} , the concentration enhancement depends on the width of the focussed zone, which in turn, depends on the steepness of the gradients. Importance, therefore, should be emphasised on controlling the balance between v_1 , v_2 and v_{EOF} to try and achieve situation 1 ($|v_2| > |v_{EOF}|$).

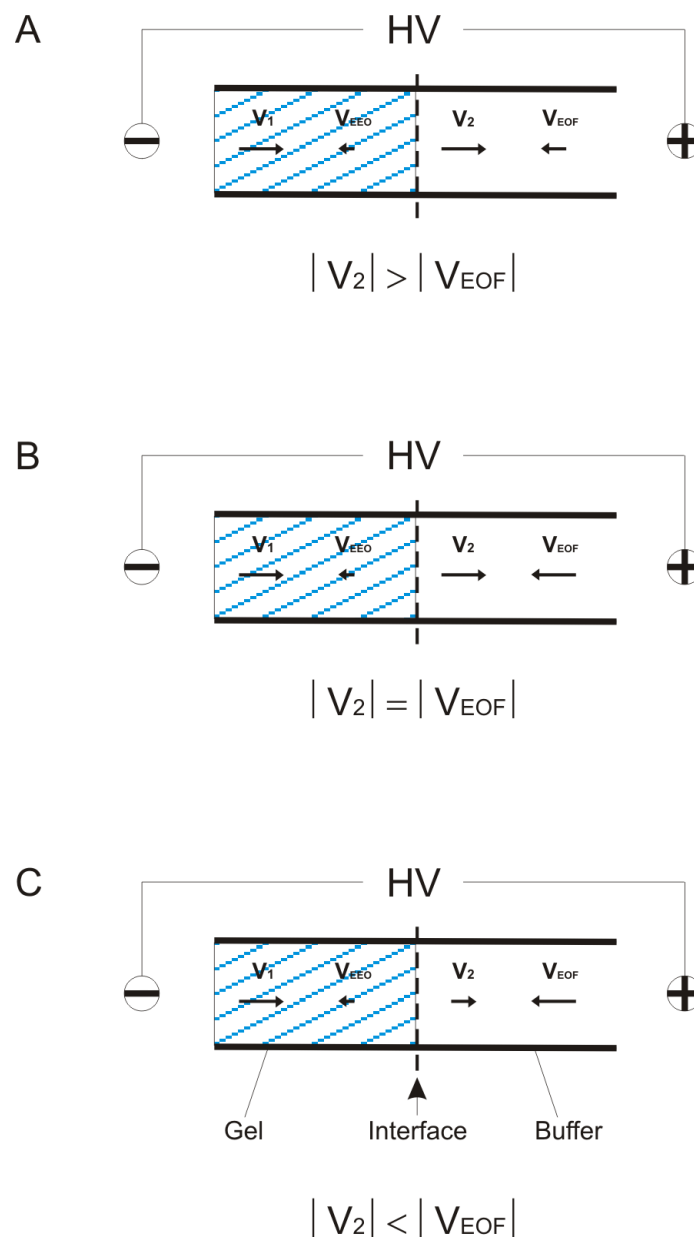


Figure 5.7: Schematic drawing showing the effect of the counteraction of the bulk flow at the gel-buffer interface. The behaviours of the ions under three different situations:

- 1). weak EOF in the channel, $|v_{EOF}| > |v_2|$. The ions slow down and stack.
- 2). Equal velocities. $|v_2| = |v_{EOF}|$, $v_{app} = 0$. The ions stop at the interface.
- 3). strong EOF, $|v_2| \ll |v_{EOF}|$. The ions are pushed back into the gel.

However, under these experimental conditions, the effect of the law of conservation of mass should also be taken into consideration. v_1 and v_2 are the movement of small ions whereas v_{EOF} is the movement of a bulk flow. When a high potential is applied across the channel, the flow dynamics in the the channel and especially in the proximity of the interface will be impacted. EOF generates a pressure against the gel. This as a result will have a negative effect on the focussing efficiency. Two plausible consequences expected are given:

A) Recirculation of the buffer may occur as a result of the higher hydrodynamic resistance of the gel compared to water and the dimensions of the gel. This phenomenon would be expected to lower the efficiency of the focussing by enhancing dispersion and to cause extra band broadening, during mobilisation.

B) The pressure generated may be strong enough to lift the gel. In this case, a water layer between gel and glass caused by the continuous convective outflow of the buffer, pushed electroosmotically toward the cathode could be postulated. Compositional changes in the gel will occur and, as a result, a conductivity gradient may be produced in the gel.

5.3.3 Effect of the electric field gradient

The electric field gradient is created initially, by the geometry of the disk electrode and then, by the drastic change in the volume through which the total current flows. The electric field concentrates closer to the gel-buffer interface, thus the velocity of the ions would increase where the field strength is higher. The existence of this electric field gradient causes electro focussing to occur in the gel, at a point where the electric force nullifies.

As an example, fluorescamine labelled glycine and aspartic acid are considered (Figure 5.8).

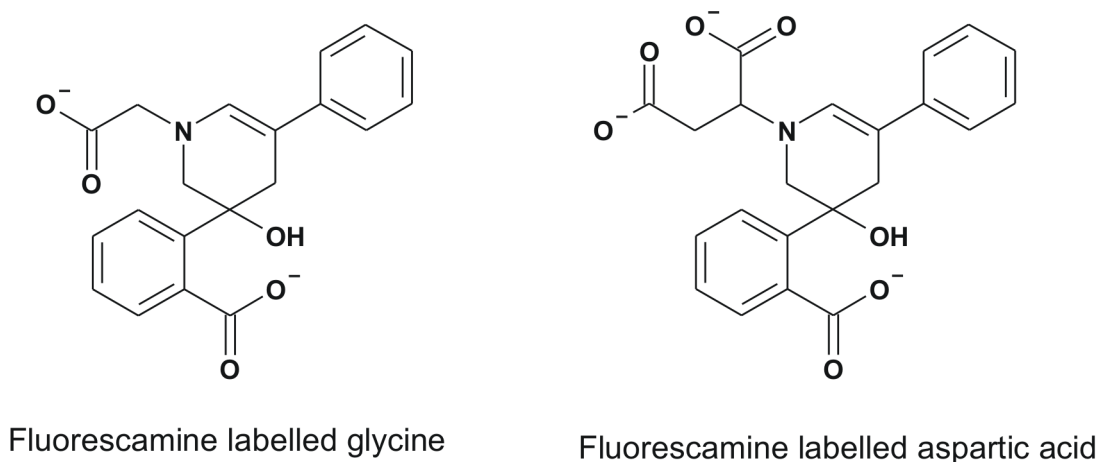


Figure 5.8: Structural formula of fluorescamine labelled aspartic and glycine under the experimental condition used (pH=9.2).

Using the Nernst-Einstein equation, it is possible to estimate the electrophoretic mobility of each amino acid on the basis of the charge.

$$\mu = \frac{ze}{k_B T} D \quad (5.13)$$

where z is the net effective charge in proton units, e is the elementary charge (1.6×10^{-19}), k_B is the Boltzmann's constant ($1.38 \times 10^{-23} \text{ JK}^{-1}$) and T is the temperature, with the diffusion coefficient $D \approx 10^{-10} \text{ m}^2 \text{ s}^{-1}$. The calculated values are shown in the Table 5.2.

Table 5.2: The electrophoretic mobility μ of aspartic acid and glycine

Amino Acid	Electrophoretic mobility ($\text{m}^2 \text{V}^{-1} \text{s}^{-1}$)
Aspartic Acid	-7.3×10^{-8}
Glycine	-4.9×10^{-8}

The ratio of the mobilities for these two amino acids is calculated to be:

$$\frac{\mu_{asp}}{\mu_{gly}} = 1.5 \quad (5.14)$$

This reflects on the fact that the negatively charged amino acids will focus at different locations from the disk electrode, i.e., aspartic acid will be detected after glycine.

5.4 Experiments, Results and Discussions

The microdomain environment enables the emergence of unique physical events. Surface-driven phenomena are dominating in the microscale world and EOF is commonly utilised for fluidic manipulations. This can, however, be effectively generated only in capillaries with dimensions in the micrometer domain, as larger dimensions do not support this fluidic transport mechanism. EOF is especially important for the generation of small flow rates, in the low micro- to nano-litre per minute region, where conventional bench-top instrumentation is not always operational.

In this context, the sample stacking method using microfluidic control was developed. The aim was to implement and adapt the pre-concentration method introduced by Valussi to analyse low-abundance small volume samples. As a model sample, amino acid was used for this purpose. Alterations, such as smaller diameter with thicker gel compartment and disk electrode shape to the original chip design were made. The reasons for the specific changes made are explained in Appendix B.1. Also in Appendix B.3, reasons for the differences in the chip resistivity, experimentally observed R_{exp} and theoretically calculated R_{theo} , are discussed. The argument emphasises the importance of EOF effect in the microdomain environment.

Two mainly differing chip designs were investigated to produce the sample pre-concentration band. In both chip designs, a 5 mm wide and 3 mm deep agarose gel compartment was used. Initially, two-electrode and later three-electrode systems were designed to realise sample stacking. In the first (Figure 5.9A), electrodes were positioned as cathode at the agarose gel surface and anode at the buffer reservoir at the start of the experiment. In the latter (Figure 5.9B), the third ground electrode was introduced at the gel-buffer interface to allow independent control of the applied potential over the gel and in the channel respectively, thus the electrophoretic velocity can be separately adjusted from the value of EOF (v_{EOF}).

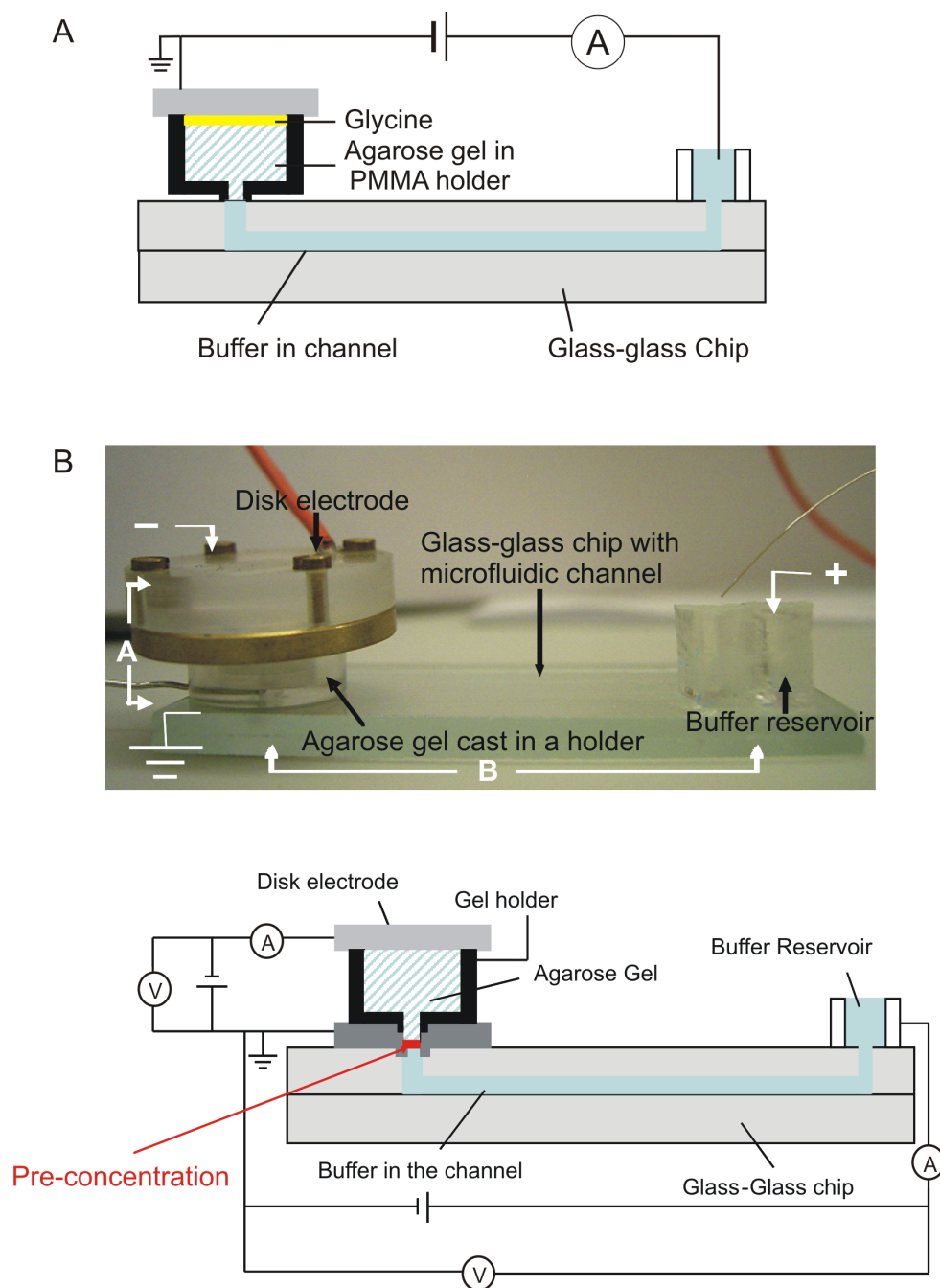


Figure 5.9: Schematic and photo showing the microfluidic chip layout for two- (A) and three-electrode (B) setup. Photo: Label A and B represent the potential control across the gel holder and the microchannel, respectively. Ground was introduced as the third electrode at the bottom of the agarose gel holder.

With the two-electrodes chip design, no sample migration nor stacking were observed. This was reasoned by the change in the geometry, influencing the electric field gradient and the total resistivity of the chip circuit. This led to the inability to predict and allocate the position of the pre-concentration band. With the three-electrodes design, sample migration was achieved successfully, however, stacking without being detected by a photomultiplier tube (PMT).

Two plausible phenomena within the microfluidic channel can be postulated. EOF internal re-circulation disturbing the stacking effect and pH value change in the buffer during the experiment, leading to a change in v_{EOF} . The first situation is based on the law of the conservation of mass and the second due to the applied potential; EOF decreases at low pH and at high pH vice versa. These two possibilities are explained next in terms of observations made from the experiments.

5.4.1 Conservation of Mass

The sample ion transport phenomenon associated with sample stacking process is in general a complex coupling of convective-diffusion, electrostatics, and electrokinetics along with the unsteady effects associated with the response of the electrical double layer to varying bulk ion concentrations.

The effects of EOF on stacking and separation are very important to studies of sample stacking as even slight EOF couples with axial conductivity gradients to generate internal pressure gradients. These internal pressure gradients disperse the sample and thereby limit the practically achievable concentration enhancement (Figure 5.10). Sounart and Baygents [122] developed a general multicomponent model for electroosmotically driven separation processes. They performed two-dimensional numerical simulations to study the effect of electro osmosis on the concentration distributions in FASS. Their simulations demonstrate that in a frame of reference moving with the bulk flow velocity, the velocity field exhibits regions of recirculating flow in the vicinity of the conductivity gradients. Their results show that the recirculating flow can drastically reduce the efficiency of sample stacking.

As described by Lin *et al.* [123] and Chen *et al.* [124], an electric field applied parallel to a conductivity gradient leads to an accumulation of net charge in the bulk liquid regions of an electrokinetic flow field, outside the electric double layer. This net charge can couple with the applied electric field in the channel and result in a body force that can introduce vorticity into the bulk flow and destabilise the flow. Moreover, it was presented by Yan *et*

al. that the finite reservoir size has an effect on electroosmotic flow in a rectangular microchannel [125]. It causes a change of the liquid levels in reservoirs, leading to an induced back pressure. As a result, the flow in the channel not only is driven by electroosmosis, but also is affected by the induced back pressure.

It is, therefore, reasonable to predict that the sample stacking phenomenon was interfered by the re-circulating bulk flow of EOF that obeys the law of conservation of mass. Even though in the three-electrodes system sample migration and slight enrichment was observed, as shown in Figure 5.11, the chip design and utilisation of gel-buffer interface is not stable enough to reproduce the result.

5.4.2 pH Change in Microchannel

Many of electrophoresis experiments use a high potential to realise sample concentration and separation and commercially available systems *e.g.*, Caliper, are designed in such a way that there is enough volume of buffer to run one experiment before the production of HO^- and H^+ start altering the initially stated experimental pH condition. Applying a high potential across a microfluidic system whereby the electrodes are placed in the buffer of a confined volume, changes in the value of the buffer pH is expected. Thus, a possible explanation for the failure to detect the signal, despite the visible sample migration, was due to the limited volume of the buffer initially apportioned in this chip design.

A typical time against current graph with the resulting sequential images of agarose gel is shown in Figure 5.12. It is evident that there is a strong dependence of current on potential that follow a plateauing effect. On every application of potential, a sharp increase in the current was seen, which then gradually decreased to zero. The steepest increase was always observed directly after the first application of the voltage. This current behaviour can be

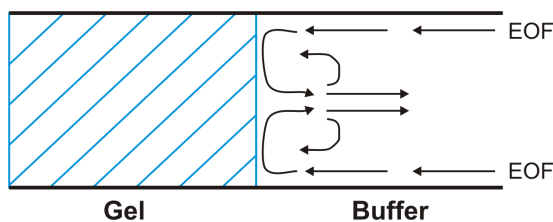


Figure 5.10: Sketch illustrating the effect of EOF at the gel-buffer interface. The law of the conservation of mass is obeyed by the bulk flow of EOF at the interface resulting in an internal circulation. This disperses or disturbs the sample focussing effect.

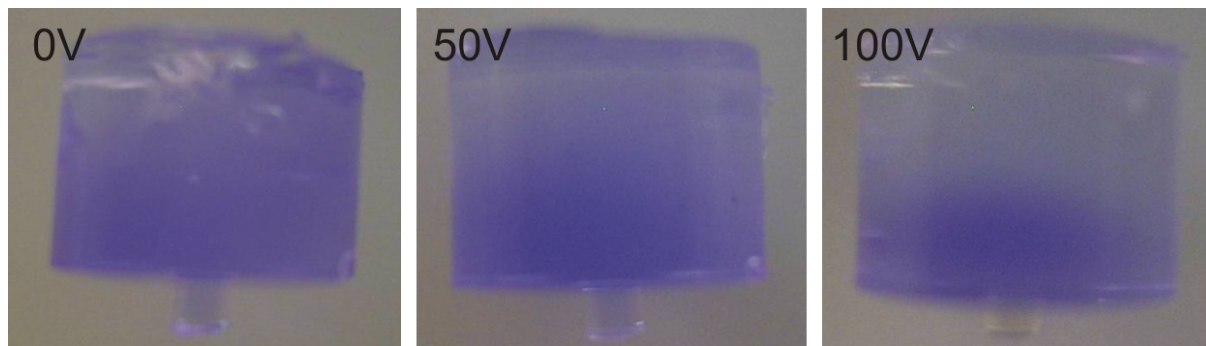


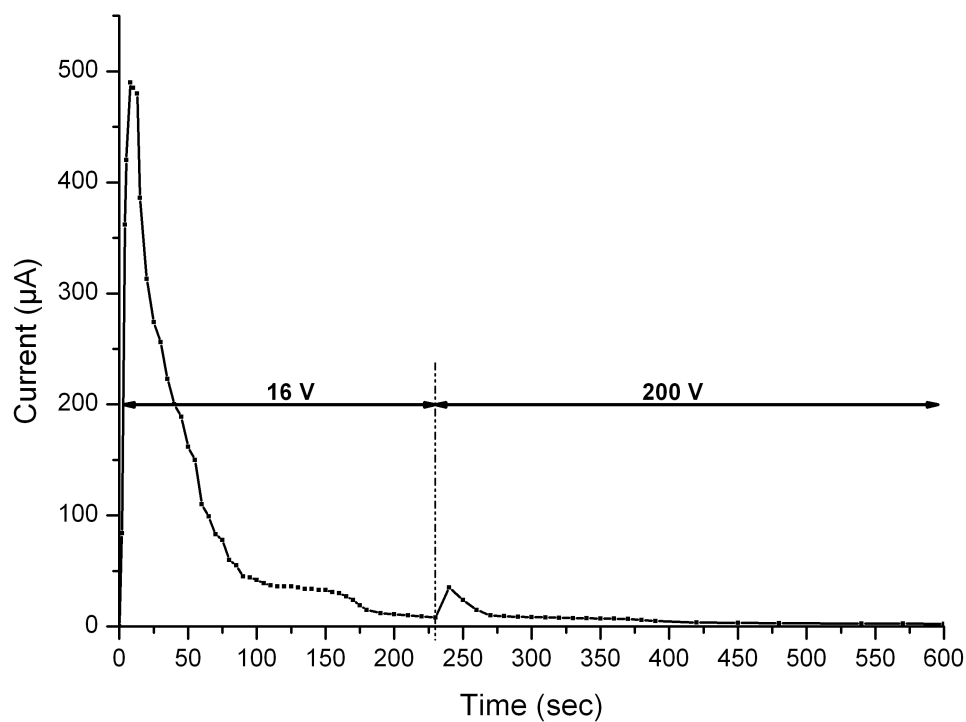
Figure 5.11: Images showing the progression of the dye through the gel matrix after 20min experiment. Potentials 0, 50 or 100V were applied across the channel and the potential across the gel holder was fixed.

rationalised by the ion transport and pH change taking place in the buffer of the gel matrix and the channel.

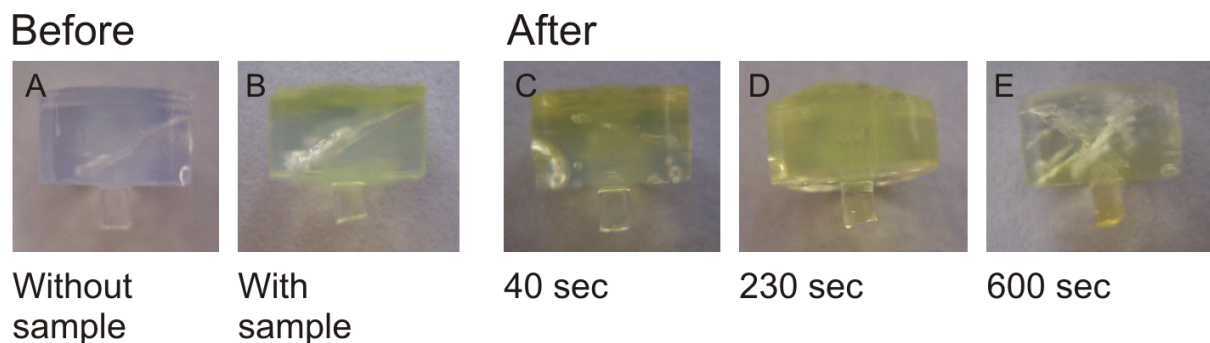
Compounds in 10 mM TRIS/2 mM borate at pH 9.2 are TRIS and borate ions where TRIS is a polyprotic acid which has pKa of 8.3 and boric acid has pKa of 9.24. Compared to HO^- and H^+ , these ions are bulky and have lower electrophoretic velocities but are still smaller than the labelled glycine. As these ions travel faster than the labelled glycine ions, it is the buffer ions, HO^- and H^+ that are responsible for the behaviour of the current curve.

As soon as the potential is applied, depletion of HO^- and buffer ions in the gel matrix is expected as they migrate toward anode. On the other hand, at anode, they are expected to stay in the reservoir. The initial buffer condition (pH 9.2) is sustained until the apportioned volume of the buffer solution in the chip system could account of HO^- and H^+ production. After this point, the pH of the buffer is expected to change from the original pH 9.2 to a more acidic state. If the buffer ions are depleted and the pH is lowered, the EOF effect starts to weaken. With the progressive decrease in the value of v_{EOF} , decline in the efficiency of focussing is anticipated as it has a reduced ability to counteract the absolute electrophoretic velocity in the gel, v_1 . Furthermore, when the polarity is altered subsequent to this phenomenon ($v_{EOF} < v_1$), it is expected that the sample impending to focus will migrate back to the gel phase since v_{EOF} generated is too small to carry the sample along the separation channel. In this hypothesis, an assumption that the reaction of the buffer ions at anode leads to a reduction of EOF efficiency is made.

As a reference, a macroscopic gel electrophoresis that corresponds to this experimental condition was carried out. It was observed that there is a successful migration of glycine



(a) The current against time graph



(b) State of the agarose gel plug at different stages

Figure 5.12: The behaviour of current with respect to time at varying potentials (a). Across A: 16 V for 230 sec, followed by 200 V. Across B: constant at 100 V. Images showing different status of the agarose gel plug (b). Before fluorescamine labelled glycine was pipetted (A). After glycine was pipetted on the gel surface (B). 40s after application of 16 V (C). 240s after application of 16 V (D). Longer than 600 s after application of 200 V (E).

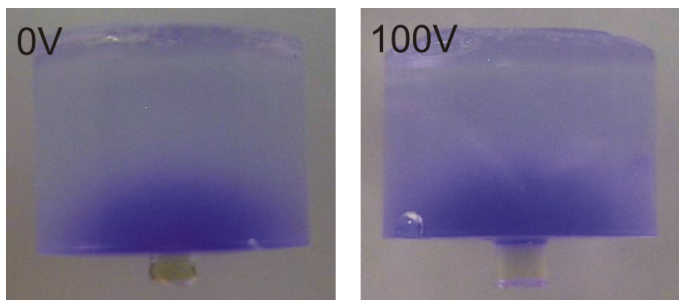


Figure 5.13: Images showing the progression of the dye through the gel matrix after 20 min. On addition of the buffer at timely interval, a slight sample concentration was observed both at 0 V and 100 V applied in the microchannel.

over 40min with the sequence of 10min at 200 V, followed by 30 min at 100 V, all at 5mA. In a similar case, using the three-electrodes system, when a drop of buffer was added to the surface of the gel at 10min interval, a prominent migration and concentration of the sample was observed (Figure 5.13). These results confirm that the amino acid can be extracted through the agarose gel matrix but only under a constant supply of buffer to keep the gel hydrated and to prevent ion depletion, leading to pH change.

To consolidate the above observations further, a graph of the Ohm's law for the ammeter as a function of the potential applied to the chip without sample was plotted for the potential increased step-wise from 0 to 3.75 kV. The value for the potential upper limit was decided as the generation of H₂ or O₂ bubbles in the separation channel was seen when potential greater than 4 kV was applied across the chip. The ohm's plot was linear, with a slope of $0.00268 \pm 0.00002 \mu\text{A}/\text{V}$ and r^2 of 0.9873 (Figure 5.14).

Based on this range of the potential, the number of protons produced, thus, the change in pH estimated to take place during the experiment was hypothetically calculated. Eq. 5.15 according to Faraday's laws of electrolysis was used to derive the result.

$$n = \frac{It}{zF} \quad (5.15)$$

where n is the amount of substance produced in number of moles, I is the electric current, t is the time, z is the valence number of ions of the substance (electron transferred per ion) and F is the Faraday constant (96485 C mol^{-1}).

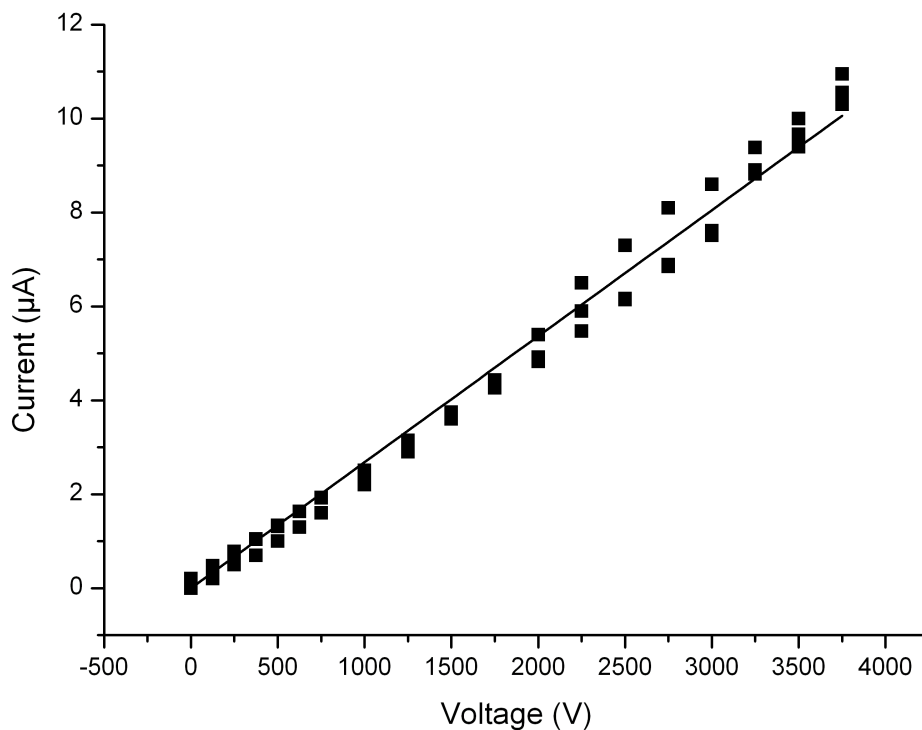


Figure 5.14: A linear Ohm's law plot from the current measurement based on the microfluidic chip circuit with no sample in the agarose gel holder. The slope of $0.00268 \pm 0.00002 \mu\text{A}/\text{V}$ and r^2 of 0.9873 was obtained.

Eq. 5.15 can be rewritten as follows to represent the number of protons produced, thus the pH change for a given time:

$$pH = -\log\left(\frac{It}{VN_Ae}\right) \quad (5.16)$$

where V is the volume of the buffer in the chip system (m^{-3}), N_A is the Avogadro's constant ($6.02 \times 10^{23} \text{ mol}^{-1}$) and e is the elementary charge ($1.60 \times 10^{-19} \text{ C}$).

In this calculation the buffer system was assumed to behave as a simple base and $10 \mu\text{A}$ was taken as the constant current value (the highest value read off the Ohm's plot). In reality, $10 \text{ mM TRIS}/2 \text{ mM borate}$ buffer is a very complex system whereby TRIS-Borate ions are present as well as the excess TRIS interacting with water molecules. These molecular interactions make it very difficult to estimate and postulate the ionic species present in the buffer system. Figure 5.15 shows the formation of TRIS-boric acid and the dissociation of protonated amino group. Despite the assumptions made, the above

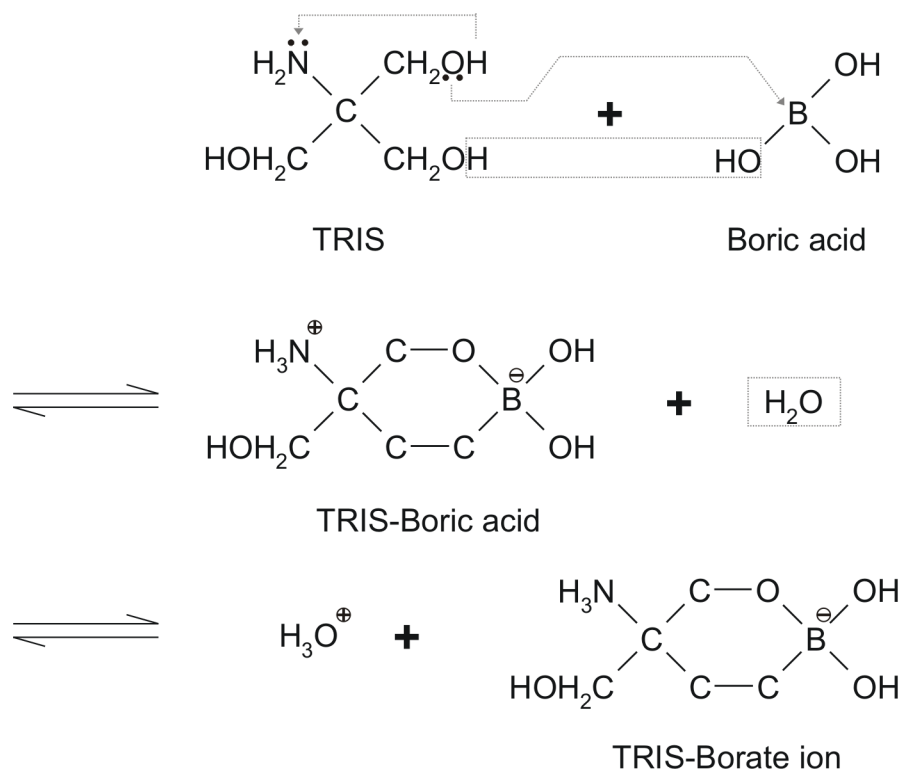


Figure 5.15: A chemical reaction scheme showing the formation of TRIS-Borate ion. TRIS-Borate buffer produces a complex species after the condensation reaction between TRIS and boric acid. TRIS-Boric acid has a zwitter ionic structure from which TRIS-borate ion is formed.

calculation using Eq. 5.16 showed more than one unit change in the pH value within the first second after applying the potential. Thus, it is reasonable to hypothesise that one of the reasons for the failure of the pre-concentration attempted using gel-buffer interface was due to the drastic change in the pH value of the buffer system before the sample migration and stacking effects were reached.

5.4.3 Summary

Despite the effort of improving the chip designs to perform sample concentration, this study was discontinued from this point onward as a realistic application and integration of this pre-concentration method was thought impractical.

Two phenomena described, namely the dispersion of stacking effect by the EOF flow and drastic pH change, could be occurring within the microfluidic channel in the presence of gel-buffer interface. These conditions make this pre-concentration method incompatible for concentrating samples, especially by extracting analyte ions through the gel matrix.

The balance between v_1 , v_2 and v_{EOF} is crucial in succeeding sample stacking. With one potential gradient, these values cannot be controlled well. With three-electrodes system, as Figure 5.12(a) represented, it was revealed that a constant supply of buffer solution is a requisite for this system to function to compensate the depleting ions, the changing EOF and the pH value of the buffer system.

It should also be noted that with the current chip design, should there be a successful outcome for producing the pre-concentration band, for 3 μL sample, the geometry of the gel holder could later on lead to band broadening at the separation stage. As seen in the images of the agarose gel, a dome shaped sample accumulation was observed after a successful migration. Too large a sample volume will reduce the focussing efficiency because analytes having the same pI value will not be able to form a concentration band along the same plane.

The articles published by Dhopeshwarkar *et al.* [99] and Astorga-Wells *et al.* [100] present pre-concentration methods that are realised on easy-to-fabricate microfluidic chip in reproducible manners. The first presents a simple and efficient method for concentration of charged molecules using a photopolymerised hydrogel plug. Enrichment factors of 500 and 50 were obtained within 150s for the two kinds of negatively charged molecules, namely single-stranded DNA (ssDNA) and fluorescein, respectively. The theory behind this method is the same principle as the work presented in this chapter, but the phases are reversed, meaning the sample is diluted in the buffer phase and the concentration occurs at the gel-buffer interface. The latter presents a separation method based on electroimmobilisation and sequential release of captured molecules whereby microfluidic electrocapture device is utilised to immobilise peptides in a microflow stream. After capture, the electric field is decreased in a stepwise manner that cause sequential release of the captured peptides according to their electrophoretic mobility. Another paper was published by Wang *et al.* [109] reporting a 10^6 - 10^8 fold concentration using electrokinetic trapping mechanism enabled by nanofluidic filters. It is possible to maintain trapping and collection for several hours.

Along with the publications of the above mentioned sample enrichment methods, it was concluded that rather than focussing on improving the current experimental chip design, the other stages of microfluidic imaging concept should be investigated to reach the goal of the research project.

Summary and Suggestions for Future Research

6.1 Summary of Achievements

Microfluidic devices are being embraced by chemists and biologists as powerful tools for performing precise experiments with high throughput and its flexibility for integration. The findings of this research project have exposed the integrability of the application of microfluidic two-phase technology towards “microfluidic imaging” concept on a microchip platform. In an era witnessing a shift toward ever-small dimensions, the concept presented here provides the path towards high throughput and automation. Its virtues are relative simplicity in fabrication, combined with the possibility for parallel data collection and serial analysis of multiplexed biological samples.

In order to test adequacy of “microfluidic imaging” concept that spatially resolved the chemical composition of biological samples, two differing chip designs were investigated to realise simultaneous injection of the samples after pixelation. The first was the use of fluidic pressure based on the geometry of the channels and the flow rate of the injected carrier fluid. The second featured micropillar manifolds that functioned like pistons, exerting mechanical force. The first heavily depended on the captured sample volume, whereas the latter not. On the basis of experimental outcomes, the final chip design comprised a PMMA perforation layer for pixelating samples, a PDMS serpentine-shaped channel for a concurrent collection and delivery of the sample droplets, and aluminum micropillar manifold. This microfluidic architecture allowed sample pixelation, injection, transfer, and detection.

Firstly, a procedure for sample uptake and pixelation was developed and optimised and secondly, the transfer of pixels into a serial droplet based system was realised. The use of soft material to pixelate targeted sample reflected a good injection ability at 41.1 ± 10.5 nL per droplet. Due to the limitation in the manufacturing ability, $10 \mu\text{m}$ gap

existing between the micropillars and perforations led to upward sample leakage. This effect was sometimes aggravated by the manual alignment and insertion of the micropillars. Nevertheless, the device was able to inject successfully at 95% of the cases. Despite the need for obvious improvements, the proof-of-principle experiments accomplished with fluorescent dyes (rhodamine B vs fluorescein) and suspended yeast cells in aqueous-in-gas flow system suggested that the microfluidic pixelation system is capable of obtaining non-averaged data from the specimen. The ability to pixelate samples in parallel reduced arduous preparation steps to recognise the sample heterogeneity while distinguishing and conserving the spatial information.

An investigation of an electrokinetic pre-concentration method, which could later on be integrated to manipulate pixelated droplets as a tool for the microfluidic imaging concept was endeavoured. When dealing with samples at very low concentration in very small volumes, sample enrichment of the analyte of interest is necessary. In spite of several efforts in altering the chip design and although migration of the sample analyte was sometimes observed, pre-concentration with high reproducibility was not fruitful. The limited volume of buffer available in the system before sample stacking occurred was thought to be the constraint in this experimental setup. It is likely that the volume of the buffer was underestimated for the time taken for bulky labelled amino acid to migrate through the gel matrix. The initial buffer condition was no longer kept the same, resulting in a drastic change in pH. The decrease in the value of v_{EOF} would weaken the stacking effect. At the same time, bulk flow of EOF obeying the law of conservation of mass would generate internal pressure gradients which disperses and prevents sample stacking.

Further experiments employing other pre-concentration methods and the integration of the two separately investigated microfluidic applications have not so far been conducted. Nevertheless, the ability of this microfluidic pixelation device to convert the acquired compartmentalised information from a parallel to serial manner was endorsed. It demonstrated its potential to approach closer to automation and to implement further preparation, separation and detection steps. In this respect, the concept has superiority over currently available techniques for capturing of cells from tissue, such as laser microdissection or capillary capture methods.

6.2 Suggestions for Future Research

The experiments carried out in this research project have demonstrated a new approach for handling chemical and biological samples via the microfluidic imaging concept. Even

though the fundament of the concept was manifested by the proof-of-principle tests, it still possesses an ample opportunities for the future development both in terms of chip designs and applications.

At the design level, an introduction of an extra chip layer can be considered as a way to implement a pre-treatment step. A possible approach could be a layer embedding a channel with a laminar flow as seen in Figure 6.1. By generating a gradient of reagent concentration, sample heterogeneity can be created or be analysed.

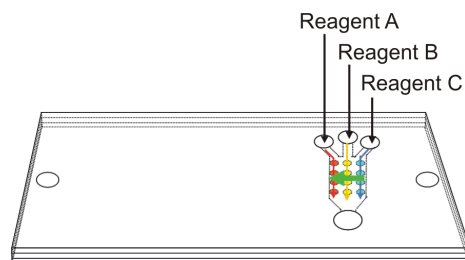


Figure 6.1: A PDMS layer with one channel to integrate the sample pre-treatment step. It relies on a laminar flow generated inside the channel that can be used to introduce different reagent conditions.

To take the micropillar manifolds approach to a more sophisticated level, the use of electronically driven micropillars could be sought. In the similar way that Braille display functions for blind and visually impaired, the microfluidic pixelation device could operate by raising and lowering different combinations of micropillars electronically to inject samples from specific locations. An electronic device is connected to a PC to control the interval and timing of the micropillar to inject the sample droplet from individual perforation. The advantage will be the exertion of an equal pressure with precise timing from a known position. As Braille displays are commercially available, they are used for mechanical valving in some scientific researches instead of chemical control (*e.g.*, hydrogel gel) [126, 127].

In this research, the injection of the droplets were realised by the introduction of the micropillar manifold. There are several other possible approaches for producing droplets; one of them being acoustically. The utilisation of acoustic transducer accompanied by solid state material set at the right frequency or the use of acoustic field using a surface acoustic wave piezoelectric substrate allow production of droplets of regular sizes with an increased automation, throughput and non-invasiveness [128]. In the pharmaceutical industry, acoustic droplet ejection (ADE) by Labcyte Inc. is commercially available and is used as the method of choice for transferring nanolitre volumes of drug candidates in high throughput screening labs. A focused pulse of sound ejects a droplet of fluid with

extraordinary accuracy and precision. An inverted microwell plate or any other suitable surface, such as a microscope slides or tissue sections, positioned over the source solution captures the droplet via surface tension. Each source well is addressed individually, so fluid from any source well can be transferred to any destination well or position. Using a similar technique, the microfluidic pixelation device can be further automated. Moreover, since no extra nozzles or perforations are present, parts which are usually associated with clogging and limited directionality, the fluid contact is lessened and cross-contamination is prevented.

A possibility to integrate pre-concentration method in the pixelation device can be realised by the use of an UV polymerisable hydrogel as an alternative to agarose gel plug. Following the example of Ref. [99], hydrogel can provide an additional ability to control the fabrication area of gel-buffer interface in the microchannel. In this manner, buffer can be steadily supplied.

The detection method utilised in this research was fluorescence microscopy. Coupling the microfluidic chip to mass spectrometry (MS) would increase the diversity of information attainable from a given sample. Recently, the demand to use image mass spectrometry (IMS) has risen as it promises dramatically enhanced discovery in proteomics, cancer research, drug metabolism and systems biology [129]. The analytical power of MS may now be linked with the localisation of histology. IMS reveals the position of proteins and small molecules in tissues such as animal models and tumor samples. In contrast to 2D gels from homogenised samples, this approach determines the concentration of specific compounds at each point in the tissue. Integrating such a detection technique, the data obtained via the pixelation device enables to produce a “protein image” of the tissue.

Alternative chip designs can be considered as the next step in using the multilayered microchip to capture and deliver voxel samples. They are shown in Figure 6.2. With respect to design A that have multiple parallel channels, the number of perforations per channel will be a crucial point. As discussed in Section 4.3.3, Pascal’s law must be considered to realise simultaneous sample injection. However, the advantage will be that the channels either on the top or the bottom layer can introduce sample pre-treatment step, reducing the need of an extra step to position the micropillar manifolds. Design B has a movable middle layer that assists single sample capturing. Although this approach reduces sample high throughput, the spatial control is enhanced.

In this research project, a yeast cell population was used as the starting point to the biological application. The aim is to expand the use of the microfluidic imaging chip to ultimately facilitate the analysis of numerous (sub)cellular biological mechanisms and

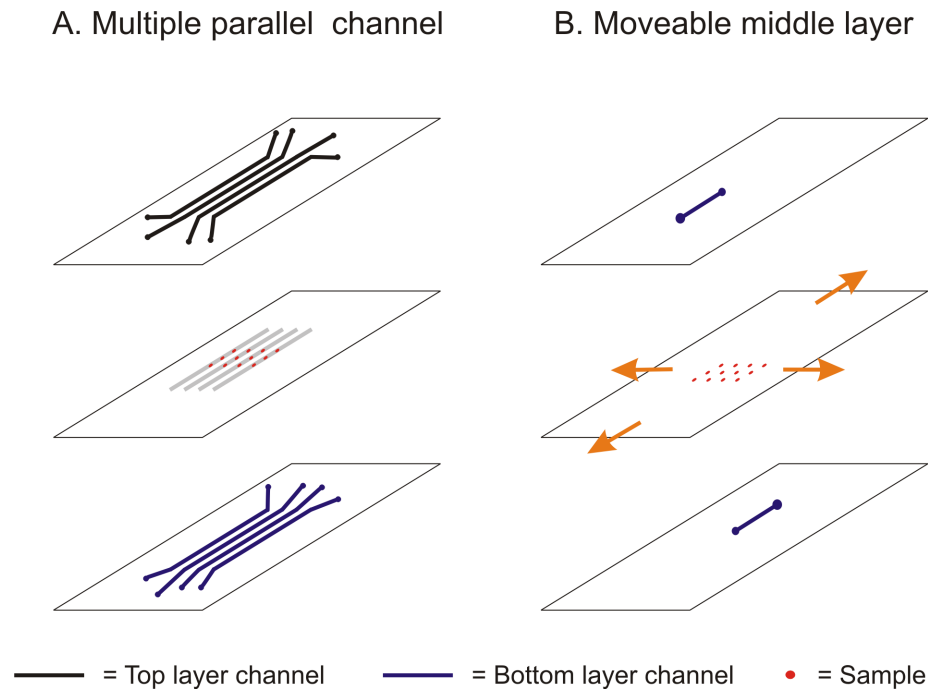


Figure 6.2: Two other designs for the total fluidic approach. Multiple parallel channels; must have the same number of channels as the pixelation rows (A). Moveable middle layer to assist single sample capturing; must be operated for the number of pixels (B).

processes without damaging or losing viability. It is suitable for demanding applications in tissue engineering and cell-based assays such as simultaneous immunochemical analyses and tests for diagnostic markers in clinical tissue specimens.

To fulfill the goal, it is logical that the focus on the model sample is moved from a yeast cell population to mammalian cells. It is a sensible choice as when conducting medical tests, mammalian cells are normally handled in tissue forms rather than in suspensions.

One realistic application of the chip would be to investigate the process of wound healing or tumour development that are heterogeneous in nature of the tissues involved. Fibroblasts¹ [130] are associated with wound healing and are morphologically heterogeneous with diverse appearances depending on their location and activity. Such features make them an attractive target for the microfluidic imaging concept, as cells can be extracted from a specific wound area and be directed to grow inside perforations after appropriate surface modifications. The diversity in chemicals secreted from the wounded area and colonial heterogeneity by subjecting them to various conditions can be analysed to study the cell activities and healing processes.

¹It is a type of cell that synthesises and maintains the extracellular matrix of many animal tissues. The cells provide a structural frame for many tissues and play a critical role in wound healing.

Nearly all cancers are a result of abnormalities in the genetic materials of the transformed cells. A study was conducted using laser capture microdissection to determine whether different zones of the same pancreatic tumor exhibited differential expression of genes [131]. The data showed zonal heterogeneity for gene expression profiles in tumors. In a similar manner, the pixelation chip can target the sample tissue and measure immunohistochemistry of tumour comparable to tissue microarray (TMAs).

On the other hand, it is also of particular importance to apply the pixelation technique to a homogeneous sample that undergoes screening assays or different sample pre-treatments, which as a consequence generates a heterogeneous environment. For example, perforations in this microfluidic pixelation device can be interpreted as equivalent to the wells of microtitration plate used in enzyme-linked immunosorbant assay (ELISA). In a comparable manner to ELISA being used for clinical medicine for detecting proteins associated with disease, antigen and antibody reactions can be pre-defined and controlled at the pixelation stage.

Lastly, the most apparent but important outlook would be the further reduction of the pixel sizes. An increase in the current 12 arrays of perforations to mega pixel range would certainly be achievable using a photolithography technique. Any of the above mentioned techniques can be integrated to actualise controlled parallel injection of the small volume samples, while retaining the spatial information. The increased number of pixels will lead to production of an image with a higher resolution. This would be most advantageous when biological samples such as cells are handled. By successful device down sizing, the ability to especially control encapsulation of single cells in single droplets or perforations comparable in size to the cell diameter at high throughput rates and with high precision can be accomplished. In this respect, the application of the concept in high throughput screening, clinical diagnosis, single cell bioreactors, and the investigation of stem cell differentiation can be appreciated, emphasising the importance of cellular heterogeneity within a population at single cell level.

Additional Information on Pixelation Study

A.1 Sample Pre-Treatment

One of the sample pre-treatment steps currently underway is the integration of a PDMS layer that embeds a channel(s) to introduce different reagent conditions. A chip design shown in Figure A.1 represents this type of work.

An example was experimentally demonstrated by testing the viability and lysis of yeast cells against different concentrations of ethanol [132]. The dye used was erythrosine B that distinguishes live and dead cells. When the membrane of the cells is ruptured, the dye enters and fluorescence can be detected. Under this experimental condition, yeast cell colonies are pixelated and subsequently subjected to three channels each having a different concentration of the ethanol. After a certain period, when the lysis or reaction has occurred, the samples are injected into the channel using the micropillars. The results can be determined in terms of fluorescence intensity.

A.2 Chip Design

Technical drawings of the channel designs manufactured by the in-house workshop are given.

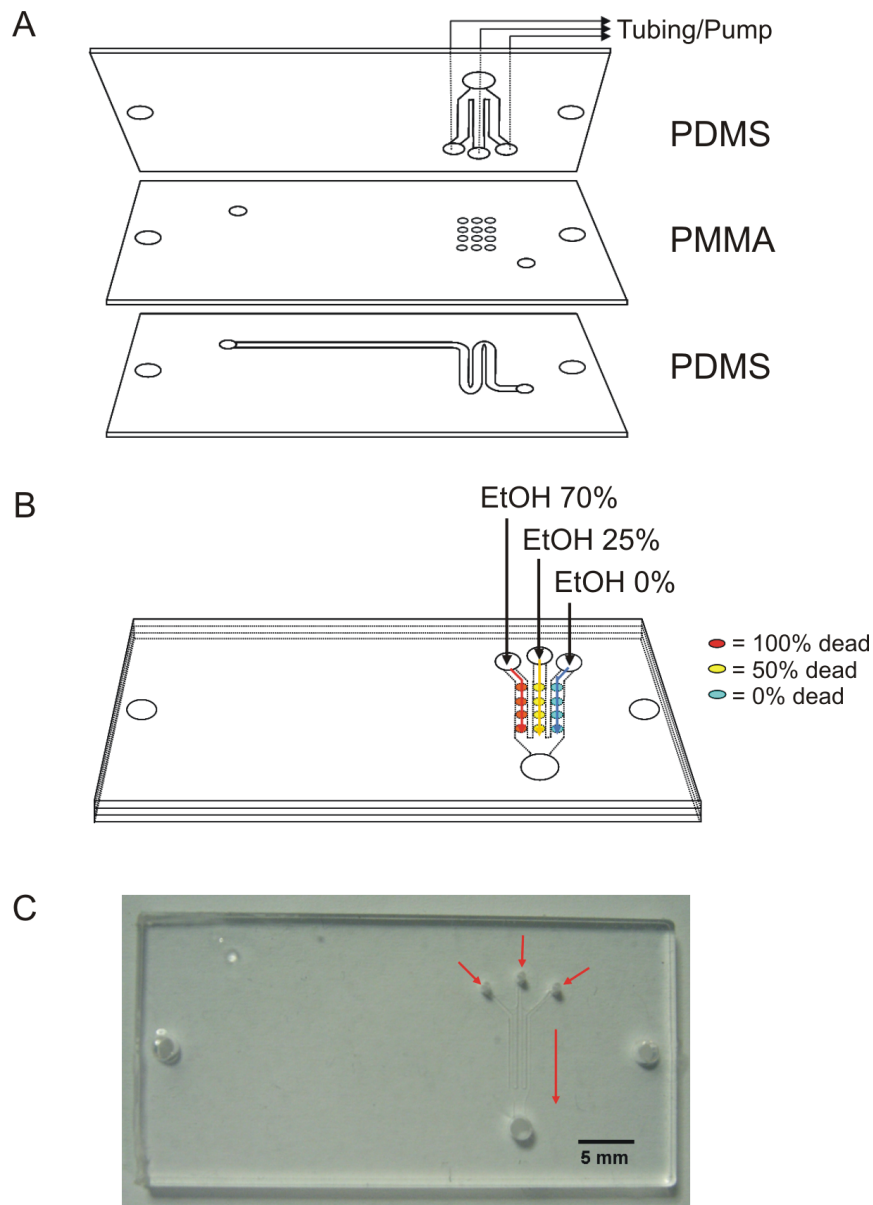


Figure A.1: A PDMS layer with three separate channels or one channel to integrate the sample pre-treatment step. The top PDMS layer design, embedding three separate channels (A), was used for introducing ethanol at different concentrations to investigate yeast cell lysis (B). A photo image of the PDMS layer cast out of the mold is shown in (C). This channel design is considered as the test phase design for easier analysis.

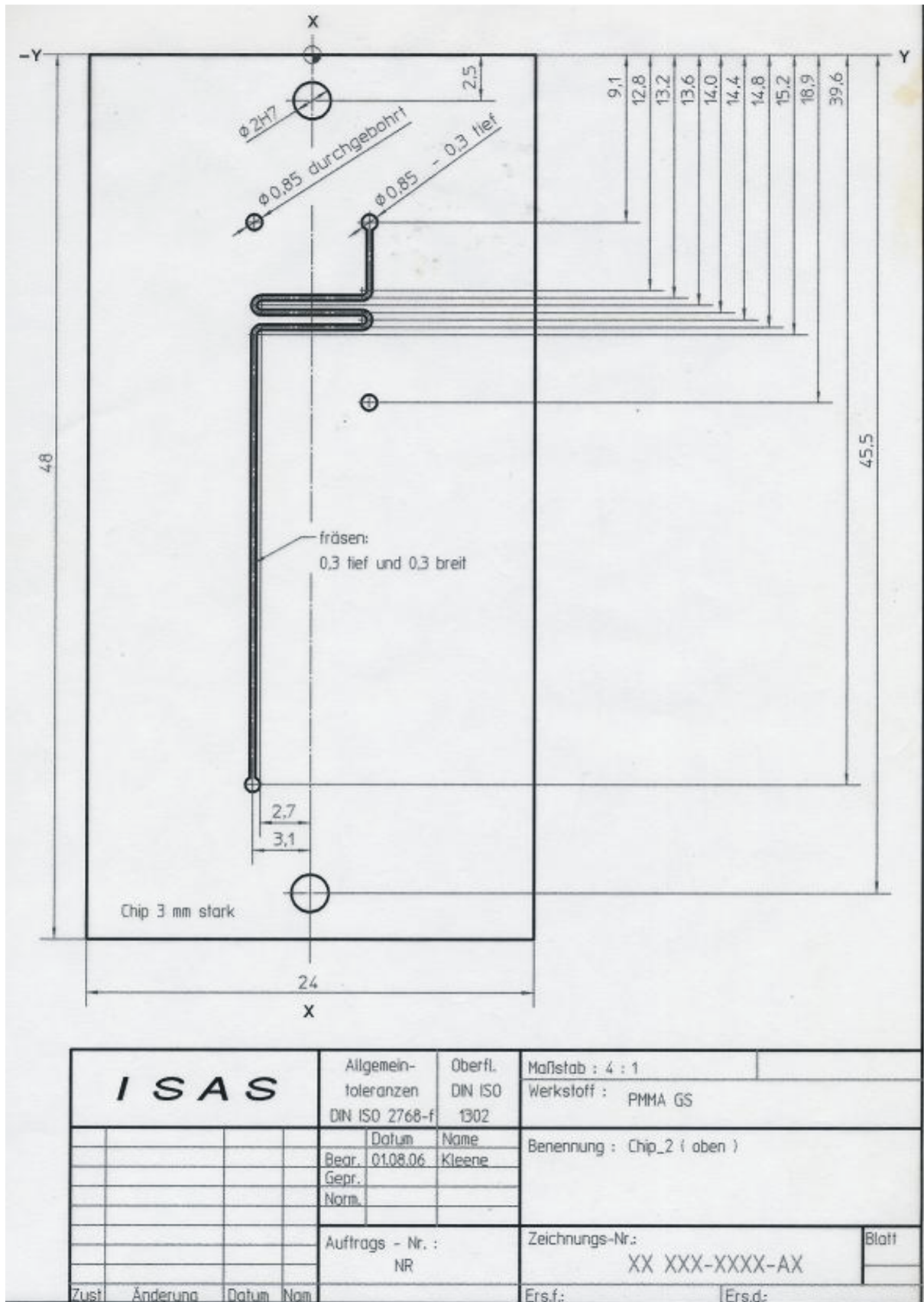


Figure A.2: A drawing of a serpentine channel design on a PMMA layer.

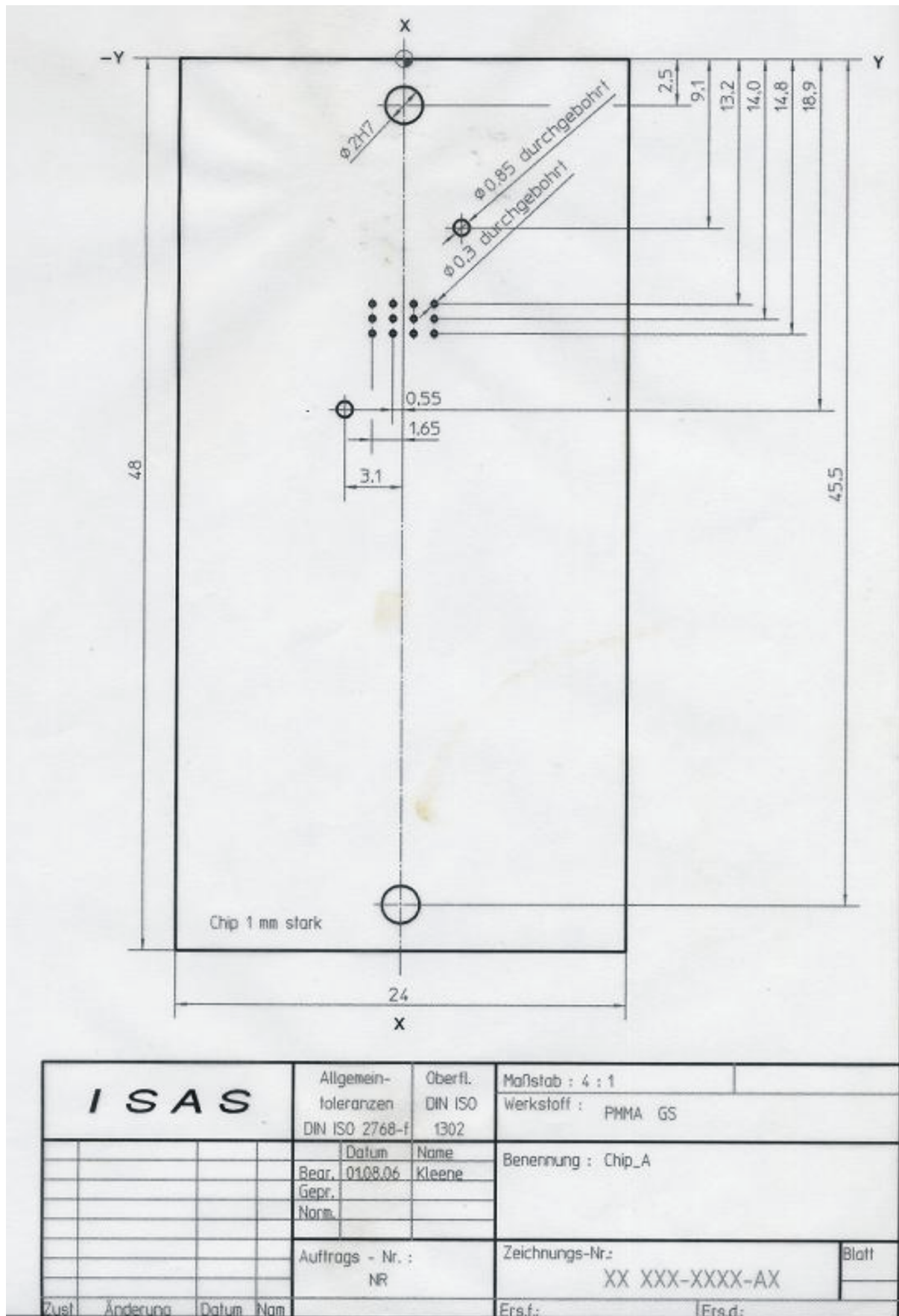


Figure A.3: A drawing of a perforations layer made of PMMA.

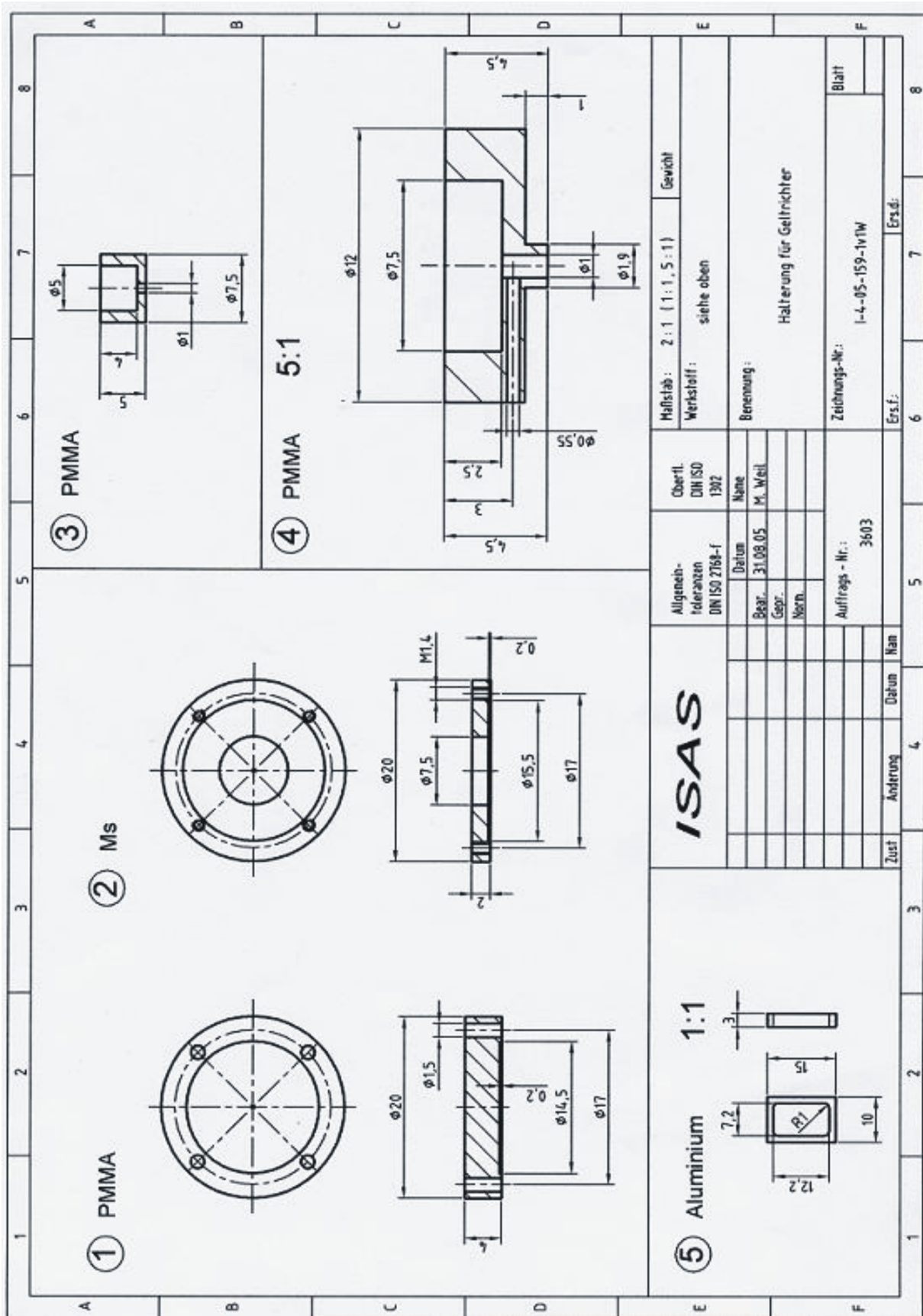


Figure A.4: A drawing of a PMMA agarose gel holder.

Adaptation of the Pre-concentration Method

B.1 Chip Design with the Circular Electrode

The aim for the novel pre-concentration technique was mainly dictated by the two major requirements of the previous project:

- 1) Direct sampling of fingerprint residues, and
- 2) Non-invasive analysis of the samples.

Among many physical phenomena involved in electrophoresis in microchannels that are often composed of different materials, the theory behind Valussi's pre-concentration mechanism exploited arises from the combination of:

- a non-linear electric field gradient and a steep conductivity gradient created due to the chip geometry,
- the counteraction of the bulk flow of the buffer, originating from electroosmosis in the microchannel.

There are two possible shapes for the electrode to pre-concentrate the samples residing on the gel compartment. A disk or a ring electrode can be placed on top of the gel that is in contact with a buffer-filled channel. In the previous work, a software package FEMLAB was used to simulate the electric field for the two cases. Figure B.1 shows the geometry of the electric field for the two electrode configurations. In the simulation, however, neither conductivity nor viscosity gradients were taken into consideration.

The conclusion drawn from the simulation for the previous work was to use a ring electrode, for there being mainly two reasons (quote from ref. [97]):

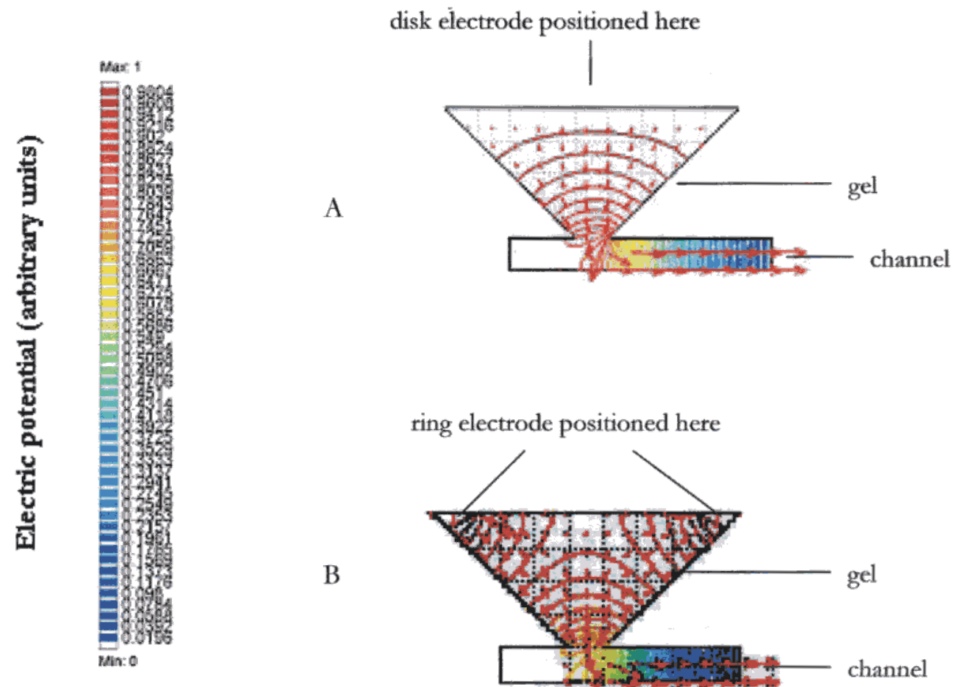


Figure B.1: Schematic representation of the electric field in the case of A) a disk electrode and B) a ring electrode. Parameters: diameter of circular electrode = 20mm, thickness of the gel = 1 mm, channel dimensions = 34 mm (L) \times 30 μ m (W) \times 10 μ m (D). The arrows model field strength vectors, while the curves represent iso-potential lines [Courtesy Thesis Valussi [97]].

- 1) to extract as much material as possible from the whole area covered by the fingerprint, and
- 2) because, as a result of the fingertip pressure applied on deposition of the print, components in the more depressed centre of the sampling area in the gel might already feel a stronger influence of electric field than the components in the peripheral areas.

The interpretation of Figure B.1, however, conflicts with the two reasons stated above, based on principles of physics and physical property of the material. With respect to statement (1), a disk electrode actually has a more uniformly distributed field strength, thus, allowing a better extraction of the material from the whole area covered by the analyte. Regarding statement (2), the pressure applied will have only a small effect on the influence of electric field, as electric field would only be applied after the pressure from the fingertip is removed. Realistically speaking, during the time taken to place the ring

electrode, the depression made by the force of the fingertip would be relieved considering the elasticity of the 2% agarose gel.

For these reasons, the following modifications were made to the original microfluidic chip design:

- 1) a disk electrode instead of a ring electrode,
- 2) a small diameter for the sample extraction area (modified to 5mm diameter instead of 2 cm), and
- 3) 3 mm rather than 2mm thick gel.

The thickness of the gel was increased by a 1mm, as the smaller the volume, the greater the effect of Joule heating leading to dehydration of the gel.

B.2 Experimental

Device fabrication

Glass microfluidic chip (60 mm×25 mm) was fabricated at the in-house clean room, using microlithographic patterning and an HF (hydrogen fluoride) etchant, as described previously (see Section 3.2). Channels were etched 50 μm deep on one glass plate. The etched glass and a cover plate with holes for external access, drilled with a 1.0mm tungsten coated grinding bit (Proxxon, Germany) were bonded by heating with the temperature programme described in Section 3.2.4. Before bonding, the two plates were cleaned with acetone, DMF, methanol and concentrated H_2SO_4 all at reagent grade and deionised water in an ultrasonic bath. The gel holder was made out of PMMA having a cylindrical shape with the diameter 5mm and the depth 3 mm.

Instrumentation

A manually controlled power supply (12.5 kV and 35 kV, HCN 7E series, Omiran Ltd, England) and multimeter (M-4650, Metex Instrument, Korea or Precision Gold, M215, UK) were used to setup the microfluidic chip circuit. Caliper 42 MDS (Caliper Life Sciences, USA) equipped with PMT (Microscope photometer D-104 and Photomultiplier Detection System 814, Photon Technology International, UK), facilitated with an electronic shutter (Melles Griot, NY, USA) was used for fluorescence intensity measurement of fluorescamine labelled glycine. Caliper was connected to a Nikon microscope with xy-stage (Eclipse TE300, Nikon, UK).

Materials and Reagents

Glycine, agarose powder, TRIS and boric acid were from Fluka and fluorescamine was

from Sigma-Aldrich. All chemicals were reagent grade and ultrapure water (Millipore) was used for all solution preparation. Fluorescamine was dissolved in 95% acetone 5% water. A stock solution of 10 mM glycine dissolved in TRIS-borate (10 mM TRIS/2 mM borate, pH 9.2) was prepared fresh for every experiment. An equal volume of fluorescamine solution and 10 mM glycine was mixed to instantaneously label glycine (Figure B.2). Solutions were introduced to the channels via syringe; a 0.22 μm pore size, syringe-mounted microfilter (Millipore). PDMS was cast on the hot plate to form a PDMS slab of approx. 1.3 mm high. The block was cut into an appropriate size and was placed at the end of the straight channel as a buffer reservoir. The reservoir was filled with the buffer solution and waited until all channels were filled. Agarose was dispersed in 10 mL TRIS-borate buffer (10 mM TRIS/2 mM borate, pH 9.2) to form 2% (w/v) agarose gel. The hot agarose solution was poured into the PMMA gel holder, left to solidify and was placed at the other end of the straight channel. A fine platinum wire was inserted into the reservoirs and a copper piece, coated with gold using sputter coating, was filed as a disk electrode to sit above the gel holder to deliver the potentials.

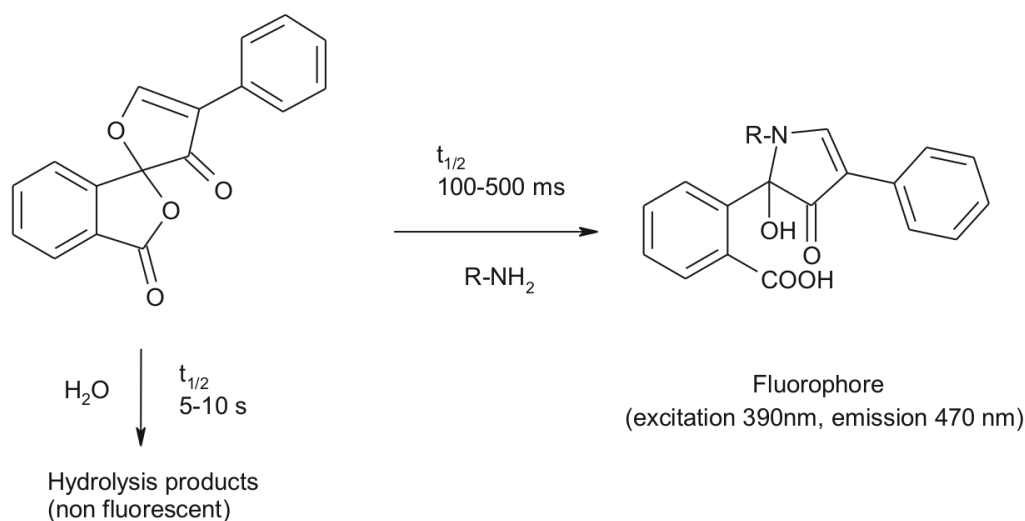


Figure B.2: Possible reaction mechanisms for fluorescamine under differently treated conditions.

Current Measurement

The circuit diagram shown in Figure B.3A was used to measure the current in the microfluidic chip circuit. The PDMS reservoir was placed at one end of the separation channel, filled with TRIS-borate buffer and the channel was filled by capillary force. It was made sure that the buffer emerged at the other end of the channel to avoid the creation of dead volume. The PMMA gel holder was filled with agarose gel and was placed at the other

end of the channel to the reservoir. After placing the electrodes appropriately, experiments were performed by placing the ammeter in the appropriate place and the potential was applied step-wise from 0 to 3.75 kV. The current was read and graph was plotted according to the Ohm's law. The same glass-glass chip was used for both experiments. The chip was washed and prepared in the same manner between experiments that the chip conditions would be the same.

Pre-concentration using Two-Electrode System

The chip layout shown in Figure B.3B was used to perform two electrodes based pre-concentration of glycine. The channel was filled and agarose gel holder was placed in the same way as described previously. 3 μL solution of the labelled glycine was pipetted on the surface of the gel and acetone was left to evaporate. On placing the electrodes appropriately, 3.75 kV was applied for 360 s for the pre-concentration. After this duration, the polarity was reversed for the separation or mobilisation step. The fluorescence emission was monitored by PMT at the detection window positioned along the straight channel.

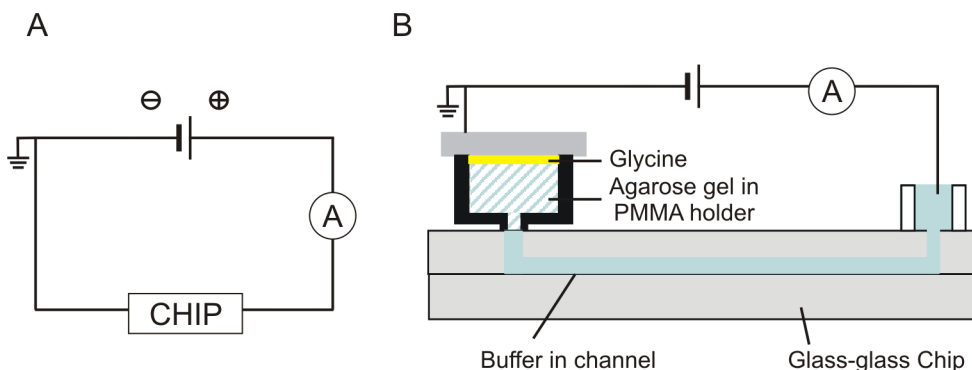


Figure B.3: The circuit diagram for measuring the current (μA) in the adapted chip design for the Ohm's plot (A). Two electrodes chip design for pre-concentrating glycine (B).

Pre-concentration using Three-Electrode System

An in-house photolithographically etched glass-glass microfluidic chip with a cast agarose gel plug, dissolved in 10 mM TRIS/2 mM Borate buffer (pH 9.2), in a PMMA gel holder, at the end of the channel was used (Figure 5.9). Potentials of 16 V for 230 s followed by 200 V across A and 100 V across B were applied separately over 10 min. PMT was used to detect the resulting concentrated band on reversal of the polarity. The current against time graph was plotted to observe the behaviour of the nature of the curve. Glycine solution (3 μL at 10 mM in TRIS-Borate) labelled with fluorescamine was utilised as the sample.

As an alternative sample to labelled glycine, bromophenol blue was used to simulate the behaviour of primary amino acids to observe the pre-concentration effect. $3\mu\text{L}$ at 7mM bromophenolblue was pipetted on the agarose gel surface. For a set of sequences of potentials applied across A and B, side view images of agarose gel were taken to observe the results. Additionally, under the same experimental condition, a drop of buffer solution was added at cathode, *i.e.*, to the surface of the agarose gel. The supply was made three times at 5, 10, 17 min during the 20min experiment. Side view images of the agarose gel were taken for a comparison to the above experiment.

B.3 Results

Ohm's Law Plot

One of the advantages offered by the microfluidic channel is the ability to employ high field strength for achieving fast separations, as the heat dissipation is faster compared to the conventional CE systems. Joule heating inside the microfluidic channels is generated by the conduction of electric current through the buffer. Therefore, the channel dimensions, the applied potential and the conductivity of the buffer will have an influence on the heat production rate.

A plot of the Ohm's law for the ammeter as a function of the potential applied to the chip without sample was linear, with a slope of $0.00268 \pm 0.00002 \mu\text{A}/\text{V}$ and r^2 of 0.9873. This calculates the experimental resistivity, R_{exp} , to be $3.73 \times 10^8 \Omega$. Using Eq. 2.1 to calculate the theoretical value of the chip resistance, R_{theo} , $2.55 \times 10^9 \Omega$ was obtained.

$$R_{theo} = \rho \frac{L}{A} \quad (2.1)$$

Conductivity of the buffer, σ	$5.66 \times 10^{-3} \Omega^{-1}\text{m}^{-1}$
Specific resistivity, ρ	$177 \Omega\text{m}$
Length of the channel, L	0.036 m
Cross sectional area of the channel, A	$2.5 \times 10^{-9} \text{m}^2$

The theoretical and experimental values of the resistivity vary by a factor of 10. This deviation can be explained by the variance in the buffer concentration, the level of the buffers and in the positioning and connection of the electrodes due to the unstability of the chip design. Leak in the setup is another possibility. However, the most important factor to be considered is the EOF effect generated in the microchannel. Assuming that

the specific resistivity for the buffer was measured in a macroscopic environment, the specific resistivity for the buffer in this dimension will be different to when the walls of the microchannel are introduced.

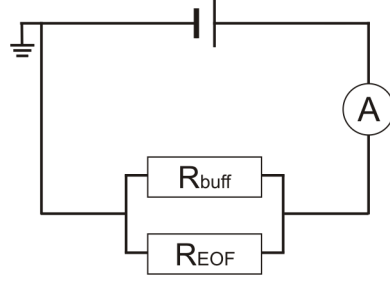


Figure B.4: The circuit diagram can be redrawn as above in the microfluidics domain. R_{chip} is the sum of R_{EOF} and R_{buff} . In microscale dimension, $R_{EOF} \ll R_{buff}$.

The microdomain environment enables the emergence of unique physical events. Under this experimental condition, the circuit diagram can, therefore, be redrawn to Figure B.4, rather than that depicted in B.3A. Under this circumstance, the following applies:

$$\frac{1}{R_{chip}} = \frac{1}{R_{EOF}} + \frac{1}{R_{buff}} \quad (2.2)$$

where $R_{chip} = R_{exp}$. From the above equation, three different situations can be postulated:

- when $R_{EOF} \gg R_{buff}$ then $R_{chip} \approx R_{buff}$
- when $R_{EOF} \ll R_{buff}$ then $R_{chip} \approx R_{EOF}$
- when $R_{EOF} = R_{buff}$ then $R_{chip} = \frac{1}{2}R_{EOF} = \frac{1}{2}R_{buff}$

EOF is one of the surface-driven phenomena dominating in the microscale world. EOF is commonly utilised for fluidic manipulations and can be effectively generated only in channels with dimensions in the micrometer domain, as larger dimensions do not support this fluidic transport mechanism. This suggests that $R_{chip} \approx R_{EOF}$ is established for the microfluidic chip circuit, which implies $R_{EOF} \ll R_{buff}$. This supports the results obtained in the experiment for R_{exp} compared against R_{theo} . From this observation, the result confirms that the resistivity for this chip circuit falls into a reasonable region and that there's no short circuit in the setup. Thus, the circuit design and the values of the applied potential were used for the rest of the experiment.

Two-Electrode System

The results from the previous experiment proved that it is appropriate to apply the potential up to 3.75 kV for this particular setup. After the expected duration for the formation of the concentration band (6 min) [97], the potential was reversed to detect the

fluorescence signal with the PMT detection window positioned along the straight channel. Despite many attempts, no signal was observed.

A possible hypothesis for this observation could be accounted for the increased height of the gel holder. The entire microfluidic chip composition can be imagined as a circuit composed of different resistors, *i.e.*, the gel holder, microchannel with the buffer and the reservoir, each having different resistances. In the previous design, the geometry of the entire chip to the total resistivity was optimal, realising the pre-concentration band. On increasing the height of the gel holder, the resistivity in the network was altered. The potential drop in the new design is greater than in the original geometry, thus, the electric field and EOF is smaller. When an equal potential was applied, this alteration led to a significant change in the position at which the sample concentrated. Thus, when the potential was reversed, no signal was detected with the PMT. It can be postulated that if v_1 was greater than v_{EOF} , the amino acid will leak away without forming the concentration band. In this case, no pronounced signal peak would be detected.

The general conclusion drawn from the series of experiments states that with two electrodes chip design, the uncertainty in predicting and allocating the position of the pre-concentration band remains. To counteract the problem, a better control over the potential applied is necessary. A balance between the EOF generated against electrophoretic mobility of the glycine ions is crucial. To satisfy this requirement, a three electrode circuit design was established.

Three-Electrode System

An attempt was made to design a chip with three electrodes after learning that the two electrodes microfluidic chip system is unable to precisely control the region where EOF and electrophoretic mobility balance. Being able to control the concentration band position, upon reversal of the polarity, loss of the sample migrating back though the gel matrix is avoided. Furthermore, the values of EOF and electrophoretic mobility can independently be controlled with a separately applied potential across the gel matrix and the microchannel.

Labelled glycine is subjected to electrophoresis in the pre-formed electric field gradient. Glycine migrates through the gel matrix until a point where buffered pH equal to its isoelectric point. In the three electrodes chip design, the purpose was to vary the value of EOF to control the position where these ions stopped for concentration.

Extraction of glycine seem to proceed because migration of the labelled glycine toward the ground electrode, distinguished by the yellow colour, was observed over the 10 min

experiment. However, the enrichment factor is negligible, thus, a thorough investigation into buffer levels, the degree of EOF effect and pH change is necessary to understand the system inside the microchannel better.

Publications

- (1) Dittrich, P., Tachikawa, K., and Manz, A.: *Micro Total Analysis Systems. Latest Advancements and Trends*. Analytical Chemistry, 2006, 78, 3887-3907. [23]
- (2) Ohno, K., Tachikawa, K., and Manz, A.: *Microfluidics: Applications for Analytical Purposes in Chemistry and Biochemistry*. (accepted), Electrophoresis.
- (3) Tachikawa, K., Dittrich, P., and Manz, A.: *Microfluidic Imaging: A novel concept for pixelation of chemical and biological samples*. (submitted), Lab-on-a-Chip.

Table of Abbreviations

ADE	Acoustic droplet ejection
CAD	Computer aided design
CE	Capillary electrophoresis
CNC	Computer numerical control
eGFP	Enhanced green fluorescent protein
EOF	Electroosmotic flow
FASS	Field-amplified sample stacking
FFE	Free-flow electrophoresis
FIA	Flow injection analysis
IC	Integrated circuit
ID	Internal diameter
IMS	Image mass spectrometry
ITP	Isotachopheresis
LOC	Lab-on-a-chip
MEKC	Micellar electrokinetic chromatography
MS	Mass spectrometry
μTAS	Micro total analysis systems
PBS	Phosphate buffered saline
PCR	Polymerase chain reaction
PDMS	Poly(dimethyl)siloxane
PMMA	Poly(methyl)methacrylate
PMT	Photo-multiplier tube
POC	Point of care
SPE	Solid-phase extraction
TGF	Temperature gradient focussing
TMA_s	Tissue microarrays
TRIS	Tris(hydroxymethyl)aminomethane
YPD	Yeast extract- peptone-dextrose medium
YPG	Yeast extract- peptone-glucose medium

Bibliography

- [1] DI CARLO, D., AGHDAM, N., and LEE, L. P.: “Single-cell enzyme concentrations, kinetics, and inhibition analysis using high-density hydrodynamic cell isolation arrays”. *Analytical Chemistry*, 2006. **78** (14): pp. 4925–4930.
- [2] TEMPLIN, M. F., STOLL, D., SCHRENK, M., *et al.*: “Protein microarray technology”. *Trends In Biotechnology*, 2002. **20** (4): pp. 160–166.
- [3] BROWN, P. O. and BOTSTEIN, D.: “Exploring the new world of the genome with dna microarrays”. *Nature Genetics*, 1999. **21**: pp. 33–37.
- [4] FREIRE, S. L. and WHEELER, A. R.: “Proteome-on-a-chip: mirage, or on the horizon?” *Lab On A Chip*, 2006. **6** (11): pp. 1415–1423.
- [5] LE, H. P.: “Progress and trends in ink-jet printing technology”. *The Journal of Imaging Science and Technology*, 1998. **42** (1): pp. 49–62.
- [6] HUGHES, T. R., MAO, M., JONES, A. R., *et al.*: “Expression profiling using microarrays fabricated by an ink-jet oligonucleotide synthesizer”. *Nature Biotechnology*, 2001. **19** (4): pp. 342–347.
- [7] COLLIER, W. A., JANSSEN, D., and HART, A. L.: “Measurement of soluble l-lactate in dairy products using screen-printed sensors in batch mode”. *Biosensors and Bioelectronics*, 1996. **11**: pp. 1041–1049.
- [8] LEMMO, A. V., ROSE, D. J., and TISONE, T. C.: “Inkjet dispensing technology: applications in drug discovery”. *Current Opinion In Biotechnology*, 1998. **9** (6): pp. 615–617.
- [9] ALPER, J.: “Bioengineering - biology and the inkjets”. *Science*, 2004. **305** (5692): pp. 1895–1895.
- [10] BOLAND, T., XU, T., DAMON, B., *et al.*: “Application of inkjet printing to tissue engineering”. *Journal of Biotechnology*, 2006. **1** (9): pp. 910–917.
- [11] THORSEN, T., MAERKL, S. J., and QUAKE, S. R.: “Microfluidic large-scale integration”. *Science*, 2002. **298** (5593): pp. 580–584.

- [12] HANSEN, C. and QUAKE, S. R.: “Microfluidics in structural biology: smaller, faster em leader better”. *Current Opinion in Structural Biology*, 2003. **13** (5): pp. 538–544.
- [13] CHIN, C. D., LINDER, V., and SIA, S. K.: “Lab-on-a-chip devices for global health: past studies and future opportunities”. *Lab On A Chip*, 2007. **7** (1): pp. 41–57.
- [14] HAEBERLE, S. and ZENGERLE, R.: “Microfluidic platforms for lab-on-a-chip applications”. *Lab On A Chip*, 2007. **7** (9): pp. 1094–1110.
- [15] STONE, H. A., STROOCK, A. D., and AJDARI, A.: “Engineering flows in small devices; microfluidics toward a lab-on-a-chip.” *Annual Review of Fluid Mechanics*, 2004. **36**: pp. 381–411.
- [16] KAERN, M., ELSTON, T. C., BLAKE, W. J., *et al.*: “Stochasticity in gene expression: From theories to phenotypes”. *Nature Reviews Genetics*, 2005. **6** (6): pp. 451–464.
- [17] RYLEY, J. and PEREIRA-SMITH, O. M.: “Microfluidics device for single cell gene expression analysis in *saccharomyces cerevisiae*”. *Yeast*, 2006. **23** (14-15): pp. 1065–1073.
- [18] DAY, P. J. R.: “Miniaturization applied to analysis of nucleic acids in heterogeneous tissues”. *Expert Review of Molecular Diagnostics*, 2006. **6** (1): pp. 23–28.
- [19] STEPHENS, D. J. and ALLAN, V. J.: “Light microscopy techniques for live cell imaging”. *Science*, 2003. **300** (5616): pp. 82–86.
- [20] LICHTMAN, J. W. and CONCHELLO, J. A.: “Fluorescence microscopy”. *Nature Methods*, 2005. **2** (12): pp. 910–919.
- [21] DITTRICH, P. S. and MANZ, A.: “Single-molecule fluorescence detection in microfluidic channels - the holy grail in mu tas?” *Analytical And Bioanalytical Chemistry*, 2005. **382** (8): pp. 1771–1782.
- [22] BONNER, R. F., EMMERT-BUCK, M., COLE, K., *et al.*: “Cell sampling: Laser capture microdissection: Molecular analysis of tissue”. *Science*, 1997. **278** (21): pp. 1481–1483.
- [23] DITTRICH, P. S., TACHIKAWA, K., and MANZ, A.: “Micro total analysis systems. latest advancements and trends”. *Analytical Chemistry*, 2006. **78** (12): pp. 3887–3907.

- [24] DITTRICH, P. S. and MANZ, A.: "Lab-on-a-chip: microfluidics in drug discovery". *Nature Reviews Drug Discovery*, 2006. **5** (3): pp. 210–218.
- [25] SIMS, C. E. and ALLBRITTON, N. L.: "Analysis of single mammalian cells on-chip". *Lab On A Chip*, 2007. **7** (4): pp. 423–440.
- [26] PRICE, A. K. and CULLBERTSON, C. T.: "Chemical analysis of single mammalian cells with microfluidics". *Analytical Chemistry*, 2007. **79** (7): pp. 2614–2621.
- [27] HUANG, B., WU, H. K., BHAYA, D., *et al.*: "Counting low-copy number proteins in a single cell". *Science*, 2007. **315** (5808): pp. 81–84.
- [28] MELIN, J. and QUAKE, S. R.: "Microfluidic large-scale integration: The evolution of design rules for biological automation". *Annual Review Of Biophysics And Biomolecular Structure*, 2007. **36**: pp. 213–231.
- [29] MANZ, A., GRABER, N., and WIDMER, H. M.: "Miniaturized total chemical-analysis systems - a novel concept for chemical sensing". *Sensors and Actuators, B: Chemical Sensors and Materials*, 1990. **1** (1-6): pp. 244–248.
- [30] HARRISON, D. J., MANZ, A., FAN, Z. H., *et al.*: "Capillary electrophoresis and sample injection systems integrated on a planar glass chip". *Analytical Chemistry*, 1992. **64** (17): pp. 1926–1932.
- [31] MANZ, A., HARRISON, D. J., VERPOORTE, E. M. J., *et al.*: "Planar chips technology for miniaturization and integration of separation techniques into monitoring systems - capillary electrophoresis on a chip". *Journal Of Chromatography*, 1992. **593** (1-2): pp. 253–258.
- [32] REYES, D. R., IOSSIFIDIS, D., AUROUX, P. A., *et al.*: "Micro total analysis systems. 1. introduction, theory, and technology". *Analytical Chemistry*, 2002. **74** (12): pp. 2623–2636.
- [33] AUROUX, P. A., IOSSIFIDIS, D., REYES, D. R., *et al.*: "Micro total analysis systems. 2. analytical standard operations and applications". *Analytical Chemistry*, 2002. **74** (12): pp. 2637–2652.
- [34] VILKNER, T., JANASEK, D., and MANZ, A.: "Micro total analysis systems. recent developments". *Analytical Chemistry*, 2004. **76** (12): pp. 3373–3385.
- [35] JANASEK, D., FRANZKE, J., and MANZ, A.: "Scaling and the design of miniaturized chemical-analysis systems". *Nature*, 2006. **442** (7101): pp. 374–80.

- [36] WILSON, D. J. and KONERMANN, L.: “Ultrarapid desalting of protein solutions for electrospray mass spectrometry in a microchannel laminar flow device”. *Analytical Chemistry*, 2005. **77** (21): pp. 6887–6894.
- [37] CHEN, H., FANG, Q., YIN, X. F., *et al.*: “Microfluidic chip-based liquid-liquid extraction and preconcentration using a subnanoliter-droplet trapping technique”. *Lab On A Chip*, 2005. **5** (7): pp. 719–725.
- [38] TAKEUCHI, S., GARSTECKI, P., WEIBEL, D. B., *et al.*: “An axisymmetric flow-focusing microfluidic device”. *Advanced Materials*, 2005. **17** (8): pp. 1067–1072.
- [39] BARRETT, L. M., SKULAN, A. J., SINGH, A. K., *et al.*: “Dielectrophoretic manipulation of particles and cells using insulating ridges in faceted prism microchannels”. *Analytical Chemistry*, 2005. **77** (21): pp. 6798–6804.
- [40] GERDTS, C. J., TERESHKO, V., YADAV, M. K., *et al.*: “Time-controlled microfluidic seeding in nl-volume droplets to separate nucleation and growth stages of protein crystallization”. *Angewandte Chemie, International Edition in English*, 2006. **45** (48): pp. 8156–8160.
- [41] FOQUET, M., KORLACH, J., ZIPFEL, W. R., *et al.*: “Focal volume confinement by submicrometer-sized fluidic channels”. *Analytical Chemistry*, 2004. **76** (6): pp. 1618–1626.
- [42] BOWDEN, M., SONG, L., and WALT, D. R.: “Development of a microfluidic platform with an optical imaging microarray capable of attomolar target dna detection”. *Analytical Chemistry*, 2005. **77** (17): pp. 5583–5588.
- [43] WU, H. K., WHEELER, A., and ZARE, R. N.: “Chemical cytometry on a picoliter-scale integrated microfluidic chip”. *Proceedings Of The National Academy Of Sciences Of The United States Of America*, 2004. **101** (35): pp. 12809–12813.
- [44] LING, Y. Y., YIN, X. F., and FANG, Z. L.: “Simultaneous determination of glutathione and reactive oxygen species in individual cells by microchip electrophoresis”. *Electrophoresis*, 2005. **26** (24): pp. 4759–4766.
- [45] THOMPSON, D. M., KING, K. R., WIEDER, K. J., *et al.*: “Dynamic gene expression profiling using a microfabricated living cell array”. *Analytical Chemistry*, 2004. **76** (14): pp. 4098–4103.

- [46] CAMPBELL, L. C., WILKINSON, M. J., MANZ, A., *et al.*: “Electrophoretic manipulation of single dna molecules in nanofabricated capillaries”. *Lab On A Chip*, 2004. **4** (3): pp. 225–229.
- [47] CHUNG, Y. C., JAN, M. S., LIN, Y. C., *et al.*: “Microfluidic chip for high efficiency dna extraction”. *Lab On A Chip*, 2004. **4** (2): pp. 141–147.
- [48] HUANG, F. C., LIAO, C. S., and LEE, G. B.: “An integrated microfluidic chip for dna/rna amplification, electrophoresis separation and on-line optical detection”. *Electrophoresis*, 2006. **27** (16): pp. 3297–3305.
- [49] MARCUS, J. S., ANDERSON, W. F., and QUAKE, S. R.: “Microfluidic single-cell mrna isolation and analysis”. *Analytical Chemistry*, 2006. **78** (9): pp. 3084–3089.
- [50] EASLEY, C. J., KARLINSEY, J. M., BIENVENUE, J. M., *et al.*: “A fully integrated microfluidic genetic analysis system with sample-in-answer-out capability”. *Proceedings Of The National Academy Of Sciences Of The United States Of America*, 2006. **103** (51): pp. 19272–19277.
- [51] LIU, P., SEO, T. S., BEYOR, N., *et al.*: “Integrated portable polymerase chain reaction-capillary electrophoresis microsystem for rapid forensic short tandem repeat typing”. *Analytical Chemistry*, 2007. **79** (5): pp. 1881–1889.
- [52] SIA, S. K., LINDER, V., PARVIZ, B. A., *et al.*: “An integrated approach to a portable and low-cost immunoassay for resource-poor settings”. *Angewandte Chemie, International Edition in English*, 2004. **43** (4): pp. 498–502.
- [53] HERR, A. E., HATCH, A. V., THROCKMORTON, D. J., *et al.*: “Microfluidic immunoassays as rapid saliva-based clinical diagnostics”. *Proceedings Of The National Academy Of Sciences Of The United States Of America*, 2007. **104** (13): pp. 5268–5273.
- [54] KOBAYASHI, J., MORI, Y., OKAMOTO, K., *et al.*: “A microfluidic device for conducting gas-liquid-solid hydrogenation reactions”. *Science*, 2004. **304** (5675): pp. 1305–1308.
- [55] TERRY, S. C., JERMAN, G. H., and ANGELL, J. B.: “A gas chromatograph air analyser fabricated on silicon wafer”. *IEEE Transactions on Electron Devices*, 1979. **12** (ED-26): pp. 1880–1886.

- [56] SONG, H., CHEN, D. L., and ISMAGILOV, R. F.: "Reactions in droplets in microfluidic channels". *Angewandte Chemie-International Edition*, 2006. **45** (44): pp. 7336–7356.
- [57] HANSEN, C. L., CLASSEN, S., BERGER, J. M., *et al.*: "A microfluidic device for kinetic optimization of protein crystallization and in situ structure determination". *Journal Of The American Chemical Society*, 2006. **128** (10): pp. 3142–3143.
- [58] HUEBNER, A., SRISA-ART, M., HOLT, D., *et al.*: "Quantitative detection of protein expression in single cells using droplet microfluidics". *Chemical Communications*, 2007. (12): pp. 1218–1220.
- [59] DITTRICH, P. S., JAHNZ, M., and SCHWILLE, P.: "A new embedded process for compartmentalized cell-free protein expression and on-line detection in microfluidic devices". *Chembiochem*, 2005. **6** (5): pp. 811–814.
- [60] MANZ, A.: *US Pat.*, 1999. **6 540 896 B1**.
- [61] MANZ, A. and BECKER, H.: "Parallel capillaries for high throughput in electrophoretic separations and electroosmotic drug discovery systems". *Transducers*, 1997. **International Conference on Solid-State Sensors and Actuators**.
- [62] TAN, W. H. and TAKEUCHI, S.: "A trap-and-release integrated microfluidic system for dynamic microarray applications". *Proceedings Of The National Academy Of Sciences Of The United States Of America*, 2007. **104** (4): pp. 1146–1151.
- [63] SITUMA, C., HASHIMOTO, M., and SOPER, S. A.: "Merging microfluidics with microarray-based bioassays". *Biomolecular Engineering*, 2006. **23** (5): pp. 213–231.
- [64] EWING, A. G.: "Molecule specific imaging in biology: What are the challenges and the important applications?" *Applied Surface Science*, 2006. **252** (19): pp. 6821–6826.
- [65] AMEMIYA, S., GUO, J. D., XIONG, H., *et al.*: "Biological applications of scanning electrochemical microscopy: chemical imaging of single living cells and beyond". *Analytical And Bioanalytical Chemistry*, 2006. **386** (3): pp. 458–471.
- [66] MILANI, M., BALLERINI, M., BATANI, D., *et al.*: "High resolution microscopy techniques for the analysis of biological samples: a comparison". *European Physical Journal-Applied Physics*, 2004. **26** (2): pp. 123–131.

- [67] VISKARI, P. J. and LANDERS, J. P.: “Unconventional detection methods for microfluidic devices”. *Electrophoresis*, 2006. **27** (9): pp. 1797–1810.
- [68] ANNA, S. L., BONTOUX, N., and STONE, H. A.: “Formation of dispersions using “flow focusing” in microchannels”. *Applied Physics Letters*, 2003. **82** (3): pp. 364–366.
- [69] JOANICOT, M. and AJDARI, A.: “Applied physics. droplet control for microfluidics”. *Science*, 2005. **309** (5736): pp. 887–888.
- [70] NISISAKO, T., TORII, T., and HIGUCHI, T.: “Droplet formation in a microchannel network”. *Lab On A Chip*, 2002. **2** (1): pp. 24–26.
- [71] SONG, H., TICE, J. D., and ISMAGILOV, R. F.: “A microfluidic system for controlling reaction networks in time”. *Angewandte Chemie, International Edition in English*, 2003. **42** (7): pp. 768–772.
- [72] SONG, H. and ISMAGILOV, R. F.: “Millisecond kinetics on a microfluidic chip using nanoliters of reagents”. *Journal of the American Chemical Society*, 2003. **125** (47): pp. 14613–14619.
- [73] OKUSHIMA, S., NISISAKO, T., TORII, T., *et al.*: “Controlled production of monodisperse double emulsions by two-step droplet breakup in microfluidic devices”. *Langmuir*, 2004. **20** (23): pp. 9905–9908.
- [74] TICE, J. D., SONG, H., LYON, A. D., *et al.*: “Formation of droplets and mixing in multiphase microfluidics at low values of the reynolds and the capillary numbers”. *Langmuir*, 2003. **19** (22): pp. 9127–9133.
- [75] GHIDERSA, B. E., WORNER, M., and CACUCI, D. G.: “Exploring the flow of immiscible fluids in a square vertical mini-channel by direct numerical simulation”. *Chemical Engineering Journal*, 2004. **101** (1): pp. 285–294.
- [76] TICE, J. D., LYON, A. D., and ISMAGILOV, R. F.: “Effects of viscosity on droplet formation and mixing in microfluidic channels”. *Analytica Chimica Acta*, 2004. **507** (1): pp. 73–77.
- [77] GUTMANN, O., NIEKRAWIETZ, R., KUEHLEWEIN, R., *et al.*: “Impact of medium properties on droplet release in a highly parallel nanoliter dispenser”. *Sensors and Actuators A: Physical*, 2004. **116** (2): pp. 187–194.

- [78] ZHENG, B., ROACH, L. S., and ISMAGILOV, R. F.: "Screening of protein crystallization conditions on a microfluidic chip using nanoliter-size droplets". *Journal Of The American Chemical Society*, 2003. **125** (37): pp. 11170–11171.
- [79] ZHENG, B., TICE, J. D., ROACH, L. S., *et al.*: "A droplet-based, composite pdms/glass capillary microfluidic system for evaluating protein crystallization conditions by microbatch and vapor-diffusion methods with on-chip x-ray diffraction". *Angewandte Chemie, International Edition in English*, 2004. **43** (19): pp. 2508–2511.
- [80] HE, M., EDGAR, J. S., JEFFRIES, G. D., *et al.*: "Selective encapsulation of single cells and subcellular organelles into picoliter- and femtoliter-volume droplets". *Analytical Chemistry*, 2005. **77** (6): pp. 1539–1544.
- [81] GARSTECKI, P., FUERSTMAN, M. J., STONE, H. A., *et al.*: "Formation of droplets and bubbles in a microfluidic t-junction - scaling and mechanism of break-up". *Lab On A Chip*, 2006. **6** (3): pp. 437–446.
- [82] SONG, H., CHEN, D. L., and ISMAGILOV, R. F.: "Reactions in droplets in microfluidic channels". *Angewandte Chemie, International Edition in English*, 2006. **45** (44): pp. 7336–7356.
- [83] PAIK, P., PAMULA, V. K., and FAIR, R. B.: "Rapid droplet mixers for digital microfluidic systems". *Lab On A Chip*, 2003. **3** (4): pp. 253–259.
- [84] SRINIVASAN, V., PAMULA, V. K., and FAIR, R. B.: "An integrated digital microfluidic lab-on-a-chip for clinical diagnostics on human physiological fluids". *Lab On A Chip*, 2004. **4** (4): pp. 310–315.
- [85] POLLACK, M. G., FAIR, R. B., and SHENDEROV, A. D.: "Electrowetting-based actuation of liquid droplets for microfluidic applications". *Applied Physics Letters*, 2000. **77** (11): pp. 1725–1726.
- [86] FAIR, R. B.: "Digital microfluidics: is a true lab-on-a-chip possible?" *Microfluidics and Nanofluidics*, 2007. **3** (3): pp. 245–281.
- [87] VELEV, O. D., PREVO, B. G., and BHATT, K. H.: "On-chip manipulation of free droplets". *Nature*, 2003. **426** (6966): pp. 515–516.
- [88] GASCOYNE, P. R., VYKOUKAL, J. V., SCHWARTZ, J. A., *et al.*: "Dielectrophoresis-based programmable fluidic processors". *Lab On A Chip*, 2004. **4** (4): pp. 299–309.

- [89] SCHWARTZ, J. A., VYKOUKAL, J. V., and GASCOYNE, P. R.: “Droplet-based chemistry on a programmable micro-chip”. *Lab On A Chip*, 2004. **4** (1): pp. 11–17.
- [90] ZENG, J. and KORSMEYER, T.: “Principles of droplet electrohydrodynamics for lab-on-a-chip”. *Lab On A Chip*, 2004. **4** (4): pp. 265–277.
- [91] ADAMSON, D. N., MUSTAFI, D., ZHANG, J. X. J., *et al.*: “Production of arrays of chemically distinct nanolitre plugs via repeated splitting in microfluidic devices”. *Lab On A Chip*, 2006. **6** (9): pp. 1178–1186.
- [92] ZHENG, B. and ISMAGILOV, R. F.: “A microfluidic approach for screening submicroliter volumes against multiple reagents by using preformed arrays of nanoliter plugs in a three-phase liquid/liquid/gas flow”. *Angewandte Chemie, International Edition in English*, 2005. **44** (17): pp. 2520–2523.
- [93] CONCUS, P. and FINN, R.: “On capillary free surfaces in absence of gravity”. *Acta. Maths*, 1974. **132**: pp. 177–198.
- [94] CUBAUD, T. and FERMIGIER, M.: “Advancing contact lines on chemically patterned surfaces”. *Journal of Colloid and Interface Science*, 2004. **269** (1): pp. 171–177.
- [95] ZIMERMANN, H., SHIRLEY, S. G., and ZIMERMANN, U.: “Alginate-based encapsulation of cells: past, present, and future”. *Current Diabetes reports*, 2007. **7**: pp. 314–320.
- [96] SHIN, S. J., PARK, J. Y., LEE, J. Y., *et al.*: ““on the fly” continuous generation of alginate fibers using a microfluidic device”. *Langmuir*, 2007. **23** (17): pp. 9104–9108.
- [97] VALUSSI, S.: “Microfluidic system for the chemical analysis of fingerprint residues”. *Thesis, Imperial College, London*, 2003.
- [98] SIMONET, B. M., RIOS, A., and VALCARCEL, M.: “Enhancing sensitivity in capillary electrophoresis”. *Trac-Trends In Analytical Chemistry*, 2003. **22** (10): pp. 605–614.
- [99] DHOPESHWARKAR, R., LI, S. A., and CROOKS, R. M.: “Electrokinetic concentration enrichment within a microfluidic device using a hydrogel microplug”. *Lab On A Chip*, 2005. **5** (10): pp. 1148–1154.

- [100] ASTORGA-WELLS, J., VOLLMER, S., TRYGGVASON, S., *et al.*: “Microfluidic electrocapture for separation of peptides”. *Analytical Chemistry*, 2005. **77** (22): pp. 7131–7136.
- [101] LIU, Y., FOOTE, R. S., JACOBSON, S. C., *et al.*: “Stacking due to ionic transport number mismatch during sample sweeping on microchips”. *Lab On A Chip*, 2005. **5** (4): pp. 457–465.
- [102] JUNG, B., BHARADWAJ, R., and SANTIAGO, J. G.: “Thousandfold signal increase using field-amplified sample stacking for on-chip electrophoresis”. *Electrophoresis*, 2003. **24** (19-20): pp. 3476–3483.
- [103] JUNG, B., BHARADWAJ, R., and SANTIAGO, J. G.: “On-chip millionfold sample stacking using transient isotachophoresis”. *Analytical Chemistry*, 2006. **78** (7): pp. 2319–2327.
- [104] JUNG, B., ZHU, Y., and SANTIAGO, J. G.: “Detection of 100 am fluorophores using a high-sensitivity on-chip ce system and transient isotachophoresis”. *Analytical Chemistry*, 2007. **79** (1): pp. 345–349.
- [105] CHIEN, R. L.: “Sample stacking revisited: A personal perspective”. *Electrophoresis*, 2003. **24** (3): pp. 486–497.
- [106] LICHTENBERG, J., VERPOORTE, E., and DE ROOIJ, N. F.: “Sample preconcentration by field amplification stacking for microchip-based capillary electrophoresis”. *Electrophoresis*, 2001. **22** (2): pp. 258–271.
- [107] SHIDDIKY, M. J. A. and SHIM, Y. B.: “Trace analysis of dna: Preconcentration, separation, and electrochemical detection in microchip electrophoresis using au nanoparticles”. *Analytical Chemistry*, 2007. **79** (10): pp. 3724–3733.
- [108] KHANDURINA, J., JACOBSON, S. C., WATERS, L. C., *et al.*: “Microfabricated porous membrane structure for sample concentration and electrophoretic analysis”. *Analytical Chemistry*, 1999. **71** (9): pp. 1815–1819.
- [109] WANG, Y. C., STEVENS, A. L., and HAN, J. Y.: “Million-fold preconcentration of proteins and peptides by nanofluidic filter”. *Analytical Chemistry*, 2005. **77** (14): pp. 4293–4299.
- [110] ZENG, Y. and HARRISON, D. J.: “Self-assembled colloidal arrays as three-dimensional nanofluidic sieves for separation of biomolecules on microchips”. *Analytical Chemistry*, 2007. **79** (6): pp. 2289–2295.

- [111] FOOTE, R. S., KHANDURINA, J., JACOBSON, S. C., *et al.*: “Preconcentration of proteins on microfluidic devices using porous silica membranes”. *Analytical Chemistry*, 2005. **77** (1): pp. 57–63.
- [112] SONG, S., SINGH, A. K., and KIRBY, B. J.: “Electrophoretic concentration of proteins at laser-patterned nanoporous membranes in microchips”. *Analytical Chemistry*, 2004. **76** (15): pp. 4589–4592.
- [113] BROYLES, B. S., JACOBSON, S. C., and RAMSEY, J. M.: “Sample filtration, concentration, and separation integrated on microfluidic devices”. *Analytical Chemistry*, 2003. **75** (11): pp. 2761–2767.
- [114] YU, C., DAVEY, M. H., SVEC, F., *et al.*: “Monolithic porous polymer for on-chip solid-phase extraction and preconcentration prepared by photoinitiated in situ polymerization within a microfluidic device”. *Analytical Chemistry*, 2001. **73** (21): pp. 5088–5096.
- [115] OLSEN, K. G., ROSS, D. J., and TARLOV, M. J.: “Immobilization of dna hydrogel plugs in microfluidic channels”. *Analytical Chemistry*, 2002. **74** (6): pp. 1436–1441.
- [116] SAAVEDRA, L. and BARBAS, C.: “Chromatography-based on- and in-line preconcentration methods in capillary electrophoresis”. *Journal Of Biochemical And Biophysical Methods*, 2007. **70** (2): pp. 289–297.
- [117] ROSS, D. and LOCASCIO, L. E.: “Microfluidic temperature gradient focusing”. *Analytical Chemistry*, 2002. **74** (11): pp. 2556–2564.
- [118] SERA, Y., MATSUBARA, N., OTSUKA, K., *et al.*: “Sweeping on a microchip: concentration profiles of the focused zone in micellar electrokinetic chromatography”. *Electrophoresis*, 2001. **22** (16): pp. 3509–3513.
- [119] RIGHETTI, P. G. and BOSSI, A.: “Isoelectric focusing of proteins and peptides in gel slabs and in capillaries”. *Analytica Chimica Acta*, 1998. **372** (1-2): pp. 1–19.
- [120] HAN, J. and CRAIGHEAD, H. G.: “Separation of long dna molecules in a micro-fabricated entropic trap array”. *Science*, 2000. **288** (5468): pp. 1026–1029.
- [121] GIDDINGS, J. C. and DAHLGREN, K.: “Resolution and peak capacity in equilibrium-gradient methods of separation”. *Separation Science*, 1971. **6** (3): pp. 345–356.

- [122] SOUNART, T. and BAYGENTS, J.: “Electrically-driven fluid motion in channels with streamwise gradients of the electrical conductivity”. *Colloids and Surfaces A: Physicochemical and Engineering Aspects*, 2001. **195** (1-3): pp. 59–75.
- [123] LIN, H., STOREY, B. D., ODDY, M. H., *et al.*: “Instability of electrokinetic microchannel flows with conductivity gradients”. *Physics of Fluids A: Fluid Dynamics*, 2003. **16**: pp. 1922–1935.
- [124] CHEN, C., LIN, H., LELE, S., *et al.*: “Convective and absolute electrokinetic instability with conductivity gradients”. *Journal of Fluid Mechanics*, 2005. **524**: pp. 263–303.
- [125] YAN, D. G., YANG, C., and HUANG, X. Y.: “Effect of finite reservoir size on electroosmotic flow in microchannels”. *Microfluidics and Nanofluidics*, 2007. **3**: pp. 333–340.
- [126] BEEBE, D. J., MOORE, J. S., BAUER, J. M., *et al.*: “Functional hydrogel structures for autonomous flow control inside microfluidic channels”. *Nature*, 2000. **404** (6778): pp. 588–590.
- [127] YU, C., MUTLU, S., SELVAGANAPATHY, P., *et al.*: “Flow control valves for analytical microfluidic chips without mechanical parts based on thermally responsive monolithic polymers”. *Analytical Chemistry*, 2003. **75** (8): pp. 1958–1961.
- [128] DEMIRCI, U. and MONTESANO, G.: “Cell encapsulating droplet vitrification”. *Lab On A Chip*, 2007. **7** (11): pp. 1428–1433.
- [129] ANDERSSON, M., GROSECLOSE, M. R., DEUTCH, A. Y., *et al.*: “Imaging mass spectrometry of proteins and peptides: 3d volume reconstruction”. *Nature Methods*, 2008. **5** (1): pp. 101–108.
- [130] GOLDEN, A. P. and TIEN, J.: “Fabrication of microfluidic hydrogels using molded gelatin as a sacrificial element”. *Lab On A Chip*, 2007. **7** (6): pp. 720–725.
- [131] NAKAMURA, T., KUWAI, T., KITADAI, Y., *et al.*: “Zonal heterogeneity for gene expression in human pancreatic carcinoma”. *Cancer Research*, 2007. **67** (16): pp. 7597–7604.
- [132] VON ROTEN, M.: “Master thesis: Treatment and analysis of biological assays using microfluidic imaging concept”, 2008.

CURRICULUM VITAE

Personal Information

Name	KAORU TACHIKAWA
Adresse	Hansastr. 44, 44139 Dortmund
E-mail	tachikawa@isas.de
Telefon	0231 1392 187
Mobil	0179 8360 170
Geburtsdatum	16.04.1980, Kanagawa, Japan
Familienstand	ledig
Nationalität	japanisch



Ausbildung

seit Okt 04	ISAS – Institute for Analytical Sciences, Dortmund, D Doktorarbeit im Projektbereich Miniaturisierung: Entwicklung von mikrofluidischen Chips zur Analyse biologischer Proben. Titel: "Microfluidic Imaging: Pixelation and Preconcentration for Biological and Chemical Sample Analyses".
Sep 03 – Sep 04	London School of Management, London, UK Postgraduate Diploma in Management Studies Hauptfächer: Strategic and financial management, IT, HR management, Managing people
Okt 99 – Sep 03	Imperial College London, London, UK MSci Chemistry (Note: Second class honours upper division; entspr: gut) Masterarbeit: "Membrane supported catalysis: its synthesis and applications". Spezialisierung: Microfluidik, Medizinische Chemie, Pharmazeutika
Apr 92 – Jul 99	St. Paul's Girls' School, London, UK (Sep 95 – Jul 99) Abschluss A-levels: Maths (A), Chemistry (B), Physics (B) The British School in the Netherlands, Den Haag, NL (Apr 92 – Aug 95)

Tätigkeiten und Praktika

seit Jul 05	Doktorandensprecherin am ISAS - Dortmund
Jul 02 – Sep 02	Praktikum bei Pfizer (Sandwich, UK) Zusammenarbeit mit verschiedenen Projektgruppen der Abteilung "Worldwide Regulatory Affairs" und Unterstützung im F&E Labor
Jul 01 – Sep 01	Praktikum bei Pfizer (Tokyo, Japan) Arbeit in der "Clinical Operation Group" der Abteilung "Clinical Trials": Vereinfachung eines Computerprogrammes, Übersetzung von Einverständniserklärungen ins Englische und Präsentation der erarbeiteten Ergebnisse.
Jul 01 – Sep 00	Praktikum bei Pfizer (Tokyo, Japan) Arbeit in BPSU (Business Process Support Unit) zur Übersetzung eines "Oracle Clinical programme" ins Japanische für Abteilung "Clinical trial"

Sep 99 – Jul 01

Sprachkenntnisse

Kassenwartin und Vizepräsidentin der Japanischen Gesellschaft des Imperial College, London

Japanisch (Muttersprache)
Englisch (Muttersprache)
Deutsch (sehr gute Kenntnisse)
Spanisch (Grundkenntnisse)

Auszeichnungen

Gold Duke of Edinburgh Award
"Personal development programme" für junge Leute unter 25
Turniertanzen Latein Amerikanisch
Ausgezeichnet als "The most promising Jive new comer"

EDV-Kenntnisse

MS Windows, Microsoft Office, Excel, PowerPoint, Origin, LaTeX, Endnote, HTML

Hobbies

Musik: Klavier und Querflöte (seit drittem bzw. dreizehntem Lebensjahr)
Sport: Turniertänzerin (Latein, Startklasse A), Klettern und Joggen
Reisen

Publikationen

Papers

Dittrich, P., **Tachikawa, K.**, and Manz, A. (2006): Micro Total Analysis Systems. Latest Advancements and Trends. *Analytical Chemistry*, **78**, 3887 – 3907.

Ohno, K., **Tachikawa, K.**, and Manz, A. (accepted).
Microfluidics: Applications for Analytical Purposes in Chemistry and Biochemistry. *Electrophoresis*.

Tachikawa, K., Dittrich, P., and Manz, A. (submitted).
Microfluidic Imaging: A novel concept for pixelation of chemical and biological samples. *Lab-on-a-Chip*

Vortrag

Microscale BioSeparations Jan 07 (Vancouver, Kanada)
"Pixelation of heterogeneous samples: A microfluidic approach towards image compilation"

Konferenz Paper und
Poster Präsentation

MicroScale Bioseparations, Mar 08 (Berlin, Deutschland)
"Microfluidic Imaging: A novel concept for pixelation of heterogeneous planar samples"

Micro Total Analysis Systems, μ TAS, Okt 07 (Paris, Frankreich)
"Pixelation of planar biochemical samples: A novel concept for microfluidic imaging"

Gordon Conference, Analytical Chemistry, Jun 05 (Roscoff, Frankreich)
"Electric field assisted extraction and focusing by means of microfluidics"

Referenzen

Prof. Dr. Andreas Manz,
Head, ISAS – Institute for Analytical Sciences
Email: manz@isas.de

Dr. Joachim Steinke,
Imperial College London
Email: j.steinke@ic.ac.uk

Nick Scott,
Pfizer Global Research and Development, Tokyo Labs.
Email: Nick.Scott@pfizer.com

Dortmund, den 19. Mai 2008